

UNIVERSITY OF CALGARY

The Influence of Macropores on Flow and Transport to Subsurface Drains in Low
Permeability, Salt Affected Soils

by

Joshua M. Bishop

A THESIS

SUBMITTED TO THE FACULTY OF GRADUATE STUDIES
IN PARTIAL FULFILMENT OF THE REQUIREMENTS FOR THE
DEGREE OF MASTER OF SCIENCE

DEPARTMENT OF GEOSCIENCE

CALGARY, ALBERTA

APRIL, 2012

© Joshua Bishop 2012



UNIVERSITY OF
CALGARY

The author of this thesis has granted the University of Calgary a non-exclusive license to reproduce and distribute copies of this thesis to users of the University of Calgary Archives.

Copyright remains with the author.

Theses and dissertations available in the University of Calgary Institutional Repository are solely for the purpose of private study and research. They may not be copied or reproduced, except as permitted by copyright laws, without written authority of the copyright owner. Any commercial use or re-publication is strictly prohibited.

The original Partial Copyright License attesting to these terms and signed by the author of this thesis may be found in the original print version of the thesis, held by the University of Calgary Archives.

Please contact the University of Calgary Archives for further information:

E-mail: uarc@ucalgary.ca

Telephone: (403) 220-7271

Website: <http://archives.ucalgary.ca>

Abstract

The use of subsurface tile drains in conjunction with surface irrigation is proposed as a method for remediating salt affected soils, which are a major environmental issue for the oil and gas industry. Understanding the influence macropores have on the effectiveness of the tile drains in removing salts from the soil is required for future development of similar remediation sites. A multi-year study using conservative benzoic acid groundwater tracers was performed at a field site located in central Alberta in order to examine the affect macropores have on fluid flow and solute transport to subsurface tile drains through low permeability salt affected soils. Regular surface irrigations occurred during the 2009 and 2010 field seasons over a 20×20 m test plot and were combined with detailed temporal monitoring of tile drain discharge rates and effluent tracer concentrations. The spatial distribution and concentration of the tracers were also monitored using soil and pore water sampling. Results were then used to construct a dual permeability flow and transport model using the software package HYDRUS to aid in the understanding of flow and transport dynamics occurring on site. The tracer breakthrough to the tile drains occurred 46.75 hours after application to the ground surface. After two field seasons, 7% of the initial applied tracer mass was recovered in the tile drains and 32% of the initial mass was accounted for in soil core extractions taken from directly below the plot which indicates solute flushing is occurring under the plot. The tile drains were able to capture 5.9% and 51% of the applied irrigation (including precipitation) water volume in 2009 and 2010 respectively. The large discrepancy between the tile drain capture volumes is thought to be a function of the antecedent conditions in 2009 and 2010. Initial modeling results were successful at simulating the

tile drain discharge, but were less successful in matching the effluent tracer concentrations. Field observations and simulation results suggested that although macropores accounted for the majority of the fluid and solute transport, flushing of tracer from the soil to the tile drains was still occurring.

Acknowledgements

I thank my supervisor Ed Cey for all his excellent feedback, support and enthusiasm throughout the research project. Additionally, Larry Bentley for all his advice and feedback given to me and the effort he put into running this research program and Gopal Achari for volunteering his time as the external examiner. Imperial Oil, the Program for Energy Research and Development (Environment Canada) and the Natural Sciences and Engineering Research Council of Canada for funding, in-kind and logistical support.

I would also like to thank Mike Callaghan for being an excellent mentor and putting up with my nonsense for three years. Soon you will find your million dollar idea. Simon Martin, Blake Hiebert, Alex Wilkinson and Jackie Randell for all their help in the field and the lab. Mike Nightingale for all the excellent analytical help throughout the research program. Leslie Harker, Anita Gue and Brad Hansen for suffering through the course work with me.

Finally, I'd like to thank my friends and family for everything.

Table of Contents

Approval Page.....	ii
Abstract	iii
Acknowledgements.....	v
Table of Contents	vi
List of Tables	ix
List of Figures and Illustrations	x
List of Symbols.....	xiii
 CHAPTER ONE: INTRODUCTION.....	 1
1.1 Objectives	2
1.2 Thesis Outline	3
 CHAPTER TWO: RESEARCH SITE BACKGROUND	 4
2.1 Historic Site Development.....	4
2.2 Summary of Previous and On-Going Research Projects	5
 CHAPTER THREE: LITERATURE REVIEW	 11
3.1 Salt Affected Soils	11
3.2 Tile Drains	12
3.3 Variably Saturated Flow in Macroporous Soils.....	14
3.4 Vadose Zone Hydrologic Tracers	16
3.5 Variably Saturated Flow and Transport Modeling	18
 CHAPTER FOUR: METHODS AND MATERIALS.....	 22
4.1 Physiographic Setting	22
4.1.1 Regional Setting and Climate.....	22
4.1.2 Lithology	22
4.1.3 Soil Properties	23
4.2 Plot Construction and Monitoring Equipment.....	23
4.2.1 Irrigation Plot (Plot A), Tile Drain and Sump Construction	24
4.2.2 Monitoring Wells.....	25
4.2.3 Suction Lysimeter Installation.....	27
4.3 Plot A Irrigation	28
4.3.1 2009 Irrigation Season.....	28
4.3.2 2010 Irrigation Season.....	29
4.4 Tracer Application	29
4.4.1 Benzoic Acid Tracer Descriptions.....	30
4.4.2 Tracer Applications	30
4.4.2.1 DFBA Application.....	30
4.4.2.2 PFBA Injection	31
4.5 Water Sampling	32
4.5.1 Tile Drain Effluent	32
4.5.2 Monitoring Well Samples.....	33
4.5.3 Suction Lysimeter Samples	33
4.6 Soil Sampling.....	34

4.7 Laboratory Analysis.....	34
4.7.1 Water Samples.....	34
4.7.2 Soil Samples.....	35
4.7.3 QA/QC.....	36
4.7.4 Spiked Experimental Samples.....	37
4.7.5 Soil Batch Tests.....	37
4.8 Hydraulic Parameters.....	39
4.8.1 Hydraulic Conductivity.....	39
4.8.1.1 Slug Testing.....	39
4.8.1.2 Permeameter Testing.....	39
4.8.1.3 Tension Infiltrometer.....	40
4.8.2 Soil Water Characteristics.....	40
CHAPTER FIVE: DEVELOPMENT OF THE NUMERICAL MODEL.....	49
5.1 Conceptual Model.....	49
5.2 Preferential Flow Models.....	50
5.3 Model Implementation.....	51
5.3.1 HYDRUS 2D.....	51
5.3.2 Governing Equations.....	52
5.3.2.1 Fluid Flow.....	52
5.3.2.2 Solute Transport.....	53
5.3.3 Equation Solutions.....	55
5.4 Model Domain and Material Distribution.....	55
5.5 Model Parameters.....	57
5.5.1 Hydraulic Parameters.....	57
5.5.2 Dual-Domain Fluid Transfer Parameters.....	58
5.5.3 Solute Transport and Reaction Parameters.....	59
5.5 Boundary and Initial Conditions - Fluid Flow.....	60
5.5.1 Boundary Conditions.....	60
5.5.1.1 Hydraulic Head Boundary Conditions.....	60
5.5.1.2 Atmospheric Boundary Conditions.....	62
5.5.1.3 Internal (Seepage Face) Boundary Conditions.....	63
5.5.2 Initial Condition - Pressure Head.....	64
5.6 Boundary and Initial Conditions - Solute Transport.....	64
5.7 Observation Nodes and Mesh Lines.....	65
5.8 Mass Balance Error.....	66
CHAPTER 6: RESULTS AND DISCUSSION.....	73
6.1 2009 Field Results.....	73
6.1.1 Soil Properties.....	73
6.1.2 Tile Drain Flow Response.....	73
6.1.3 2009 DFBA Results.....	75
6.1.3.1 Tile Drain Effluent.....	75
6.1.3.2 Monitoring Wells.....	76
6.1.3.3 Tracer Degradation and Sorption Tests.....	78
6.1.3.4 Soil Extractions.....	79
6.2 2010 Field Results.....	80

6.2.1 Tile Drain Flow Response	80
6.2.2 Hydraulic Response in Monitoring Wells	82
6.2.3 2010 DFBA Results.....	84
6.2.3.1 Tile Drain Effluent Concentrations.....	84
6.2.3.2 Monitoring Well Detections	86
6.2.3.3 Suction Lysimeter Concentrations.....	87
6.2.3.4 Soil Extraction	88
6.2.3.5 DFBA Mass Balance	91
6.2.4 PFBA Injection Results	91
6.3 Model Calibration and Sensitivity Analysis	93
6.3.1 Calibration	93
6.3.1.1 Flow Parameters	93
6.3.1.2 Transport Parameters	94
6.3.2 Sensitivity Analysis	94
6.4 Simulated Flow Results	96
6.4.1 Tile Drain Discharge	96
6.4.2 Hydraulic Head Response	98
6.4.4 Simulated Fluid Mass Balance	99
6.5 Simulated DFBA Transport.....	100
6.5.1 Tile Drain Effluent Concentrations	100
6.5.2 Lysimeter Concentrations.....	103
6.5.3 Simulated Tracer Migration	104
CHAPTER SEVEN: CONCLUSIONS AND FUTURE WORK.....	132
7.1 Conclusions.....	132
7.2 Future Work.....	134
REFERENCES	136
APPENDIX A: TRACER DATA.....	143
APPENDIX B: SOIL BATCH TESTS.....	167
APPENDIX C: FIELD SOIL EXTRACTIONS	174
APPENDIX D: QA/QC	182
APPENDIX E: BOREHOLE LOGS	186
APPENDIX F: HYDRUS INPUTS	198
APPENDIX G: SOIL DATA.....	199

List of Tables

Table 4.1. Geometric mean of hydraulic conductivities at three different depths calculated from single well rising head slug tests completed in 2010.....	48
Table 4.2. Calculated van Genuchten (1980) parameters using the RETC software program.	48
Table 5.1. Summary of node spacing refinements used while constructing the unstructured finite element grid.	69
Table 5.2. Summary of depth material depth intervals used in numerical simulations	70
Table 5.3. Summary of dual-domain fluid mass transfer parameters used in the base case simulation.	71
Figure 5.5. Initial pressure head distribution for the 138 day simulation period. Blue colours indicate pressure head values greater than 0 (saturated). Yellow – red colours indicate pressure head values less than 0 (unsaturated).	71
Table 6.1. Properties of soils on site	107
Table 6.2. Summary of DFBA mass recovery at the end of the 2009 season. Soil corrected values indicate the total DFBA mass accounted for after a correction had been applied based on the DFBA soil extraction method (Section 4.5.2.2). ..	111
Table 6.3. Summary of DFBA mass recovery at the end of the 2010 season compared against the total mass applied (M_0) at the beginning of the 2009 season. Soil extraction numbers have been corrected based on the DFBA soil extraction method (Section 4.5.2.2)	118
Table 6.4. Summary of the reported literature values of the main calibration variables K_{sf} , ω and a as well as their effect on the simulated tile drain flow.	119
Table 6.5. Parameters used in base case simulation for matrix, macropore, fluid mass transfer and solute mass transfer.	120
Table 6.6. Results of sensitivity analysis normalized against base case simulation. Values less than 1 indicate the simulation results fit closer to observed data than base case results.	121

List of Figures and Illustrations

Figure 2.1. Airphoto of site.....	8
Figure 2.2. Site map showing spatial distribution of apparent electrical conductivity with the installed tile drain layout (red lines running west – east). High levels of electrical conductivity (warm colours) correspond to high levels of in-situ salt. Distribution of installed tile drains focus primarily in high electrical conductivity regions.....	9
Figure 2.3. Photos of a) fractures and roots observed during site excavation and b) fractures observed in recovered soil cores.	10
Figure 3.1. Schematic depicting a) flow and solute transport in a dual porosity domain and b) flow and solute transport in a dual permeability domain. Modified from Simunek and van Genuchten, 2008.....	21
Figure 4.1. Cross-section of sediment lithology beneath plot A. Cross-section stretches approximately 20 meters from north to south as shown in the key. Includes monitoring well and tile drain depths. Modified from Wilkinson (2011).....	42
Figure 4.2. Photo of Plot A in 2009 during irrigation. The location of the meterological along with tensiometer and thermocouple nests are indicated. Photo was taken prior to monitoring well installation.	43
Figure 4.3. a)Photo of monitoring equipment located inside the sump. Photo includes both north and south tile drain outlets, tipping buckets and sample collection tubing. b) Cross-section of sump system with tile drain outlets, location of sample devices and location of ISCO sample collection outlets *Note, cross-section not to scale*.....	44
Figure 4.4. Illustrated plan view map of Plot A at the end of the 2010 season. Legend indicates if monitoring well was installed in 2009 or 2010.	45
Figure 4.5. Schematic of the suction lysimeter installation at depths below 30 cm. Note, not to scale.....	46
Figure 4.6. Schematic of drip irrigation line configuration with tie-ins to the pump and irrigation tank.	46
Figure 4.7. Plan view map of sampling locations for the 2009 and 2010 DFBA soil sampling locations.	47
Figure 5.1. Summary of fluid flow parameters. Flow in both the matrix and macropore domain using the Richards' equation and mass transfer between each domain and a short description of the variables used in the calculations.	67

Figure 5.2. Summary of solute transport parameters. Solute transport in both the matrix and macropore domain using the advection-dispersion equation and mass transfer between each domain and a short description of the variables used in the calculations.	68
Figure 5.3. Model domain and flow boundary conditions used for all simulations. Location of cross-section shown in key in Figure 5.1.	69
Figure 5.4. Material distribution used in simulations.	70
Figure 5.6. Initial DFBA concentration distribution. Concentrations were set using results from the calculated pore water concentration extracted from the 2009 soil cores (Section 6.1.3.4).	72
Figure 5.7. Solute transport boundary condition used for all simulations.	72
Figure 6.1. Applied irrigation/precipitation (mm), measured tile drain flow (L/hr) and DFBA concentration in water samples recovered from the north and south tile drains in 2009. DFBA surface application occurred August 18 (day 230).	108
Figure 6.2. Plan view map of monitoring well DFBA concentrations in 2009.	109
Figure 6.3. Depth profile of average DFBA soil pore water extract concentrations in Plot A. Data are derived from 2:1 soil extracts collected in 2009 (blue) and 2010 (red). Error bars represent the standard error calculated from the sample population.	110
Figure 6.4. Applied irrigation/precipitation (mm), measured tile drain flow (L/hr) and DFBA concentration in water samples recovered from the north and south tile drains in 2010.	112
Figure 6.5. Plan view map of DFBA detections in A series monitoring wells during 2009 and 2010.	113
Figure 6.6. Plan view map of DFBA detections in B series monitoring wells in 2010.	114
Figure 6.7. Plan view map of DFBA detections in C series monitoring wells in 2010.	115
Figure 6.8. North (a) and south (b) lysimeter DFBA depth profiles from June 2010 to October, 2010. The north nest lies above the north tile drain and the south nest lies in the center of the plot, between the tile drains.	116
Figure 6.9. Plan view map showing DFBA depth distribution of 2010 soil extractions. Boreholes outside of plot are not included due to non-detects. Extracted DFBA concentration and sampling depth shown in legend unless otherwise indicated.	117
Figure 6.10. Monitored breakthrough of PFBA in North tile during the 2010 season. .	118

Figure 6.11. Sensitivity of simulated tile drain flow when specific glaciolacustrine hydraulic parameters were changed. Variables tested were a , n_m , α_m , K_{sf} , ω , K_{sa} . Results are shown with the base case simulation results and the observed 2010 south tile drain flow. Note the different scale used for the ω simulations.....	122
Figure 6.12. Sensitivity of simulated south tile drain effluent DFBA concentration to specific glaciolacustrine hydraulic parameters. Variables tested were a , n_m , α_m , K_{sf} , ω , K_{sa} and the solute mass transfer coefficient α_s . All scenario results are shown with the base case simulation and the observed 2010 south DFBA effluent concentration.	123
Figure 6.13. Results of base case 2010 simulation of south drain tile flow. Flow measured in tile drain is separated into matrix, macropore and combined flow components all of which are compared to the observed 2010 south tile drain flow.	124
Figure 6.14. Comparison of observed and simulated hydraulic heads selected monitoring wells at 37 different times throughout the simulation period. Locations of wells are indicated in the map and cross-section shown below.....	125
Figure 6.15. Comparison of simulated and observed hydraulic heads measured throughout the simulation period of 2010. Monitoring wells compared are MW09-01 (a), MW09-03 (b), MW09-05 (c), MW09-13A (d) and MW09-13B (e).	126
Figure 6.16. Results of base case simulation of the 2010 south drain effluent DFBA concentration. DFBA transport into tile drain is separated into matrix, macropore and combined flow components all of which are compared to the observed 2010 south effluent DFBA measured concentration.	127
Figure 6.17. Schematic diagram comparing how DFBA tracer mass is spatially distributed in (a) the numerical model versus (b) the field at the start of the 2010 season.	128
Figure 6.18. Results from the simulated lysimeters (a) observed in the base case scenario shown with the observed lysimeters (b).	129
Figure 6.19. Time lapse of simulated DFBA concentrations in the matrix domain at (a) $t=0$ days, (b) $t=36$ days, (c) $t=51$ days, (d) $t=80$ days, (e) $t=138$ days.	130
Figure 6.20. Time lapse of simulated DFBA concentration in the macropore domain at (a) $t=0$ days, (b) $t=36$ days, (c) $t=51$ days, (d) $t=80$ days, (e) $t=138$ days.....	131

List of Symbols

Symbol	Definition
h	Pressure Head
ρ_b	Dry Bulk Density (M/L^3)
K_{sat}	Saturated Hydraulic Conductivity (L/T)
K_{sf}	Saturated Hydraulic Conductivity of the Macropores (L/T)
θ_r	Residual Water Content of the Matrix (L^3/L^3)
θ_{rf}	Residual Water Content of the Macropores (L^3/L^3)
θ_s	Saturated Water Content of the Matrix (L^3/L^3)
θ_{sf}	Saturated Water Content of the Macropores (L^3/L^3)
α_m	Measure of the Inverse of the Air Entry Pressure in the Matrix ($1/L$)
α_f	Measure of the Inverse of the Air Entry Pressure in the Macropores ($1/L$)
n_m	Empirical Parameter Describing the Pore-Size Distribution of the Matrix (unitless)
n_f	Empirical Parameter Describing the Pore-Size Distribution of the Macropores (unitless)
S_m	Matrix Sink Term (T^{-1})
S_f	Macropore Sink Term (T^{-1})
Γ_w	Transfer Rate of Water between Domains (T^{-1})
ω	Volume of the Macropore System Relative to the Total Rock or Soil Volume (unitless)
α_w	Fluid Mass Exchange Coefficient ($L^{-1}T^{-1}$)
a	Characteristic Half Width of a Matrix Block (L)

β	Dimensionless Geometry Coefficient (unitless)
γ_w	Dimensionless Scaling Factor (unitless)
K_{as}	Effective Hydraulic Conductivity of the Interface between Matrix and Macropore Domains (L/T)
D	Dispersion Tensor (L ² /T)
q	Darcian flux (L/T)
φ	Reaction Parameter (M/L ³ T)
Γ_s	Solute Mass Exchange Parameter (T ⁻¹)
α_s	Solute Mass Transfer Coefficient (L ⁻¹)
C	Specified Concentration in the Respective Pore System (M/L ³)
D_a	Effective Dispersion Coefficient (L ² /T)
α_L	Lateral Dispersivity (L)
α_T	Transverse Dispersivity (L)
K_d	Distribution Coefficient (L ³ /M)

CHAPTER ONE: INTRODUCTION

When the Leduc No. 1 well discovered crude oil in 1947, oil and gas exploration and production in Alberta became one of the largest industries in the province. In Alberta there are currently 275,000 jobs directly and indirectly linked to the oil and gas industry as of 2011 (Government of Alberta, 2011). The increased development and expansion of oil and gas facilities in Alberta has resulted in an increased risk to the environment. These hazards can include the occurrences of industrial spills that have the potential to release large volumes of harmful chemicals (metals, volatile organic compounds), hydrocarbons and produced water (brine containing high levels of dissolved ions, produced along with oil and gas) at the ground surface. One of the more common and difficult environmental issues to deal with in oil and gas production facilities is release of produced water. Produced water spills have the ability to alter the geochemistry of the affected soils due to the addition of large volumes of chloride, calcium, magnesium and various other ions. This can result in both sodic (high sodium content, high pH, high sodium adsorption ratio (SAR)) and saline (high salt content, low pH, low SAR) soil conditions (Government of Alberta, 2010). The impact these spills have on the affected area can decrease the infiltration capacity of the soils and alter the soil structure; all of which can potentially result in a major reduction in soil fertility and crop production potential.

Several difficulties arise when developing a remediation strategy for salt affected soils. These include the location of the spill (remote or centered in a highly congested area), size of spill area ($m^2 - km^2$), spill composition (non-reactive, highly

reactive and harmful) and composition of affected soils (low permeability, presence of fractures, high permeability). One remediation method for treating saline/sodic soils is the installation of subsurface tile drains used to leach the salts from the soil and drain them away from the affected area. The effectiveness of the drains depends primarily on the permeability of the soil, tile drain spacing and the total volume of water passing through the soil. Closer drain spacing typically results in larger volumes of water removed from the soil, thereby increasing the leaching rate of the salts (Kladivko et al., 1999). Another factor that may influence the tile drain effectiveness is the presence of macropores (fractures, root holes), which have the ability to transport infiltrating water straight to or beyond the installed tile drains and reduce the efficiency of salt flushing from the soil profile. Preferential flow along macropores causes large volumes of water to bypass sections of soil matrix, reducing the amount of salt being flushed.

1.1 Objectives

In 2008, a research project was initiated to determine the effectiveness of subsurface drains (tile drains) for the removal of salts from low permeability, fractured soils and to examine whether surface applied irrigation could enhance the leaching of salts from the soils into the tile drains. Due to the large scope of the research, several projects were created with the intent of contributing to the overall research goal. The primary objective of this research project is aimed at furthering the understanding of how macropores influence solute transport to subsurface tile drains in low permeability, salt affected soil. This was accomplished by completing two tracer experiments over an irrigated, tile drain plot. The results from the tracer experiments were then used to

construct a calibrated 2-dimensional, dual permeability numerical flow and transport model using the HYDRUS software package. The numerical model will help quantitatively determine the influence macropores have on tile drain flow dynamics and solute transport through the low permeability soils.

1.2 Thesis Outline

This chapter introduces the scope of the research problem as well as the main objectives of the completed research. Chapter 2 will introduce the research site including its historical development and a discussion of previous and current research being conducted at the site by the University of Calgary. Chapter 3 is a literature review that discusses the occurrence and treatment of salt affected soils, the use of tile drains as a remediation strategy, macroporosity and their impacts, the use of benzoic acids as groundwater tracers and variably saturated flow and transport modeling. Chapter 4 describes the fieldwork and laboratory methodology used to characterize flow and tracer transport at the site. The development and calibration of the numerical flow and transport model are discussed in Chapter 5. Chapter 6 presents the results and discussion of the benzoic acid tracer experiments and the flow and transport simulations. Chapter 7 contains the final conclusions of the research along with recommendations for future work.

CHAPTER TWO: RESEARCH SITE BACKGROUND

2.1 Historic Site Development

The research site under investigation is located southwest of Edmonton, Alberta in a region used primarily for agriculture (Figure 2.1). The site was originally used as an oil and gas battery to facilitate oil and gas production activities in the region. Air photos of the property show that development of the site as an oil and gas production facility was established prior to 1962 (Komex International, 1999). Ongoing development occurred from the early 1960's through until the 1980's. Throughout the history of the site, multiple small releases of produced water occurred, negatively impacting the soil conditions. During the mid 1980's (exact date unknown) a pipeline spill on site released an unknown volume of hydrocarbons and produced saline water (Komex International, 1997). Removal of 6085 m³ of hydrocarbon contaminated soil in 2001 left approximately 27000 m³ of shallow, salt affected soil on site (Komex International, 2005). The addition of calcium soil amendments along with the installation of subsurface tile drains in 2003 acted as an in-situ remediation strategy with the intent to remove salt from the soil via flushing to the tile drains (Komex International, 2003). Drains were installed in locations of high salinity at a depth of approximately 2.1 meters below ground surface in a west – east direction with 10 meter separation (Figure 2.2). All drains are connected to main lines that discharge into a wet well located on the south edge of the property. A summary of work completed by various environmental consulting firms between 1998 and 2006 is as follows (Smith, 2008)

- Four electromagnetic (EM) surveys completed between 1998 and 2004
- Seven shallow (approx. 3-5 meters) monitoring wells installed in 1998 and re-installed in 2004; three deep (below 5 meters) monitoring wells installed in 1999
- Monitoring well sampling in 1998 and 2004 for groundwater chemical analysis.
- Excavation of hydrocarbon impacted soils in 2001
- Soil sampling and analysis in 1998, 1999 and 2004
- Installation of subsurface tile drain system and application of calcium amendments in 2003

2.2 Summary of Previous and On-Going Research Projects

Research done by the University of Calgary on the site began in the mid 2000's with multiple near surface geophysical surveys being conducted (Electrical Resistivity Tomography (ERT), EM and push tool electrical conductivity (EC)). Multiple ERT surveys were run in two separate locations on the property (south and western edge), both of which were used to characterize and monitor the depth of the salt impacted soil over time. Additional site wide EM and push tool electrical conductivity surveys were conducted to determine the spatial extent of the salt impacted soil as shown in Figure 2.2. Numerical models were developed by Smith (2008) to estimate the time required to remove salt from the soils under natural climatic conditions and to determine what effect the tile drain spacing had on salt flushing. The models developed were also used to investigate the role density dependent flow had on salt transport in variably saturated conditions. Results from the simulations suggested that surface irrigation over the tile drain area could enhance the salt production in the tile drains. Additional experiments were conducted in 2008 using tension infiltrometers and Guelph permeameters to examine the variance of surface hydraulic conductivities under varying soil conditions (tilled, irrigated, natural).

A second phase of the monitoring program investigating the effectiveness of subsurface tile drains for remediation of salt affected, low permeability soils was initiated in 2008. The 2008 program built on the previous monitoring work with the completion of several push tool conductivity surveys performed throughout the full site coupled with soil core analysis. Six additional full site EM surveys were completed in 2010 that were used to determine if measurable changes have been observed in the salt distribution compared to previous surveys and to ultimately determine the total mass of salt residing on site.

Furthermore, an experimental irrigation test plot and control plot were constructed in 2008 to examine whether surface irrigation could enhance salt flushing from the soil into the tile drains. The experimental and control plots were constructed in areas of high salinity (Figure 2.2) so that greater decreases in soil salinity could be observed. The experimental plot (Plot A) was outfitted with drip line irrigation system and monitoring equipment, while the control plot (Plot B) was left without irrigation. In the experiment, irrigation water was regularly applied to the surface of the plot along with routine measurements of tile drain effluent chemistry (chloride). Additional monitoring focused on changes in soil geochemistry and differences observed in the ERT and EM surveys, which could be used to measure and monitor the performance of the tile drains. Observed decreases in the soil's electrical conductivity would indicate a removal of salts. ERT surveys were completed over the experimental plot (Plot A) throughout the course

of the research program to track the changes in soil electrical conductivity over and between the tile drains.

Increasing evidence has shown the influence macropores have on preferential flow and transport in soils (Bouma, 1981; Beven and Germann, 1982; Jarvis, 2007). Initial results from the 2008 irrigation season, tension infiltrometer measurements and analysis of soil cores indicated that preferential flow pathways were affecting the flow and transport of water and salts in the soil on site. Analysis of soil cores recovered on site and observations made during excavation of the tile drains confirmed the presence of macropores (fractures and root holes) (Figure 2.3). To test the influence macropores have on solute flow and transport, two tracer experiments were conducted in 2009 and 2010. Results from the tracer experiments were then used to construct a calibrated numerical flow and transport model that could help quantify the role macroporosity has on tracer transport to the tile drains. This model could then be adapted in the future to examine other salt flushing issues (e.g., soil swelling, geochemical alterations) and assess alternative remedial design options.



Figure 2.1. Airphoto of site.

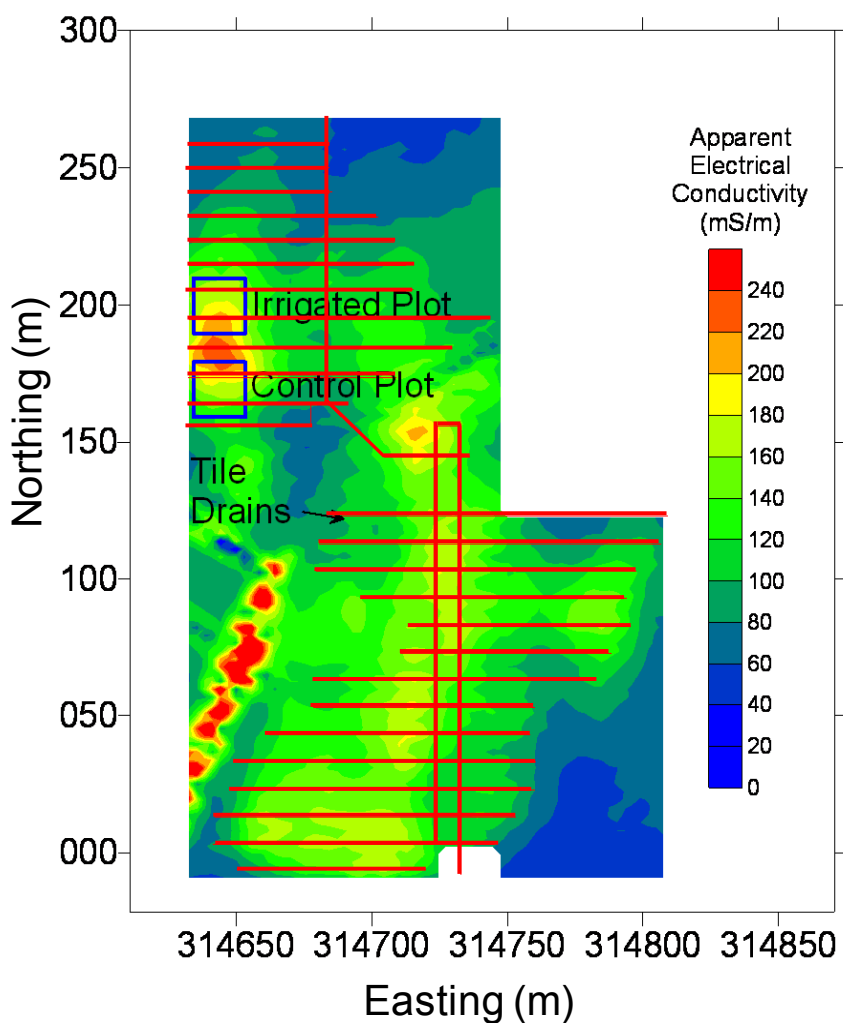


Figure 2.2. Site map showing spatial distribution of apparent electrical conductivity with the installed tile drain layout (red lines running west – east). High levels of electrical conductivity (warm colours) correspond to high levels of in-situ salt. Distribution of installed tile drains focus primarily in high electrical conductivity regions.

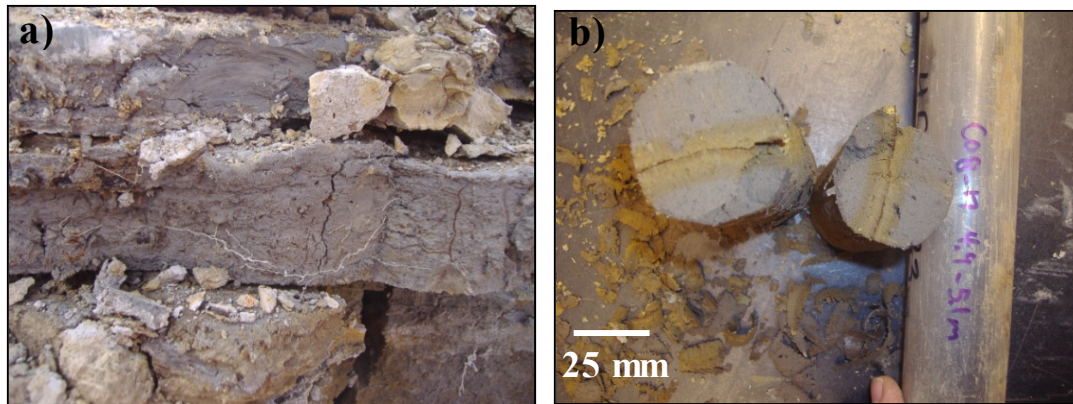


Figure 2.3. Photos of a) fractures and roots observed during site excavation and b) fractures observed in recovered soil cores.

CHAPTER THREE: LITERATURE REVIEW

3.1 Salt Affected Soils

In Alberta, approximately 1.6 million acres of land suffers from complications associated with high salt concentrations resulting in a reduced crop yield of up to 25% (Alberta Agriculture, 1991). Salt affected soils are characterized by higher amounts of soluble salts that can cause negative impacts on crop yields (Abrol et al., 1988). They can be caused by the use of saline groundwater for irrigation, excessive irrigation in arid regions, poor subsurface drainage, or result from industrial spills releasing large volumes of brine over the land surface (Abrol et al., 1988). There are two main classifications for salt affected soils: saline and sodic. Common characteristics for saline soils include having a pH less than 8.2 in the saturated paste test (Abrol et al., 1988) and an electrical conductivity greater than 4 dS/m at 25°C. Saline soils tend to exhibit white patches of precipitated salts, especially in elevated areas where evaporation occurs (Tanji, 1990). Generally, the permeability of the soil is not impacted by the increased salinity. Common characteristics of sodic soils include having a pH greater than 8.2 in the saturated paste test, increased levels of sodium relative to the levels of calcium and magnesium, and at times an electrical conductivity greater than 4 dS/m at 25°C (Abrol et al., 1988). Visually, sodic soils will display a brown crust and have a lower infiltration capacity caused by the swelling and dispersion of clay minerals due to an increased proportion of sodium ions (Tanji, 1990). The increase in sodium ions causes the clay particles to repel each other, decreasing the pore size of the clay, which in turn decreases the permeability of the soil (Appelo and Postma, 2005).

Remediation strategies used to treat salt affected soils include the addition of a soil amendment (e.g., gypsum), scraping of precipitated surface salts, planting salt tolerant crops, physical excavation and removal of the affected soils, or leaching the salts from the soil with the aid of subsurface drains (Abrol et al., 1988). The addition of gypsum ($\text{CaSO}_4 \cdot 2\text{H}_2\text{O}$) acts to replace sodium on cation exchange sites by supplying sufficient quantities of the divalent calcium ion (Tanji, 1990). The sodium – calcium ion substitution aids in decreasing the clay particle repulsion, preventing clay mineral dispersion and the reduction of soil permeability. Another strategy used is the leaching of salts with subsurface drains. This allows for salts to pass through the soil column and into the drains, removing the salts from the affected area. This technique can potentially lower the soil salinity of the affected area quicker if used in conjunction with surface irrigation when compared to soil flushing under natural climatic conditions although soil sodicity issues may arise as a result of poor irrigation water quality (high TDS).

3.2 Tile Drains

Subsurface tile drains can be a useful remediation method for the reclamation of contaminated sites. Traditionally, tile drains have been used in agricultural practice as a method for regulating the water table and improving subsurface drainage. In contaminated sites, they act as a tool to enhance the flushing and removal of harmful solutes from the affected area. The efficiency of tile drains in site remediation is dependent on tile drain spacing, magnitude and frequency of irrigation, time of initial irrigation after solute application, soil structure, and contaminant mobility (Balasubramanian et al., 1973; Kladvko et al., 2004). It is thought that tile drain fields

with a close spacing will naturally collect more solute/contaminant than a tile drain field with wider tile drain spacing. Furthermore, managing the irrigation rates and volumes applied can be important to ensure the right soil moisture conditions exist for leaching of potential contaminants. A study performed by Balasubramanian et al. (1973) found that nitrate transport rates to tile drains were influenced by the timing of intermittent irrigation (surface flooding) events following a application of nitrate to the ground surface. The study suggested that the management of irrigation rates and fertilizer application can help reduce nitrate losses to subsurface drains. Allowing the nitrate time to migrate from the more permeable macropores into the less permeable matrix after application reduced nitrate losses in comparison to quickly irrigating after nitrate application. This has implications in salt flushing scenarios in which irrigations using large volumes of water shortly after salt application should enhance the salt removal to subsurface drains by not allowing the salt to migrate from the macropores into the less permeable matrix.

Several other issues can be encountered with the use of subsurface drains that can negatively impact the surrounding environment. Drain outlets generally discharge into surface waters, which can have an adverse impact on surface water quality. Levels of nitrate and fecal bacteria exceeding drinking water guidelines have been measured at tile drain discharge outlets in studies completed by Jaynes et al. (2001) and Jamieson et al. (2002). This is not likely a major issue for remediation schemes as the tile drain effluent is generally not discharged into surface water bodies, but is instead treated or disposed of after collection.

Low permeability soils such as the glacial sediments found throughout Alberta, can increase the time required for solute removal using tile drains. The low permeability soils decrease the speed at which fluids and solutes can travel through the soil, increasing the required remediation time. The effectiveness of tile drains as a remediation strategy for reclaiming saline-sodic soils in Southern Alberta was investigated by Van Schaik and Milne (1961). The researchers found that tiles installed at a relatively shallow depth (0.76 meters) in low permeability glacial tills were able to successfully flush the soils after 3 years while applying a total of 1.8 meters of irrigation water (roughly 6 pore volumes). A decrease in salt concentration was also observed beneath the drains suggesting that the tile drains were able to flush soils underlying the drains. Another study that focused on tile drain usage in low permeability glacial sediments in Alberta found that a decrease in salinity was observed only within the top 30 cm of the soil profile after 2 years of irrigation (Paterson and Brook Harker, 1980). Both of these studies indicate that although remediation times may be lengthy and variable due to the low permeability soils, tile drains can be a useful technique for flushing salts.

3.3 Variably Saturated Flow in Macroporous Soils

Flow and transport in variably saturated conditions is a function of a soil's ability to retain and drain water due to the dependence between hydraulic conductivity (K) and pressure head (h) (Freeze and Cherry, 1979). In conditions of $h < 0$, the soils will be under tension, causing preferential draining of the larger pores, reducing the effective hydraulic conductivity of the soil. As $h \ll 0$ and the tension placed on the soil increases, the remaining smaller saturated pores begin to drain further reducing the soil's

hydraulic conductivity. The complexity of the relationship between hydraulic conductivity, pressure head and moisture content leads to nonlinear flow equations that are not subject to easy solutions (Fetter, 2001).

Furthermore, the presence of macropores adds to the complexity of variably saturated flow and transport. The term macroporosity can be given to any large continuous soil pores that influence the flow and transport of fluids and solutes (Beven and Germann, 1982). Although there is much debate among researchers on how large the opening must be to be deemed a “macropore” (Bouma, 1981), most can agree on the influence macropores have on preferential flow and transport in the subsurface (Bouma, 1981; Beven and Germann, 1982; Jarvis, 2007). These preferential flow paths are most often generated in the soil due to desiccation or previous stress, root holes, animal burrows or natural soil pipes (Beven and Germann, 1982). Under unsaturated conditions, fluid flow in macropores is initiated or “turned on” once the soil has reached near saturation and the large radius macropores are able to fill up and transmit water (Weiler and Naef, 2003). Rapid transport of solutes is generally a characteristic behaviour of macropores. Macropores have been found to decrease the breakthrough time of solutes to tile drains, due to these preferential flow pathways acting as a “short cut” to the drains (Kung et al., 2000; Kohne and Gerke, 2005; Stone and Wilson, 2006). The majority of flow in the soil is channelled through the macropores, while only a small fraction of the soil matrix is exposed to any infiltrating water. This can be troublesome when attempting to completely flush a solute (i.e. salt) from the soil matrix as only portions of soil matrix will be exposed to infiltrating fresh water.

Understanding the dynamics between the matrix and macropore domains is important when studying the influence macropores have in a low permeability soil. Fluid and solute transfer between the matrix and macropore region is a highly complex process that can depend on variables such as macropore geometry, the hydraulic conductivity of the matrix and macropore regions, soil moisture content and the solute concentrations present in the matrix and macropore domains (Gerke and van Genuchten, 1996).

3.4 Vadose Zone Hydrologic Tracers

The ability to identify the influence soil macropores have on flow and solute transport is commonly accomplished with the use of conservative tracers. Monitoring the breakthrough to subsurface monitoring locations allows physical measurements of travel time and velocities to be made. Additionally, studying the spatial distribution of tracers within the soil column helps understand the influence heterogeneities have on flow. Multiple natural tracers exist in the form of isotopes (^3H , ^{14}C , ^{36}Cl , ^{18}O), all of which can help calculate recharge, infiltration rates and transport times of groundwater (Allison et al., 1994). The anions chloride and bromide are commonly used as conservative tracers because they do not degrade, react or adsorb in the subsurface, are cost efficient, and easily detectable at low concentrations. One potential setback is both chloride and bromide are not effective tracers in areas with high pre-existing concentrations (i.e. salt affected soils).

Recently, the use of benzoic acids as groundwater tracers has become increasingly popular. Multiple studies have examined whether benzoic acids could be used as suitable non-reactive tracers in the subsurface. These studies have shown that two specific benzoic acids, 2,6-Difluorobenzoic acid (DFBA) and Pentafluorobenzoic acid (PFBA), act similar to bromide in that they have the same measureable breakthrough times and show no signs of sorption (Bowman, 1984a; Bowman, 1984b; Jaynes, 1994). Commonly, DFBA and PFBA are analyzed using High Precision Liquid Chromatography (HPLC), which is able to simultaneously detect both acids at relatively low concentrations and offers a relatively precise and accurate measurement technique (Bowman, 1984a; McCarthy et al., 2000; Dahan and Ronen, 2001). Both DFBA and PFBA have been used in several field studies as conservative groundwater tracers and have been typically applied on the soil surface, or injected at depth (Bowman and Gibbens, 1992; Jaynes, 1994; Kung et al., 2000). A series of laboratory column tests, soil batch experiments, aquifer and vadose tests were performed by Bowman and Gibbens (1992) and found that both DFBA and PFBA showed no signs of degradation, sorption and each recorded breakthrough times similar to that of bromide. Other experiments performed by Kung et al. (2000), Dahan and Ronen (2001) and Johnson et al. (2003) all found that both DFBA and PFBA acted similar to bromide and chloride under field conditions in that they showed no degradation or sorption. An experiment completed by Jaynes (1994) did not obtain full recovery of DFBA in soils saturated with a known concentration of DFBA over a 60 day period. The lab batch test measured a total decrease in DFBA concentration of 0.6 mg/L from an initial concentration of 2 mg/L over the study period. No measureable decrease in concentration was noted for PFBA

under the same conditions. It was noted that the decrease in mass is not necessarily due to the degradation of the benzoic acid but could be due to a decrease in the recovery of DFBA from the solution over time. Another study by Hu and Moran (2005) supported the findings of Jaynes (1994) in that the transport of the benzoic acid tracers could be retarded by changes in the pH of the soil, presence of organic matter, iron oxide content and clay mineralogy.

3.5 Variably Saturated Flow and Transport Modeling

When numerically defining flow and transport in variably saturated media, a mathematical relationship termed the soil water characteristic model must be developed to describe the dependence among hydraulic conductivity, water content, and the applied pressure head. One method for describing the unsaturated hydraulic properties for an individual soil is the van Genuchten model (van Genuchten, 1980). The relation between pressure head (h) and soil water content (Equation 3.1) or hydraulic conductivity (Equation 3.2) is as follows:

$$\theta(h) = \theta_r + \frac{\theta_s - \theta_r}{[1 + |\alpha h|^n]^m} \quad (3.1)$$

$$K(h) = \frac{\{1 - (\alpha h)^{n-1} [1 + (\alpha h)^n]^m\}^2}{[1 + (\alpha h)^n]^{\frac{m}{2}}} \quad (3.2)$$

where θ_r is the residual water content (L^3/L^3), θ_s is saturated water content (L^3/L^3), α ($1/L$) is the measure of the inverse of the air entry pressure, n (unitless) is an empirical parameter describing the pore-size distribution and $m = 1 - \frac{1}{n}$ (Wise et al., 1994). The

van Genuchten – Mualem model predicts how a specific soil's water content reacts to changing negative pressures (or tensions) allowing for unsaturated hydraulic conductivities to be calculated for a specific soil tension or water content.

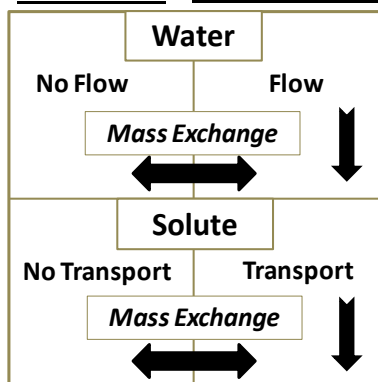
The use of numerical flow and transport models has become an important part of hydrogeological studies due to their ability to provide useful information on how a subsurface flow system operates, and how that system will behave when exposed to varying forcing factors (Fetter, 2001). Simulating fluid flow and solute transport in a variably saturated system can be accomplished using Richards' equation for a single matrix domain. When soil heterogeneities in the form of macropores begin to influence flow and transport, a single domain model is no longer useful in representing the physical processes occurring. Macropores are often represented in numerical simulations either discretely or using dual continuum formulations. Modeling macropores discretely requires that each macropore be represented by a group of model elements with a specific geometry, hydraulic conductivity and storage capacity. To accurately represent such a system, a large amount of information on the geometric distribution and connectivity of the macropores is needed. Using the software program HydroGeoSphere, this is accomplished numerically by representing discrete fractures with 2-dimensional planes of connected nodes that form part of a 3 dimensional grid. The matrix and macropore domains are then coupled by their collocation (Weatherill et al., 2008). Generally, large numbers of nodes are needed to simulate flow through discrete macropores. Alternatively, the dual continuum method represents the matrix and macropores as two separate, but overlapping domains. This allows for flow to occur in both domains with

fluid and solute transfer occurring between them. This typically decreases the number of elements needed because the full spatial distribution of macropores does not need to be defined, thus reducing simulation times.

There are two main types of dual continuum models currently in use: dual porosity and dual permeability models. The dual porosity model assumes flow and solute transport occurs only through the macropores, making fluid in the matrix immobile while still allowing fluid and solute transfer between the matrix and fracture domains (Simunek et al., 2003) (Figure 3.1a). Mass exchange between the two domains is determined by a combination of the hydraulic head, soil moisture or concentration gradients and varying mass exchange parameters (Gerke and van Genuchten, 1993a; Jarvis, 1995). Commonly the dual porosity model requires fewer input parameters when compared to the dual permeability model, and is generally more stable numerically and requires less time to generate a solution. Alternatively, the dual permeability model allows fluid and solute flow in both matrix and fracture domains, which are coupled to allow mass transfer between domains (Simunek et al., 2003) (Figure 3.1b). Numerically, flow within the domains is described using Richards' equation for both the matrix and macropores. Transfer between each domain is accomplished with the use of a coupling term. Solute transport in each domain is determined with the use of the advection-dispersion equation. Similar to fluid flow, solute mass transfer between domains is accomplished with the use of a coupling term which accounts for solute transfer via diffusion and advection.

a) Dual Porosity Model

Matrix Domain Macropore Domain



b) Dual Permeability Model

Matrix Domain Macropore Domain

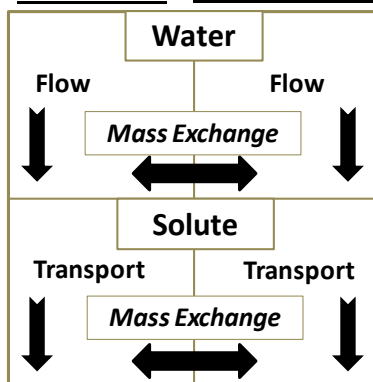


Figure 3.1. Schematic depicting a) flow and solute transport in a dual porosity domain and b) flow and solute transport in a dual permeability domain. Modified from Simunek and van Genuchten, 2008.

CHAPTER FOUR: METHODS AND MATERIALS

4.1 Physiographic Setting

4.1.1 Regional Setting and Climate

The research site is located approximately 10 km southwest of Devon, Alberta at XX-XX-50-26 W4M on an abandoned oil and gas satellite. Located in the arid region of central Alberta, the nearby town of Camar (approximately 2 km south) historically receives 521 mm of annual precipitation and reaches annual average maximum and minimum temperatures of 9.3°C and -3.5°C, respectively (Environment Canada, 2011). Located within the Parkland Natural Eco-region, topography can be characterized as gently undulating with no significant topographic relief (Natural Regions Committee, 2006).

4.1.2 Lithology

The region is located east of the front ranges of the Canadian Rockies and has been heavily influenced lithologically by previous glaciations. Prior to the glaciations the topography was characterized by broad north-east to southeast trending valleys (Mossop and Shetsen, 1994). Regionally, glaciations occurred at least five times with the earliest likely 1.8 million years ago (Mossop and Shetsen, 1994). Each glacial advance deposited high levels of glacial and non-glacial sediments in lakes and depressions (Mossop and Shetsen, 1994). Regionally, the surficial sediments rest upon the top of the Upper Horseshoe Canyon formation. These surficial sediments can reach thicknesses of up to 300 m in some locations. Locally, the top of the Upper Horseshoe Canyon formation is located 20 m below ground surface (Mossop and Shetsen, 1994).

Analysis of soil cores show that the site is underlain by a layer of top soil roughly 0.20 m thick, followed by a low permeability glaciolacustrine silt layer with a thickness of 2.2 m extending to a depth of 2.4 m below ground surface. Below the glaciolacustrine silt unit exists a fractured dense glacial till unit extending below 7.0 m that is interrupted by two fine to medium sand units at depths of 4.0 m and 6.0 m with thicknesses of approximately 0.5 m (Figure 4.1).

4.1.3 Soil Properties

Particle size distribution, dry bulk density, porosity and cation exchange capacity were analyzed for the top soil, glaciolacustrine, glacial till and the B series sand unit. Particle size distribution for the glaciolacustrine and glacial till units were measured using the Mastersizer 2000 (Malvern Instruments). Particle size distribution of the B series sand unit was completed by sieve analysis. Particle size classifications for each material were taken from The Canadian System of Soil Classification (Haynes, 2005). Cation exchange capacity of the glaciolacustrine and glacial till units was calculated using the procedure found in Amrhein and Suarez (1990). A summary of the soil properties can be found in Table 6.1

4.2 Plot Construction and Monitoring Equipment

In 2003, site wide subsurface tile drains were installed 2.1 m below ground surface at 10 m spacings in areas shown to be highly affected by salts. Each tile drain was originally installed resting on top of a 1.0 m wide by 0.35 m thick

gravel pack. All tile drains were installed by excavating a trench causing a large zone of disturbed soil above the tile drains (Figure 4.1). Dimensions of the trench were constructed at a 1:1 ratio, meaning the depth of the trench corresponds to the width of the trench measuring from the center out to the edge. Previous modeling completed by Smith (2008) suggested that surface irrigation could enhance the flushing of salts from the soil and decrease the time required for remediation. In order to test this, two plots were constructed on the western edge of the property in a location with the highest measured electrical conductivity (Figure 2.2), with each plot constructed directly over a pair of tile drains. The experimental plot (Plot A) was constructed with surface irrigation drip lines while the control plot (Plot B) was constructed without drip lines. Throughout the course of the program, both plots were monitored (soil core salinity, push tool conductivity, ERT surveys) for changes in soil salinity. Furthermore, tile drains beneath the experimental plot were diverted into a sump, which allowed monitoring of the tile drain effluent and discharge rates.

4.2.1 Irrigation Plot (Plot A), Tile Drain and Sump Construction

Construction of Plot A and B began in 2008. Both 20 m × 20 m plots were deep tilled, levelled, and surrounded by a compacted soil berm designed to limit any runoff or runoff during irrigation and precipitation events (Figure 4.2). The focus of this study was Plot A, where irrigation was used to enhance salt leaching. To enable monitoring of flow and water quality in the tiles, the two tile drains (North and South) beneath Plot A were isolated from the surrounding tile drainage system. In 2009, a 3.5 m deep by 1.5 m diameter sump was installed approximately 15 meters east of Plot A. Both tile drain

discharge outlets were directed into the sump to allow for effluent monitoring (Figure 4.3). Discharge rates were monitored using tipping buckets (TB1L, Hydrological Services Pty Ltd) calibrated to 0.73 L /tip that allowed for a maximum flow rate of 25 L/min. Regular sampling every 3 – 8 hrs was conducted using ISCO (model 6712) automated samplers.

A meteorological station (Figure 4.2) located at the center of the plot contained a data logger (CR1000, Campbell Scientific) that recorded net radiation (NRLITE2, Campbell Scientific), surface temperature (SI-111, Campbell Scientific), and soil heat flux (HFT3, Campbell Scientific). The data logger was programmed to record measurements at 5 second intervals while recording the average value every 20 minutes. A second weather station (WatchDog Model 2900ET, Spectrum Technologies) was located at the south end of the site and was used to monitor precipitation, relative humidity, wind speed and direction, and air temperature. Measurements were taken using built in measurement devices recording average readings at 15 minute intervals.

4.2.2 Monitoring Wells

Three series (A, B, C) of monitoring wells were installed throughout the course of the research program (Figure 4.1). The A series wells have been installed to a depth of 2.0 – 2.5 meters below ground surface, in the glaciolacustrine sediments. These wells were installed to target the unit most affected by the salt. Additionally, the A series wells were completed shallow enough to enable accurate water table monitoring. The B series wells were installed at approximately 4.5 meters below ground surface and were

completed in the B series sand unit while the C series wells were installed at approximately 6 meters below ground surface in the C series sand unit. The wells were used to monitor water levels and solute concentrations (salt and tracers) in each unit.

In 2009, twelve PVC 2.54 cm diameter A series monitoring wells (Figure 4.4) were installed manually using a soil core auger and screened over a 0.5 meter interval with a 1.0 meter sand pack. Bentonite chips were placed in the borehole annulus from the top of the sand pack up to ground surface to seal the remaining hole. In 2010, 14 new PVC 2.54 and 5.08 cm A, B and C monitoring wells were installed (Figure 4.4) using either 4.45, 10.21 or 15.24 cm solid stem auger. Wells were installed with a screen length of 0.5 meters and a sand pack of 1.0 meter. Similar to the 2009 wells, bentonite chips were placed in the borehole above the sand pack and hydrated to seal the borehole annulus. Well logs of 11 of the monitoring wells can be found in Appendix E.

Hydraulic head measurements in the monitoring wells were recorded using pressure transducers (Level Troll 500 & 700, Level Logger Gold). The transducers recorded the water levels in the wells to the nearest millimetre every 20 minutes, starting in 2009 and continuing until the end of the 2010 season. The Level Troll transducers were vented; therefore no barometric pressure correction was needed. Level Logger Gold transducers were not vented; therefore a separate transducer was used to record the barometric pressure, allowing for corrections to be made during data processing. Manual water level measurements were also taken using a water level tape in order to ensure the pressure transducer data quality.

4.2.3 Suction Lysimeter Installation

Ten stainless steel single chamber suction lysimeters (Soil Measurement Systems Model SW-071) were installed in two locations on the site at the beginning of the 2010 field season, in the centre of Plot A and directly above the north tile drain. The lysimeters were used to sample in situ pore water at five sampling depths. Five lysimeters were installed above the north tile drain with sampling ports located at depths of 0.15, 0.30, 0.56, 0.72 and 1.46 m below ground surface. The remaining five lysimeters were installed at the center of the plot with sample ports located at 0.15, 0.30, 0.73, 0.88 and 1.38 m below ground surface. Lysimeters were installed using a 10.16 cm diameter solid stem auger for bore holes deeper than 30 cm and by a 5.08 cm diameter hand auger for holes shallower than 30 cm. Holes that were drilled with the 10.16 cm auger were stopped at a depth 20 cm shallower than the final borehole depth. The remaining portion of the borehole was dug using the smaller diameter hand auger to improve the contact between the lysimeter and the surrounding soil. Boreholes deeper than 30 cm were augered vertically. The shallower 15 and 30 cm boreholes were augered at a 30° angle from the ground surface to minimize potential for short circuiting from the ground surface directly to the sampling port. Once each hole was drilled, a slurry of water and silica flour was mixed and poured into the hole and the lysimeter was inserted with the remaining slurry poured in to the hole until a tight seal was formed. Lysimeters were attached to a 2.54 cm PVC pipe that housed two plastic tubes, which extended to ground surface for sampler evacuation/pressurization and sample collection. Once the lysimeter was in place, a 10.16 cm PVC casing was inserted into the hole to a depth approximately

10 cm above the sampling port of the lysimeter (Figure 4.5). The PVC casing was capped and bentonite chips were used to seal the space between the borehole walls and casing in order to ensure no surface water infiltration occurred into the borehole.

4.3 Plot A Irrigation

Routine Plot A irrigation events occurred in summer and fall of 2009 and 2010. The purpose of the irrigation was to examine whether surface applied irrigation could enhance salt flushing. The plot was irrigated using 13.6 mm diameter polyethylene drip lines supplied by Rain Bird. Drip lines ran east – west and the irrigation lines were spaced 1.2 meters apart from each other covering Plot A (Figure 4.6). The irrigation lines were fed from a pump that was connected to a 10,000 L irrigation tank. Irrigation was applied manually using a gas pump for the early part of the 2009 field season. The remainder of the irrigation program used an automated system powered by solar panels. The system was programmed to apply a set volume of water beginning at a preset time. Irrigation frequency varied based on the amount of surface ponding observed and the amount precipitation received during the previous days. Irrigation events typically occurred every 1-2 days or at times longer depending on precipitation.

4.3.1 2009 Irrigation Season

Irrigation in 2009 began on July 9 and continued until October 1 with a cumulative irrigated water depth of 612 mm and 56 mm of precipitation making the cumulative water applied 668 mm (Appendix A). During irrigation of the plot it was noted water would preferentially pond in the northeast corner of the plot. In an attempt to

prevent this, irrigation volumes were applied to the plot in order to minimize the amount of ponding that occurred. Once any observable amount of ponded water began to form, irrigation was shut off. Irrigation would resume either the following day or the next scheduled irrigation session.

4.3.2 2010 Irrigation Season

Prior to the 2010 irrigation season, plot A was levelled by adding top soil to the surface in order to avoid surface ponding that was observed during the 2009 season. Irrigation of the plot began on May 2 and ended on October 5. A total of 385 mm of irrigation water was applied to the plot over 157 days. The total amount of precipitation that fell on the plot in the same time period was 293 mm making the cumulative amount of water applied to the plot 678 mm (Appendix A).

4.4 Tracer Application

In order to characterize the influence macroporosity had on salt flushing to subsurface tile drains, two conservative benzoic acid tracers were used in experiments in plot A. The first tracer experiment occurred in 2009 and was designed to study to how solutes move throughout the subsurface in soils containing macropores. Breakthrough of the tracer into the tile drains was monitored in addition to monitoring the spatial distribution of the tracer in the soil profile at the end of the 2009 and 2010 field seasons. The second tracer experiment occurred in 2010 and was designed to help determine the hydraulic connection between the different lithological units present on site and aid in

understanding the macropore influence above the tiles in the lower portion of the glaciolacustrine unit.

4.4.1 Benzoic Acid Tracer Descriptions

The conservative tracer used for the 2009 surface application was 2,6 – Difluorobenzoic acid (DFBA) (98% purity, Oakwood Products, West Columbia, South Carolina). Pentafluorobenzoic acid (PFBA) (99% purity, Oakwood Products, West Columbia, South Carolina) was used as a groundwater tracer for the second experiment that took place in 2010. Application of DFBA and PFBA as conservative tracers in hydrogeological investigations initially began in the early 1980's (Bowman, 1984a) and has become a popular alternative to traditional groundwater tracers (bromide, chloride). The two tracers are generally conservative in the subsurface (Bowman, 1984a), have low measureable detection limits (Bowman, 1984b), and can be detected without analytical interference using HPLC (Bowman and Gibbens, 1992; Kung et al., 2000; Dahan and Ronen, 2001).

4.4.2 Tracer Applications

4.4.2.1 DFBA Application

The surface application of DFBA occurred on August 18, 2009. The procedure for the mixing and application of DFBA was adapted from previous studies (Kung et al., 2000; Gish and Kung, 2007). The dry DFBA powder was added to fresh irrigation water and mixed in small batches. Once the DFBA was completely dissolved, potassium

hydroxide (KOH) was added in small increments until the pH reached near neutral levels (6.5 – 7.5). In total, 4.5 kg of DFBA was added to 5200 L (13 mm equivalent depth) of water in the irrigation tank, which resulted in a DFBA solution with a concentration of 866 mg/L. Once all batches were added to the irrigation tank, the DFBA solution was then applied to the surface of the experimental plot via irrigation drip lines over a period of 1.5 hours. Sample collection from the tile drains to monitor DFBA breakthrough began immediately after DFBA application and continued for the remainder of the 2009 and 2010 field seasons.

4.4.2.2 PFBA Injection

Two PFBA injections occurred on July 20 and July 21, 2010. The first injection occurred July 20 and was located directly above the north tile at a depth of 1.72 m below ground. Two separate batches of PFBA were mixed prior to injection, both consisting of 10 L of deionized water mixed with 43 g each of PFBA making a solution of 4.3 g/L. Small portions of KOH were added to each mixture until a pH of approximately 7 was reached. The borehole previously used to house the 1.46 m lysimeter was used for the injection hole. The lysimeter was removed and purged of water prior to the PFBA injection. A total of 20 L of 4.3 g/L PFBA solution was injected over a one hour period. The injection was separated into two batches due to the length of time required for the acid to completely dissolve into solution. Monitoring the breakthrough of the PFBA into the north tile drain began immediately after the first injection.

Monitoring well MW09-13A was used as the location of the second injection, which occurred on July 21. Similar to the previous injection, two batches consisting of 43 g of PFBA each were mixed with 10 L of deionized water and KOH and the solution was injected into MW09-13A over a 2 hour time period. A pneumatic pressure slug (a device used to pressurize a well, forcing water out of the well, into the formation) was required to inject the full solution into the well due to the relatively low permeability material surrounding the well screen. The breakthrough of the PFBA tracer in monitoring well MW09-13B was observed by sampling immediately after the first injection and continuing to sample at every 6 hours for the next 72 days.

4.5 Water Sampling

4.5.1 Tile Drain Effluent

Effluent samples from the tile drain were recovered via ISCO automated sampling devices. One sampler was dedicated to each of the north and south tile drains and was programmed to collect samples at regular time intervals between 3 and 8 hours. Samples were then transferred from the internal 1 L, plastic ISCO sampling bottles to clean 125 mL Nalgene sample bottles and placed into a cooler. ISCO sampling bottles were then rinsed with acetic acid followed by deionized water then returned back into the ISCO sampler. The ISCO was then reprogrammed to continue sampling. Samples were then placed in a cooler and transported back to the University of Calgary for analysis. Electrical conductivity and temperature of each sample was measured in the lab.

4.5.2 Monitoring Well Samples

Monitoring well samples were collected at the beginning of every month (June – October) over a two day period using a peristaltic pump (Geotech, Geopump) connected to 5 mm diameter polyethylene sample tubing. Monitoring wells completed at 2 m (A series), and 6 m (C series) were purged dry the day prior to sample collection to ensure the sample collected was representative of the surrounding formation waters. B series monitoring wells (completed at 4.5 m) were completed in a slightly higher hydraulic conductivity unit; therefore, low flow sampling techniques were used (Puls and Barcelona, 1996). For low flow sampling the well was pumped at a low rate (to limit drawdown) while electrical conductivity, pH and temperature were monitored in a flow-through cell. Once the indicator parameters stabilized the sample was collected and placed into a clean 125 mL Nalgene sample bottle. Field parameters for all samples (electrical conductivity, pH and temperature) were recorded at the time of sample collection. Samples were placed in a cooler, transported back to the lab and stored in a refrigerator until analyzed.

4.5.3 Suction Lysimeter Samples

Lysimeter samples were collected monthly, five times (June – October) during the 2010 season. Sample collection required a two day setup to prepare and sample the lysimeters. On the first day, the lysimeters were purged dry and a suction of approximately 50 – 60 kPa was applied to each lysimeter by hand pump. After approximately a 24 hour period, samples were collected by releasing the applied suction and pumping the sample into a plastic flow through cell using a hand pump. Similar to

the monitoring wells, field parameters (EC, pH and temperature) were recorded immediately after sample collection. Each sample was then placed in a clean, 125 mL Nalgene bottle and stored in a cooler until transported back to the university.

4.6 Soil Sampling

Soil samples were collected at the end of both the 2009 and 2010 field seasons to evaluate the concentrations and spatial distribution of salt and the DFBA tracer. Collection of soil samples was done by G & R Remediation with the use of a direct-push Geoprobe rig while under the supervision of University of Calgary personnel. Soil samples for the 2009 season were collected November 2. Samples were collected along a N-S transect (Figure 4.7). For the 2010 season, soil samples were collected October 20 through to October 22 and were collected following a grid pattern. Sample depths for both sampling programs ranged from 1.5 – 7 m. All core samples were placed in clear plastic tubing, sealed at both ends and transported back to the University of Calgary for analysis.

4.7 Laboratory Analysis

4.7.1 Water Samples

Prior to analysis, water samples were filtered using 0.45 µm syringe filters and placed in 2 mL glass vials (supplied by Agilent Technologies, Canada). Analysis of DFBA and PFBA was accomplished via ion exclusion chromatography. A 25 µL aliquot of each sample was injected onto a Transgenomic ICSep ORH-801 column (6.5 x 300 mm) then separated by isocratic elution using 0.01N H₂SO₄ mobile phase, with a flow rate of

0.8 mL/min and column temperature of 45°C. A UV detection wavelength of 210 nm was used for both DFBA and PFBA. Prior to sample analysis, a calibration was completed using three concentration standards (predetermined based on expected measured concentrations). To ensure accuracy, the concentration of the analyzed sample had to be within the range of the concentration standards (i.e. if concentration of sample = 5 mg/L, then concentration standards would be 1, 5 and 10 mg/L). If the measured concentration was out of the calibrated range (e.g., if concentration of sample = 20 mg/L and concentration standards were 1, 5 and 10 mg/L), the sample was retested using a new set of concentration standards. The analytical error using this method has been calculated to be 5%.

4.7.2 Soil Samples

Soil samples were brought back to the University of Calgary soil laboratory, removed from their tubes, trimmed, separated into 10 cm sections and air dried. Once air dried, samples were crushed using a mortar and pestle and sieved using a 2 mm mesh following the procedure of Bowman (1984b). A 15 g sample of the sieved material was placed in a 50 mL Greiner polypropylene centrifuge tube along with 30 mL of deionized water. Samples were vigorously agitated, placed on a shaker table for 20 minutes and left to sit overnight. The following day, samples were suction filtered through Whatman 0.45 micron filter paper and the resulting filtrate was then sent to the lab for DFBA and PFBA analysis using the same procedure described in Section 4.7.1.

The resultant concentrations recovered by the soil extractions were then used to calculate the DFBA mass still residing within the soil. This calculated mass helped determine the vertical and lateral DFBA distribution in and around the plot. DFBA mass calculations were done using the 2:1 extracted concentration analyzed using high precision liquid chromatography. The following equation outlines how the total DFBA mass was determined

$$M_t = C_{2:1} \times 2 \times \rho_b \times 1000 \times d \times a \quad (4.1)$$

where M_t (mg) is total mass calculated for the depth interval corresponding to the representative surface area (area each borehole represents on the surface), $C_{2:1}$ (mg/L) is the 2:1 concentration result determined from the lab analysis, ρ_b (g/cm³) is the dry bulk density of the soil sample, d (m) is the depth interval the soil sample represents and a (m²) is the surface area each specific borehole represents.

4.7.3 QA/QC

Throughout the duration of the field sampling programs, QA/QC samples were collected on a regular basis. Split samples were used to test for the precision of the tracer analysis, sample duplicates were used to test the sampling procedure/sampling bias, equipment/sample/trip blanks were used to ensure no sample cross contamination throughout the analysis and spiked samples were run through the lab to test the accuracy and precision of the lab equipment and sampling procedure. These procedures were performed for both the water and soil analysis. Results from the QA/QC sampling are found in Appendix D.

4.7.4 Spiked Experimental Samples

To be confident that the extraction procedure recovered 100% of the acid tracers, several spiked samples with known initial concentrations were analyzed. Soil was crushed and 50 g of sample was placed in 125 mL Nalgene bottles after which 40 mL of 100 mg/L DFBA solution was added. Once the samples were air dried, they were crushed again and processed following the same procedure as described above. Results showed that the tracer mass recovered from the extraction procedures was less than the initial applied tracer mass. Additional extractions were done using calcium chloride, methanol and sodium hexametaphosphate solution in place of deionized water to test whether they would improve the recovery of the DFBA soil extraction. Test results from the spiked samples showed that deionized water provided the highest recovery rate with an average of 67.5%. Results from this experiment can be found in Appendix B.

Results from the spike samples showed on average that 32.5% of the DFBA mass remains on the soil after the extraction procedure using deionized water (Appendix B). Using this information, a corrected tracer recovery was calculated by adding 32.5% to the lab analyzed 2:1 extract concentrations. The soil tracer extract values reported in the thesis represent the corrected values.

4.7.5 Soil Batch Tests

Soil batch tests were performed on four soils found at varying depths on the site. Although both PFBA and DFBA have generally been found to show limited retardation

or degradation (Bowman, 1984a; Bowman and Gibbens, 1992; Jaynes, 1994), the batch tests were performed to assess this for soils found on the experimental site. Soil samples were prepared in the same manner as the previous soil extractions (Sec. 4.7.2). Once the soils were crushed and sieved, 15 g of soil was placed in a 50 mL Greiner polypropylene centrifuge tube with 30 mL of DFBA or PFBA solution (ranging from 1 mg/L – 200 mg/L in concentration). The samples were vigorously agitated, placed on a shaker table for 20 minutes and let sit over night. The following day each sample was suction filtered through Whatman 0.45 micron filter paper and the resulting filtrate was analyzed. In total 102 samples were run and results can be found in Appendix B.

A second, small-scale experiment was created to test whether DFBA degraded over time as mentioned in Jaynes (1994). Two 50 g soil samples were ground and each placed in 1 L Nalgene bottles with 100 mL of 100 mg/L DFBA solution. The soil test solutions were placed in a refrigerator and samples were subsequently collected and analyzed for DFBA concentrations over a two month period. Water samples were taken from the prepared solutions without agitation, filtered through a 0.45 μm filter and analysed using the method discussed in Section 4.7.1. Samples were collected in duplicate roughly every 15 days. Results indicated no measurable degradation occurred over the experiment and are shown in Appendix B. This is consistent with previous studies that have reported little to no mass loss of and DFBA over time in field soils (Bowman, 1984; Bowman and Gibbens, 1992).

4.8 Hydraulic Parameters

4.8.1 Hydraulic Conductivity

4.8.1.1 Slug Testing

Single well hydraulic conductivity testing was performed on all monitoring wells during the 2010 field season. Testing was done by either adding a slug of known volume, or by purging the well dry and monitoring the rate at which the water well recovered to its static level. Calculation and analysis of results was done using the Kansas Geological Survey Model (Wilkinson 2011) and are summarized in Table 4.1.

4.8.1.2 Permeameter Testing

A series of constant headwater, rising tailwater permeameter tests (Test Method C) (ASTM International, 2007) were performed using intact soil cores collected from the site to determine matrix hydraulic conductivity measurements. Intact soil cores (50.8 mm diameter by 100 mm nominal length) were prepared and placed into a rigid walled permeameter similar to the procedure used in Kodikara et al. (2002). A total of four cores for each of the glaciolacustrine and glacial till units were used to determine the matrix hydraulic conductivity of the soils. Prior to running the experiment, cores were inspected to ensure no fractures or roots were observed in the core. A constant hydraulic head was placed on the upstream end of the soil core and periodic measurements of the hydraulic head values on the rising, downstream end of the soil core were taken.

4.8.1.3 Tension Infiltrometer

Tension infiltrometer measurements were performed to estimate the surface hydraulic conductivity of the soil at various times throughout the research project. A series of tension infiltrometer experiments were conducted in 2008 to test the surface hydraulic conductivities in and around Plot A. Results from the 2008 tests were combined with additional measurements taken during the 2010 season to determine a bulk hydraulic conductivity of the top soil on site. The five tests performed between August and September of the 2010 season combined with 5 tests used from the summer of the 2008 season provided a useful data set needed to calculate a representative top soil hydraulic conductivity value.

4.8.2 Soil Water Characteristics

Soil water retention curves were estimated by performing pressure plate extractions on 5 soil cores collected from the top soil unit, and 2 soil cores taken from the glaciolacustrine unit in 2010. Each core was first saturated and placed in the pressure extraction chamber. Water contents of these cores were measured while exposed to pressures at 10 different intervals ranging from 1 to 7500 mbar, and results were used to create soil water characteristic drying curves. The details of the test procedure can be found in Klute (1986). No wetting curves were evaluated for the soil cores. Measured soil water content data from the pressure plate extractions were input into the RETC computer (van Genuchten et al., 1991) program and fitted to the van Genuchten model parameters. The RETC analysis results are presented in Table 4.2 for each individual soil. These hydraulic parameters were then used as input parameters for the flow and

transport numerical model. Raw data from the pressure plate extraction tests and the RETC fits can be found in Appendix G.

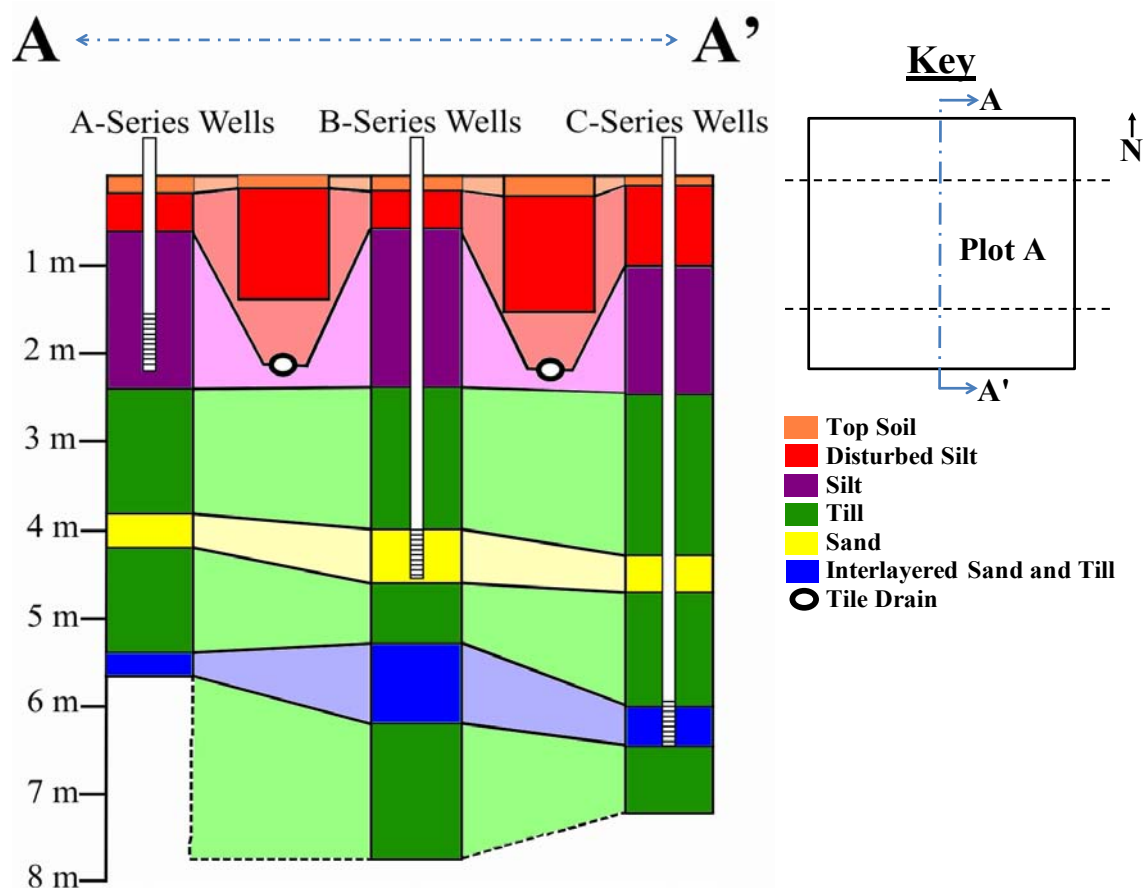


Figure 4.1. Cross-section of sediment lithology beneath plot A. Cross-section stretches approximately 20 meters from north to south as shown in the key. Includes monitoring well and tile drain depths. Modified from Wilkinson (2011).

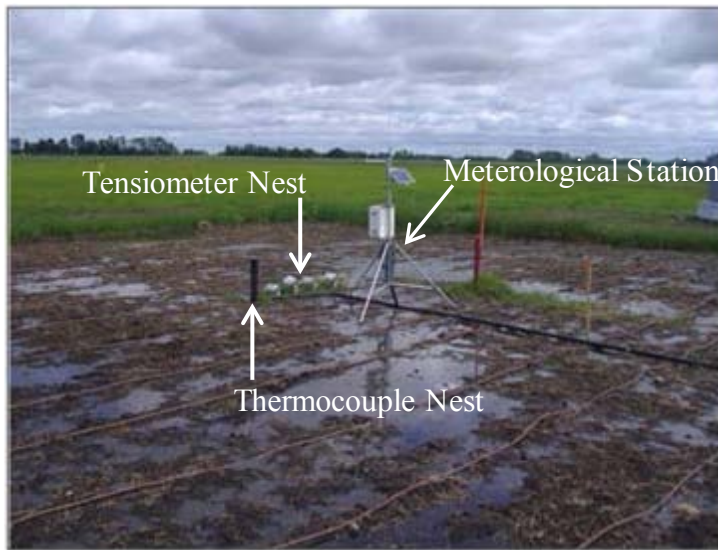


Figure 4.2. Photo of Plot A in 2009 during irrigation. The location of the meterological along with tensiometer and thermocouple nests are indicated. Photo was taken prior to monitoring well installation.

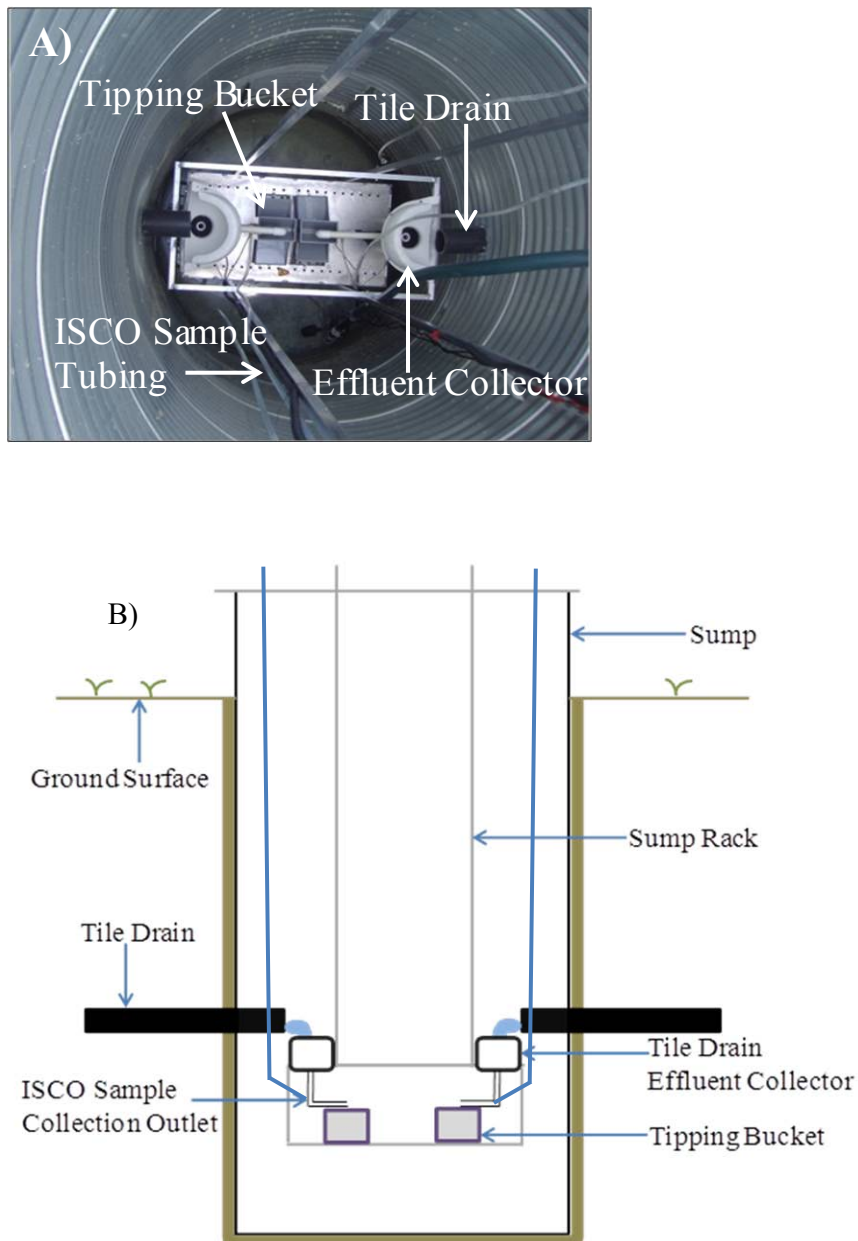


Figure 4.3. a) Photo of monitoring equipment located inside the sump. Photo includes both north and south tile drain outlets, tipping buckets and sample collection tubing. b) Cross-section of sump system with tile drain outlets, location of sample devices and location of ISCO sample collection outlets *Note, cross-section not to scale*.

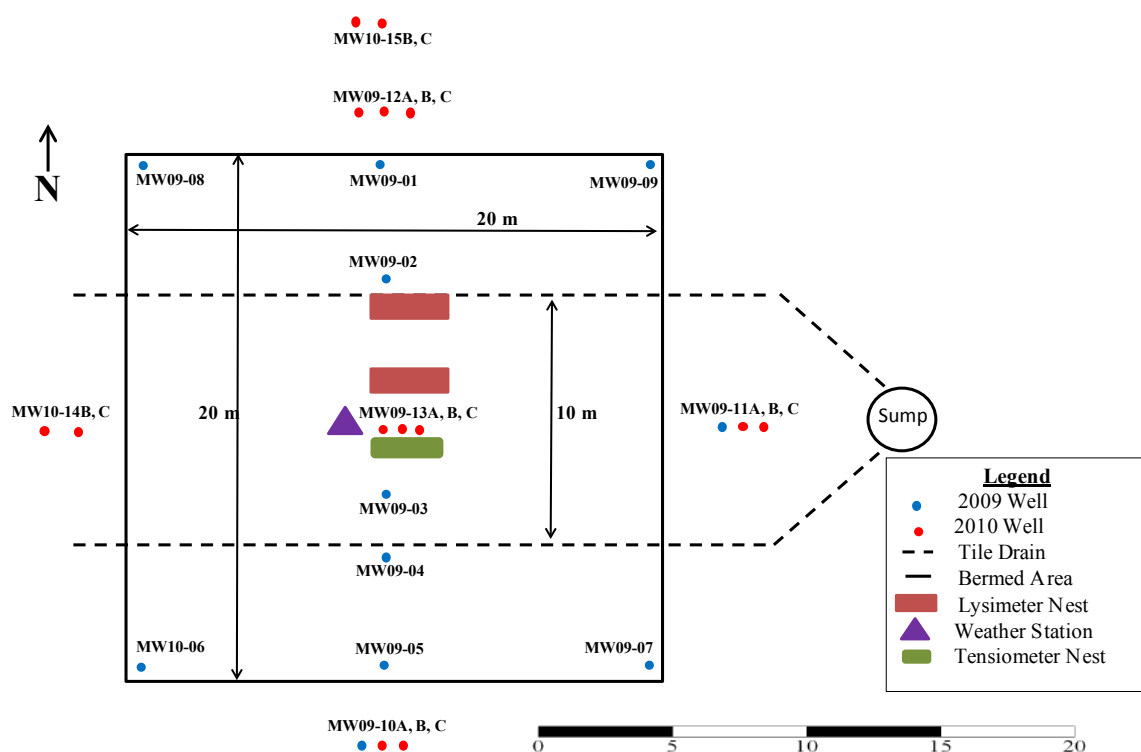


Figure 4.4. Illustrated plan view map of Plot A at the end of the 2010 season. Legend indicates if monitoring well was installed in 2009 or 2010.

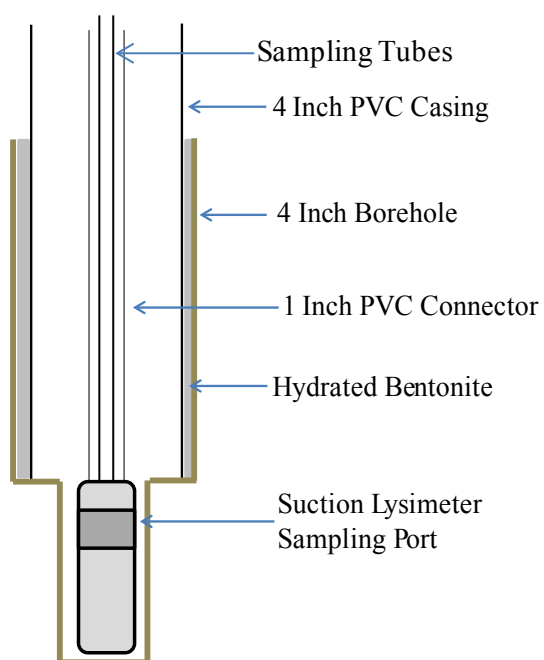


Figure 4.5. Schematic of the suction lysimeter installation at depths below 30 cm.
Note, not to scale.

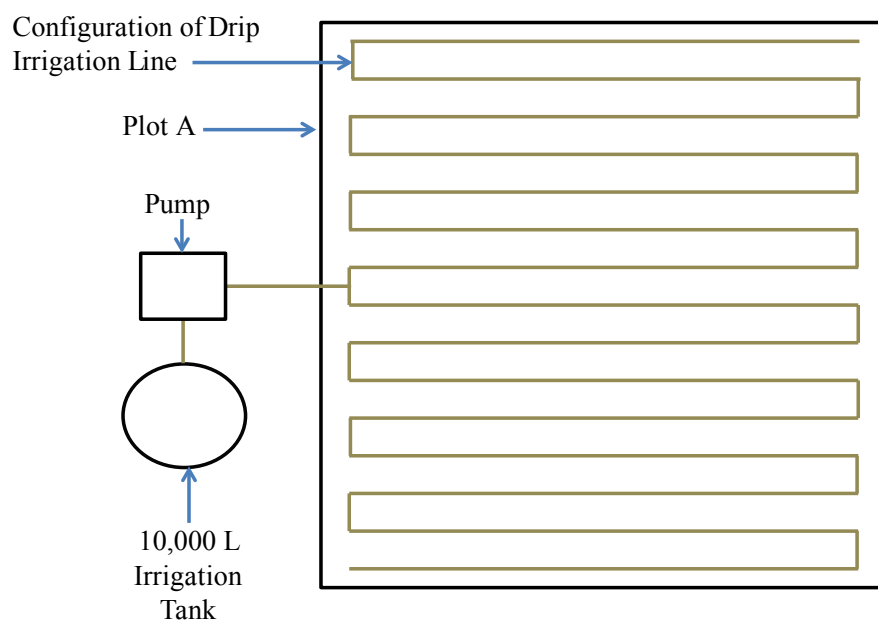


Figure 4.6. Schematic of drip irrigation line configuration with tie-ins to the pump and irrigation tank.

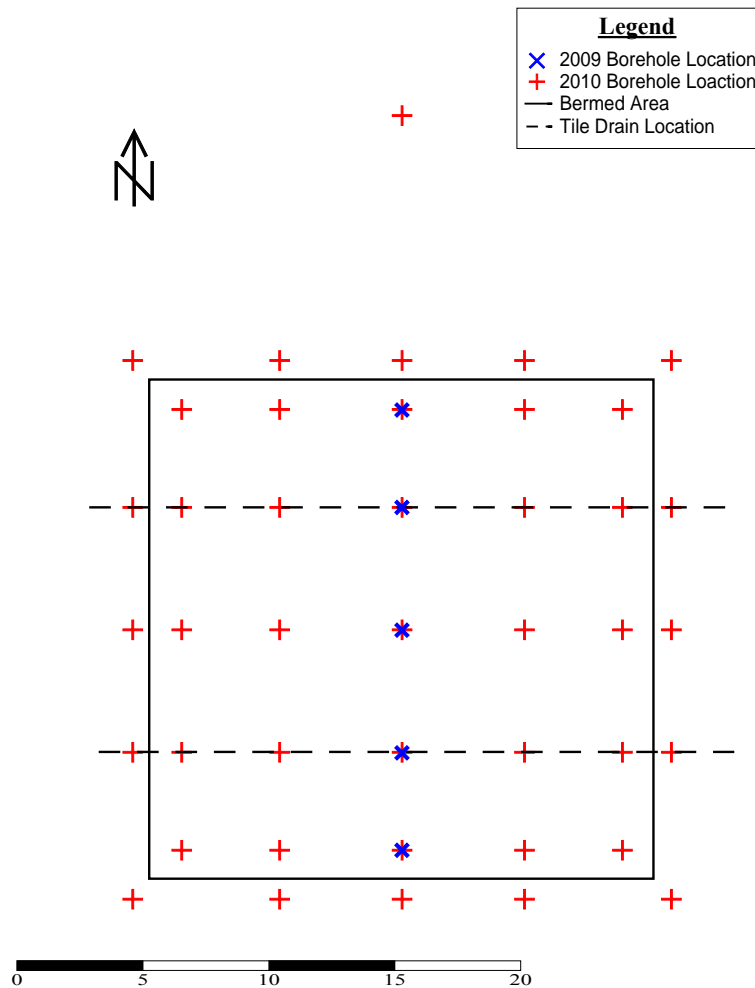


Figure 4.7. Plan view map of sampling locations for the 2009 and 2010 DFBA soil sampling locations.

Table 4.1. Geometric mean of hydraulic conductivities at three different depths calculated from single well rising head slug tests completed in 2010.

Series (Depth)	Number of Tests	Geometric Mean K (m/s)	Variance (m/s) ²
A – 2.0 meters	39	6.0E-08	9.30E-11
B – 4.0 meters	15	1.3E-06	1.00E-11
C – 6.0 meters	15	1.2E-07	1.40E-13

Table 4.2. Calculated van Genuchten (1980) parameters using the RETC software program.

Material	θ_r	θ_s	α (mm ⁻¹)	n	l
Top Soil	0	0.489	0.0016	1.091	0.5
Glaciolacustrine Silt	0	0.395	0.0045	1.083	0.5

CHAPTER FIVE: DEVELOPMENT OF THE NUMERICAL MODEL

The development of a numerical flow and transport model of the DFBA tracer experiment serves multiple purposes. Primarily, the model will help to better understand the processes influencing water flow and solute transport in a macroporous, tile-drained system. The flow and transport simulations will allow fluid and DFBA tracer mass balances to be calculated, which will help further define the role macropores play on the flow and transport in low permeability glacial soils. Model simulations will help quantify the flow dynamics of the preferential flow pathways as well as help conceptualize the effect the tile drains have on bulk (matrix and macropore) subsurface flow. The calibrated flow and transport model will then allow for future simulations pertaining to salt flushing, including estimation of remediation times and optimization of irrigation and drainage designs.

5.1 Conceptual Model

The conceptual model developed for the site involves several key hydrostratigraphic units. A cross-section below plot A (Figure 4.1) produced by Wilkinson (2011) illustrates these key units. In order for the tile drains to produce effluent the water table must be above the tile drains. Therefore, the assumption can be made that during periods of tile drain flow only the topsoil and glaciolacustrine unit will undergo variably saturated flow conditions, while saturated flow conditions will exist for all stratigraphic units below the tile drains. To accommodate variably saturated flow modeling, additional unsaturated flow parameters were needed for the glaciolacustrine

and top soil units. Additionally, a large zone of disturbed soil was created during the tile drain installation directly over the north and south tile drains beneath Plot A that likely altered the hydraulic parameters of the disturbed soil. This disturbed soil zone was not simulated in the numerical model for simplicity.

5.2 Preferential Flow Models

Both glaciolacustrine and glacial till layers are known to have a large preferential flow component due to fractures and root holes that have been observed during the analysis of core extracted from the plots and from the results of the tracer tests. Previous modeling of the Devon research site conducted by Smith (2008) suggested that preferential flow is an influential process and must be accounted for in future model simulations. Although macropores were not simulated in the modeling experiment conducted by Smith (2008), macropores were observed during analysis of soil cores. In order to properly simulate preferential flow and transport, it is important to capture the relevant processes in the numerical model. Macropores can either be represented numerically as discrete fractures or by the use of a dual-continuum formulation. As mentioned earlier in Section 3.5 representing discrete fractures numerically generally requires an extremely fine mesh, a large number of nodes and large amounts of data. The dual continuum method represents the matrix and macropores as two separate but overlapping domains. The matrix and macropore domains are connected with a coupling term that allows for fluid and solute transfer to occur between domains. The dual continuum method is generally more applicable to the field scale due to the smaller

number of nodes/elements required, and therefore will be used for simulating the Devon site.

5.3 Model Implementation

5.3.1 HYDRUS 2D

HYDRUS 2D is the dual permeability flow and transport modeling code that was selected for this study. The software program solves Richards' equation for flow and the advection-dispersion equation for transport under partially saturated conditions in both the matrix and macropore domains. The model contains two overlapping domains (matrix and macropore) each with individual van Genuchten soil hydraulic parameters (n , α , θ_r , θ_s and K_{sat}) to describe the unsaturated flow conditions and a coupling term to account for mass transfer between matrix and macropore domains (Simunek et al., 2003). As shown in Figure 3.1b, flow and transport occurs individually in each domain and exchange between the two domains is driven by hydraulic head differences for flow and a concentration gradient for solute transport. The model requires a large number of input parameters, many of which cannot be physically measured. Therefore, a lengthy literature review and calibration procedure was needed to choose physically reasonable variables. Future model development will require multiple geochemical simulations (cation exchange, variable hydraulic conductivity) to be completed and these can also be modeled using the HYDRUS 2D software.

5.3.2 Governing Equations

5.3.2.1 Fluid Flow

Equations 5.1 and 5.2 (Gardenas et al, 2006) are coupled Richards equations that describe unsaturated flow in the matrix (5.1) and macropore (5.2) domains. Variables containing the subscript f denote macropore domain parameters, while the subscript m denotes matrix domain.

$$\frac{\partial \theta_m(h_m)}{\partial t} = \frac{\partial}{\partial x_i} \left[K_m(h_m) \left\{ K_{ij}^A \frac{\partial h_m}{\partial x_j} + K_{iz}^A \right\} \right] - S_m(h_m) + \frac{\Gamma_w}{1 - \omega} \quad (5.1)$$

$$\frac{\partial \theta_f(h_f)}{\partial t} = \frac{\partial}{\partial x_i} \left[K_f(h_f) \left\{ K_{ij}^A \frac{\partial h_f}{\partial x_j} + K_{iz}^A \right\} \right] - S_f(h_f) - \frac{\Gamma_w}{\omega} \quad (5.2)$$

Within both equations, K_f and K_m represent the unsaturated hydraulic conductivity of the pore system (L/T), K_{ij}^A is the components of a dimensionless anisotropy tensor K^A that when medium is isotropic reduces to unit matrix (Simunek et al., 2006), θ is the water content (L^3/L^3), h is the pressure head (L), S is a sink term (used to simulate water root uptake by plants) (T^{-1}), Γ_w is the transfer rate of water between domains (T^{-1}) and ω is the ratio of the volume of macropores relative to the total soil system (unitless) (Gerke and van Genuchten, 1993a).

Mass exchange between the two domains is controlled by the Γ_w (mass exchange) parameter. Expanding this parameter yields Equation (5.3), which shows that exchange between each domain is proportional to the difference between the macropore and matrix heads multiplied by the fluid mass exchange coefficient, α_w ($L^{-1}T^{-1}$).

$$\Gamma_w = \alpha_w (h_f - h_m) \quad (5.3)$$

The mass exchange coefficient α_w (L/T), expanded yields Equation (5.4)

$$\alpha_w = \frac{\beta}{a^2} K_{as}(h) \gamma_w \quad (5.4)$$

Where a is the characteristic half width (L) of a matrix block, β is a dimensionless geometry coefficient, γ_w is a dimensionless scaling factor, and K_{as} is the effective hydraulic conductivity of the interface between matrix and macropore domains (L/T) that expanded yields Equation 5.5

$$K_{as}(h) = 0.5 [K_{as}(h_m) + K_{as}(h_f)] \quad (5.5)$$

where h_m is the matrix pressure head at a corresponding node and h_f is the macropore pressure head at the same node. A summary of the equations and physical description of each parameter are shown in Figure (5.1).

5.3.2.2 Solute Transport

Equations (5.6) and (5.7) (Gardenas et al, 2006) represent the modified advection-dispersion equations used to simulate solute transport in a variably saturated, dual permeability model. Coupling terms are used to simulate the transfer of solute mass between the matrix (subscript m) and macropore (subscript f) domains.

$$\frac{\partial \theta_m C_m}{\partial t} + \frac{\partial \rho S_m}{\partial t} = \frac{\partial}{\partial x_i} \left(\theta_m D_{ij}^m \frac{\partial C_m}{\partial x_i} \right) - \frac{\partial q_i^m C_m}{\partial x_i} - \phi_m - \frac{\Gamma_s}{1 - \omega} \quad (5.6)$$

$$\frac{\partial \theta_f C_f}{\partial t} + \frac{\partial \rho S_f}{\partial t} = \frac{\partial}{\partial x_i} \left(\theta_f D_{ij}^f \frac{\partial C_f}{\partial x_i} \right) - \frac{\partial q_i^f C_f}{\partial x_i} - \phi_f - \frac{\Gamma_s}{\omega} \quad (5.7)$$

where D is the dispersion tensor (L^2/T), q is the Darcian flux (L/T), ϕ is the reaction parameter (M/L^3T) which accounts for the increase or decrease of a solute due to reaction (degradation, volatilization etc.), Γ_s is the mass exchange parameter (T^{-1}) and ω is the volume of the fracture pore system as described above. The solute mass exchange parameter Γ_s expanded (Equation 5.8) is,

$$\Gamma_s = \alpha_s (1 - \omega_f) \theta_m (C_f - C_m) + \Gamma_w C^* \quad (5.8)$$

where α_s is a first-order solute mass transfer coefficient (L^{-1}), C is the concentration in the respective pore system, and C^* is equal to C_f for $\Gamma_w > 0$ and C_m for $\Gamma_w < 0$. This determines the advective solute transport direction (flowing from matrix into the macropores or vice versa). Expanding the α_s term yields Equation (5.9)

$$\alpha_s = \frac{\beta}{a^2} D_a \quad (5.9)$$

where D_a is the effective dispersion coefficient (L^2/T), and a and β are defined previously. A summary of the equations and physical description of each solute parameter are shown in Figure (5.2).

5.3.3 Equation Solutions

The HYDRUS software package uses the Galerkin finite element method with linear basis functions to develop a solution for the flow equation (Simunek et al., 2006). An implicit finite difference scheme is used for time discretization (Simunek et al., 2006). To solve the transport equation, the Crank-Nicholson scheme, which sets the temporal weighting coefficient to 0.5, was used for the time weighting method (Simunek et al., 2006). The Galerkin finite element method with artificial dispersion was used for the spatial weighting scheme. Artificial dispersion was used to decrease computational time by stabilizing the numerical solution and limiting the spatial oscillations within the results (Simunek et al., 2006).

5.4 Model Domain and Material Distribution

The model domain used in this study is a two-dimensional (2D) vertical cross section taken along a 30 m long north – south transect centered on plot A. The south edge ends at MW09-10 and the north edge extends to MW09-12 (Figure 5.3) with each lateral boundary situated at exterior tile drains. The domain runs perpendicular to the north and south tile drains, with the drains running in and out of the model domain. The vertical depth of the domain extends down to the base of the first sand unit at 4.5 m. The center of the tile drains are located at horizontal distances of $x = 10$ and 20 m and a depth of 2.15 m below ground surface. It is acknowledged that the implementation of a 2D model is not ideal for simulating a dynamic 3 dimensional (3D) system and may not fully capture the system flow behaviour (e.g., plot edge effects). However, due to

computational and data limitations, simplifying the model as a 2D cross-section was deemed necessary.

The depth of the lower boundary and the extent of the model domain were based on the monitoring well chemistry results from monitoring well samples. EC measurements from water samples collected from the C series monitoring wells were significantly lower than those from the A and B series wells. This indicated decreased hydraulic connection between the B (4 m depth) and C series (6 m depth) sand intervals below the plot. Therefore, the lower boundary for the model domain was selected as the base of the B series sand unit.

Surface ponding in Plot A regularly occurred during the irrigation events and larger precipitation events. Numerically, HYDRUS assumes that all water applied to the soil surface in excess of the infiltration amount for a given time step is removed from the system via overland flow (Simunek et al., 2006). In this study, plot A was carefully levelled and surrounded by compacted soil berms to restrict overland flow. Therefore, an artificial infiltration layer was constructed above the topsoil in HYDRUS to act as a temporary storage unit for all ponded water. The material properties of this infiltration layer were selected such that it permitted rapid infiltration of water (high K), and had sufficient storage volume (high θ_s) to retain any ponded water for eventual infiltration into the soil.

The finite-element grid was constructed using the CAD MESHGEN program (Simunek et al., 2006) included in HYDRUS. A default global element size of 250 mm was used with grid refinements around the tile drains, material boundaries and near the top boundary that contained the atmospheric condition (Table 5.1). Finer node spacing (125 mm) was used for the upper materials (surface infiltration layer, topsoil) to limit the amount of numerical instability that occurs at infiltration boundaries. Due to the high flow velocities that occur around the tile drains, additional grid refinement was needed to stabilize the model solution. The grid was automatically generated using the MESHGEN program, which adheres to the rule that the ratio of element sizes between neighbouring elements should not exceed more than 1.5 (Simunek et al., 2006). This ensures that grid spacing changes occur gradually with no sharp element size boundaries. The final model domain consisted of 10,627 nodes, 20,704 2-D elements and 1094 1-D elements.

The model domain was subdivided into five distinct horizontal layers; surface infiltration layer, top soil, glaciolacustrine unit, glacial till unit and the B series sand unit (Figure 5.4). Material properties assigned to each layer were assumed to be homogenous and isotropic. Material boundaries and depths were set by averaging the contact depths between each layer found in soil cores taken across Plot A (Table 5.2).

5.5 Model Parameters

5.5.1 Hydraulic Parameters

The van Genuchten soil hydraulic parameters for the matrix were determined by importing pressure plate extraction data into the curve-fitting program RETC (van

Genuchten et al, 1991). Output values were then averaged and single n_m , α_m , θ_{rm} and θ_{sm} values were used to describe each of the topsoil and glaciolacustrine units. The glaciolacustrine and glacial till matrix hydraulic conductivity values were determined using the results of the constant headwater, rising tailwater tests (Sec 4.8.1.2).

The van Genuchten (VG) parameters for the macropore domain cannot be physically measured in the same fashion as the matrix parameters. Therefore, VG macropore domain parameters n_f , α_f , θ_{rf} and θ_{sf} were estimated from literature values (Simunek et al., 2003; Gerke and Kohne, 2004; Gardenas et al., 2006) while K_{sf} was used as a calibration parameter to match tile drain responses for both high and tracer concentrations. Values acquired from the tension infiltrometer and slug tests were used as guidelines for bulk (combined matrix and macropore) hydraulic conductivity values. Due to the absence of macropores in the B series sand unit, VG matrix parameters were used for both the matrix and macropore domains. Although most macropores have been observed to be near vertical, which would imply a certain degree of anisotropy, the HYDRUS model currently does not include anisotropy in the macropore domain.

5.5.2 Dual-Domain Fluid Transfer Parameters

Transfer of fluid between the matrix and macropore domain is controlled by five specified parameters; β , γ_w , ω , a and K_{as} . The parameters β and γ_w were held constant during model development, while ω , a and K_{as} were modified to optimize the results during model calibration. Table 5.3 summarizes the value and source used for each

variable in the base case simulation. The β parameter is used to represent the size and shape of matrix blocks (Gerke and van Genuchten, 1996) with β values of 3 used for rectangular slabs, 8 for solid cylinders and a value of 15 used to represent spheres. The input parameter γ_w is described as a dimensionless scaling factor and a value of 0.4 was used based on the literature values found (Gerke and van Genuchten, 1993b). The parameter ω is used to represent the volume fraction of macropores found in a matrix block. The a parameter is used to describe the distance from the center of the matrix to the closest macropore and the K_{as} parameter is used to describe the hydraulic conductivity of the matrix-macropore interface.

5.5.3 Solute Transport and Reaction Parameters

The solute mass transfer coefficient is a key factor that determines how much and how quickly the solute is transferred (Brusseasu and Rao, 1990), therefore the solute mass transfer coefficient (α_s) was the primary calibration parameter used for the solute transport simulations. Calibrated values were compared with values reported in the literature, which ranged from 0.001 to 7.2 d⁻¹ (Gardenas et al., 2006; Gerke and Kohne, 2004; Lee et al., 2000).

The lateral and transverse dispersivities (α_L and α_T) were set to 100 mm and 10 mm, respectively, which are within the range of values found in literature with comparable scales of observation (Gelhar et al., 1992). The molecular diffusion coefficient for DFBA set at 7.6×10^{-10} m²/s based on values found in literature (Bowman and Gibbens, 1992). Sorption was not used in the base case simulation but was tested

during the sensitivity analysis. The distribution coefficient, K_d that was input into the model was calculated using the results from the laboratory batch tests (Appendix B). A linear isotherm was created that represented the maximum observed soil sorption. This isotherm was calculated using measured values of the highest sorption from all 4 soils at each concentration tested in all available lab data. A DFBA distribution coefficient of $0.0789 \text{ cm}^3/\text{g}$ was used in the simulation sensitivity analysis to examine the affect retardation had on solute transport in our system.

5.5 Boundary and Initial Conditions - Fluid Flow

5.5.1 Boundary Conditions

5.5.1.1 Hydraulic Head Boundary Conditions

The boundary conditions used for the model are shown in Figure 5.3. Fixed head boundary conditions (1st type) were used to simulate the measured pressure head values from monitoring wells on the lateral boundaries of the model domain. Hydraulic head readings from MW09-10A and MW09-12A were used for the specified head boundary condition in the glaciolacustrine unit on the south and north edges of the domain, respectively (Figure 5.3). Likewise, the heads from wells MW10-11B and MW10-14B were used as boundary conditions for the B series sand unit in the south and north edges of the domain, respectively (Figure 5.3). Through development of the model complications arose due to the lack of water exiting the model from the lower sand boundaries. A large portion of this problem stems from attempting to model a 3D problem in 2D. The lower boundary condition heads were only allowing small amounts of lateral flow to pass through the model in the X direction, while realistically a large

amount of radial flow occurs both in the X and Y directions (in and out of the model domain). Therefore it was decided to use hydraulic heads taken from only MW10-14B for both sand boundary conditions, allowing for symmetrical radial flow to occur, thereby increasing the amount of water removed from the sand unit.

Theoretically, flow symmetries (mid-point between tile drains) should allow for no flow boundaries to be implemented between each tile drain because of groundwater flow divides. But a system failure occurring in mid-July 2010 caused the tile drain system across the entire site to stop draining water (while Plot A drains continued to function). This resulted in the water table surrounding Plot A to rise and there was a lateral influx of water to the plot during this period. Consequently, the rise in the site-wide water table during this time period was simulated using the specified head boundaries in the glaciolacustrine units rather than no flow boundaries to account for the lateral inflows.

A no flow boundary condition was used along the lateral boundary of the glacial till unit and at the base of the B series sand unit (Figure 5.3). A limited hydraulic connection is assumed between the B series sand unit and the C series sand unit, allowing for a no flow boundary condition at the base of the B series unit. Additionally, it was assumed there was a negligible amount of lateral flow through the till unit (relative to the sand units above and below the till) therefore a no flow boundary was used for the lateral boundaries of the glacial till unit.

5.5.1.2 Atmospheric Boundary Conditions

The irrigation plot area on the top boundary was simulated using an atmospheric boundary condition (2nd – Type Neumann). The HYDRUS 2D program simulates atmospheric boundary conditions by requiring the user to specify a precipitation rate (L/T) and an evaporation rate (L/T). Evaporation is subtracted directly from the precipitation in the numerical solution, which results in a fluid mass flux that is applied directly to the atmospheric boundary (Simunek et al, 2006). Transpiration was calculated separately from evaporation using the FAO Penman-Monteith dual-crop coefficient (Allen et al., 1998) and was simulated numerically using the Feddes root water uptake model implemented within HYDRUS (Simunek et al, 2006). Maximum potential transpiration rates were calculated on a daily basis in units of mm/day. A root zone distribution profile was constructed with a maximum rooting depth of 1.0 m and a rooting depth intensity set to the upper top soil boundary. The root water uptake is simulated as a sink term in the solution. Numerically, two conditions must be met with regard to the root water uptake in order to obtain a numerical solution. First, the absolute value of the flux must not exceed the infiltration or evaporation rate. Second, the pressure head at the soil surface must remain between the minimum pressure head value and zero (Simunek et al, 2006).

A 2nd type, specified flux boundary was implemented on top of the remaining model domain outside of plot A (i.e., on both sides of the atmospheric boundary condition as shown in Figure 5.3). This boundary was meant to simulate precipitation occurring outside of the irrigation plot. Daily rain gauge measurements taken from the

nearby weather station were used to calculate a daily specified flux. Calculated evaporation rates were subtracted directly from the measured precipitation similar to the atmospheric boundary condition. Sign convention dictates water being added to the system is negative. Therefore, when precipitation > evaporation, all fluxes would carry a negative (-) sign. When precipitation < evaporation, all fluxes carry a positive (+) sign indicating a mass flux out of the system or, evaporation from the soils. Transpiration was also implemented by the same procedure used in the atmospheric flux boundary.

5.5.1.3 Internal (Seepage Face) Boundary Conditions

To simulate the north and south tile drains; an internal circular opening was constructed inside the model domain with the diameter equal to the tile drain diameter (200 mm). The nodes surrounding this internal boundary were fixed as a seepage face boundary condition that allows water to pass through and be removed from the system (Figure 5.3). The seepage face boundary is numerically represented by assigning a 1st type condition at each specified node to a value of h (pressure head) = 0 (atmospheric). When nodes surrounding the seepage face boundary are saturated ($h > 0$), water will flow across the internal boundary and be removed from the domain. When nodes surrounding the seepage face boundary are unsaturated ($h < 0$), the seepage face boundary will turn off, and no flow conditions will occur between seepage face nodes and surrounding nodes, thereby preventing flow from the seepage face back into the domain (Simunek et al, 2006).

5.5.2 Initial Condition - Pressure Head

The initial pressure head distribution (Figure 5.5) was calibrated by matching the simulated tile drain flux to the initial observed tile drain flux during the first 20 days of the 2010 field season. A hydrostatic pressure head distribution was first set by fixing the model's top and bottom pressure head values and applying a linear distribution between the two values. Specified precipitation fluxes were then applied to the top boundary over a 20 day period until the simulated tile drain fluxes matched the initial 2010 observed tile drain fluxes. Once the observed and simulated tile drain fluxes were equal, the domain pressure head distribution was imported into a new simulation as the initial pressure head distribution.

5.6 Boundary and Initial Conditions - Solute Transport

DFBA was applied on the surface of plot A in 2009 and subsequently infiltrated in the soil profile. In order to simulate the 2010 field season, the initial in-situ DFBA distribution was required. The DFBA concentration profiles from the soil core extractions at the end of the 2009 field season (Figure 6.3) were used to represent the initial solute distribution in the model (Figure 5.6). The lateral extent of the modeled DFBA distribution was limited to directly beneath the irrigation plot with no spreading beyond the vertical boundary of the irrigation plot. In the absence of measured data to indicate the lateral extent of the DFBA tracer, the bulk of the tracer mass was assumed to be retained within the plot due to the limited amount of lateral flow that occurs in the vadose zone. Requirements within the HYDRUS software made all non zero fluid flux boundary conditions to be specified as a 3rd – Type (Cauchy) boundary condition (Figure

5.7) for the solute transport. The Cauchy boundary condition is a mass conservative boundary condition (Simunek et al., 2006) used for simulating mass flux in and out of the domain (i.e. mass leaving through tile drains or laterally out of domain). No DFBA mass entered the domain during 2010 because all water infiltrating (irrigation and precipitation) was tracer free. Thus, only mass exiting the system through the tile drains and specified head conditions was considered.

5.7 Observation Nodes and Mesh Lines

Observation nodes were inserted into the domain to simulate monitoring wells MW09-01, MW09-03, MW09-05, MW09-13A, MW09-13B and the south lysimeter sampling units at 0.15, 0.30, 0.60, 0.90 and 1.50 meters. Each node recorded the matrix and macropore pressure heads as well as the matrix and macropore DFBA concentrations at each time step. Observation node data was compared against the measured monitoring well hydraulic heads and lysimeter concentrations during model calibration.

Mesh lines are a series of connected elements in the model domain used to calculate fluid and solute fluxes passing through the constructed line. They were used to calculate the instantaneous and cumulative fluid and solute mass fluxes in both the matrix and macropore domains throughout the simulation period. Mesh lines were inserted at both tile drains and each specified head boundary condition to calculate the fluid and solute fluxes leaving or entering the domain.

5.8 Mass Balance Error

A mass balance error was calculated by comparing the total change in volume of the system throughout the simulation time against the measured cumulative fluxes (evaporation, irrigation, root uptake, tile drains etc.). A relative water balance error of 0.20% was calculated for the 138 day simulation period. The same procedure was used to determine the solute mass balance error by subtracting the initial and final solute volumes present in the domain, and comparing them against cumulative solute volumes measured exiting the system through the mesh lines. A relative error of 0.24% was calculated, indicating the model accurately accounted for all mass within the system throughout the simulation period.

FLUID FLOW

DOMAIN - MATRIX	DOMAIN - MACROPORE
Modified Richards' Eqn.	Modified Richards' Eqn.
$\frac{\partial \theta_m(h_m)}{\partial t} = \frac{\partial}{\partial x_i} \left[K_m(h_m) \left(K_{ij}^A \frac{\partial h_m}{\partial x_j} + K_{iz}^A \right) \right] - S_m(h_m) - \frac{\Gamma_w}{1-\omega}$	$\frac{\partial \theta_f(h_f)}{\partial t} = \frac{\partial}{\partial x_i} \left[K_f(h_f) \left(K_{ij}^A \frac{\partial h_f}{\partial x_j} + K_{iz}^A \right) \right] - S_f(h_f) - \frac{\Gamma_w}{\omega}$
MASS TRANSFER BETWEEN DOMAINS $\Gamma_w = \alpha_w (h_f - h_m) \quad \alpha_w = \frac{\beta}{a^2} K_a(h) \gamma_w \quad K_{as}(h) = 0.5 [K_a(h_m) + K_a(h_f)]$ <p>Where: ω = volume of fractures to total volume (macropore porosity) β = geometry coefficient of matrix (3 = rectangular slabs, 8 = cylinders, 15 = spheres) a = Half width of matrix block (distance from center of matrix to matrix/macropore interface) γ_w = dimensionless scaling factor K_{as} = effective hydraulic conductivity of matrix/fracture domain interface</p>	

Figure 5.1. Summary of fluid flow parameters. Flow in both the matrix and macropore domain using the Richards' equation and mass transfer between each domain and a short description of the variables used in the calculations.

SOLUTE TRANSPORT

DOMAIN - MATRIX	DOMAIN - MACROPORE
Advection-Dispersion Eqn.	Advection-Dispersion Eqn.
$\frac{\partial \theta_m C_m}{\partial t} + \frac{\partial \rho S_m}{\partial t} = \frac{\partial}{\partial x_i} \left(\theta_m D_{ij}^m \frac{\partial C_m}{\partial x_j} \right) - \frac{\partial q_i^m C_m}{\partial x_i} - \phi_m - \frac{\Gamma_s}{1-\omega}$	$\frac{\partial \theta_f C_f}{\partial t} + \frac{\partial \rho S_f}{\partial t} = \frac{\partial}{\partial x_i} \left(\theta_f D_{ij}^f \frac{\partial C_f}{\partial x_j} \right) - \frac{\partial q_i^f C_f}{\partial x_i} - \phi_f - \frac{\Gamma_s}{\omega}$
MASS TRANSFER BETWEEN DOMAINS	
$\Gamma_s = \alpha_s (1 - \omega_f) \theta_m (C_f - C_m) + \Gamma_w C^* \quad \alpha_s = \frac{\beta}{a^2} D_a$	
<p>Where: ω = volume of fractures to total volume (macropore porosity) β = geometry coefficient of matrix (3 = rectangular slabs, 8 = cylinders, 15 = spheres) α_s = solute mass transfer rate that determines how quickly solute passes between the matrix and macropore domain (L^{-1}) a = Half width of matrix block (distance from center of matrix to matrix/macropore interface)</p>	

Figure 5.2. Summary of solute transport parameters. Solute transport in both the matrix and macropore domain using the advection-dispersion equation and mass transfer between each domain and a short description of the variables used in the calculations.

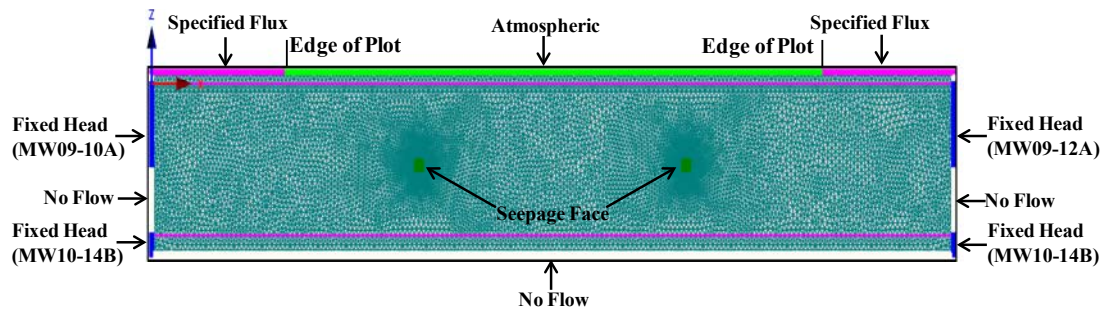


Figure 5.3. Model domain and flow boundary conditions used for all simulations. Location of cross-section shown in key in Figure 5.1.

Table 5.1. Summary of node spacing refinements used while constructing the unstructured finite element grid.

Boundary	F-E Node Spacing (mm)
Top of Domain	125
Gravel - Topsoil	150
Topsoil - Glaciolacustrine	175
Glacial Till - Sand	175
Sand - Bottom of Boundary	150
Tile Drains	21

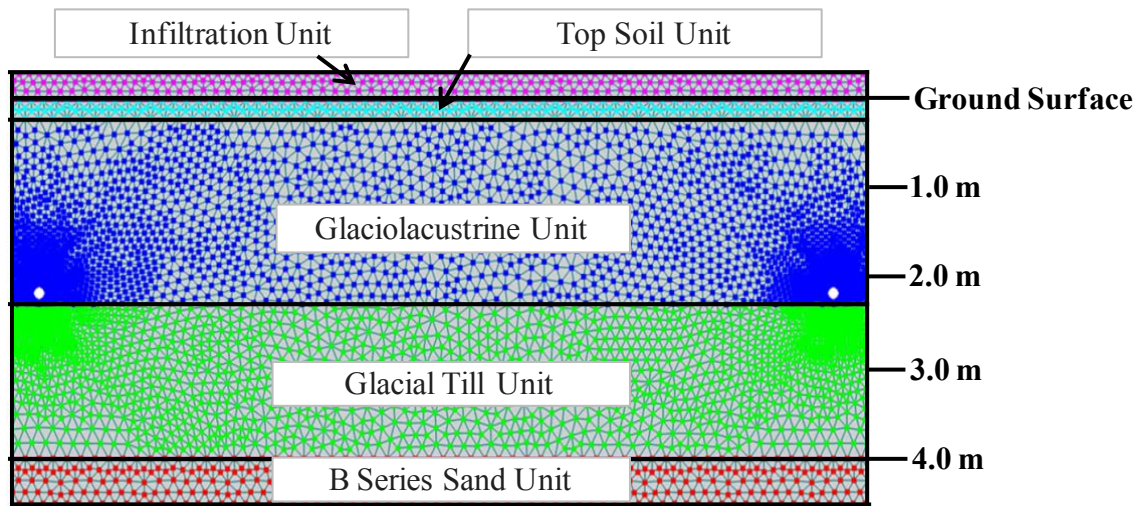


Figure 5.4. Material distribution used in simulations.

Table 5.2. Summary of depth material depth intervals used in numerical simulations

Material	Depth Interval (mm below ground)
Surface Infiltration Layer	+300 - 0
Topsoil	0 – 200
Glaciolacustrine	200 - 2400
Glacial Till	2400 - 4000
B Series Fine – Medium Sand	4000 - 4500

Table 5.3. Summary of dual-domain fluid mass transfer parameters used in the base case simulation.

Fluid Transfer Parameter	Value	Range of Literature Values	Calibration Parameter	Literature Sources
β	3	3-14	No	Gerke and van Genuchten, 1993a; Simunek et al., 2003; Gerke and Kohne, 2004
γ	0.4	0.4	No	Gerke and van Genuchten, 1993b; Simunek et al., 2003
ω	0.0025	0.03-0.05	Yes	Simunek et al., 2003; Gerke and Kohne, 2004; Gardenas et al., 2006
K_{as} (mm/day)	0.01	0.01-.25	Yes	Simunek et al., 2003; Gerke and Kohne, 2004; Gardenas et al., 2006
a (mm)	5-25	10	Yes	Simunek et al., 2003; Gerke and Kohne, 2004

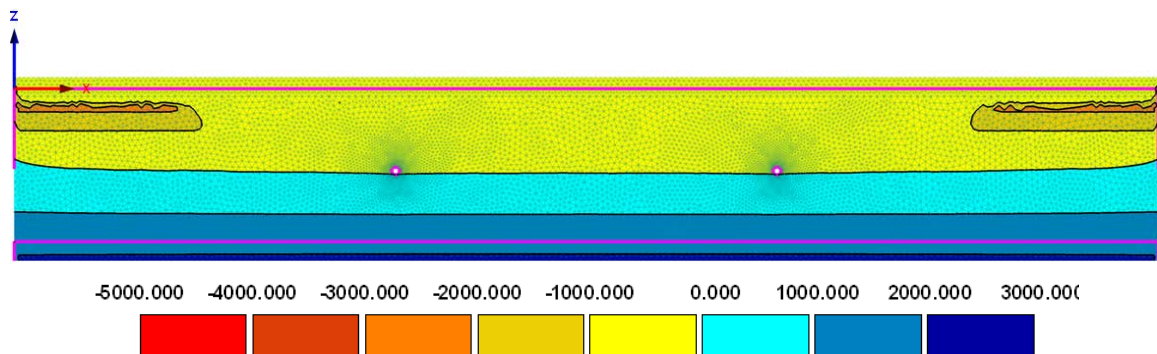


Figure 5.5. Initial pressure head distribution for the 138 day simulation period. Blue colours indicate pressure head values greater than 0 (saturated). Yellow – red colours indicate pressure head values less than 0 (unsaturated).

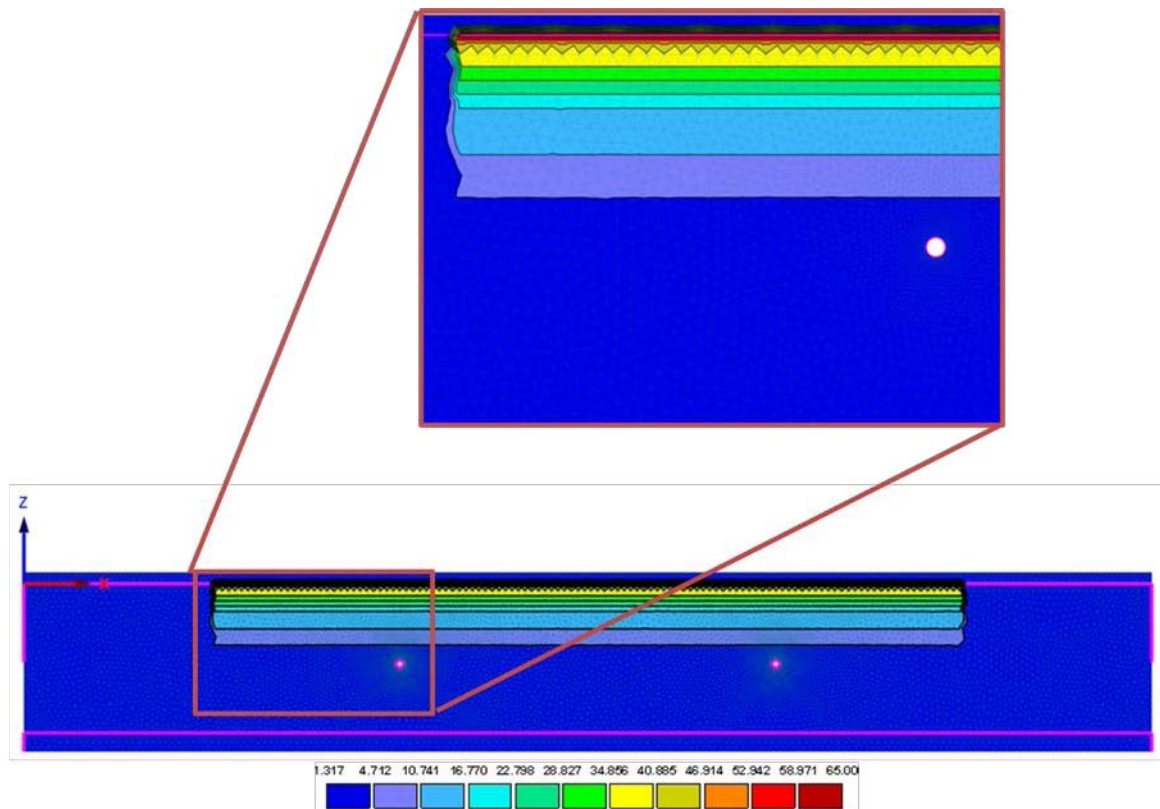


Figure 5.6. Initial DFBA concentration distribution. Concentrations were set using results from the calculated pore water concentration extracted from the 2009 soil cores (Section 6.1.3.4).

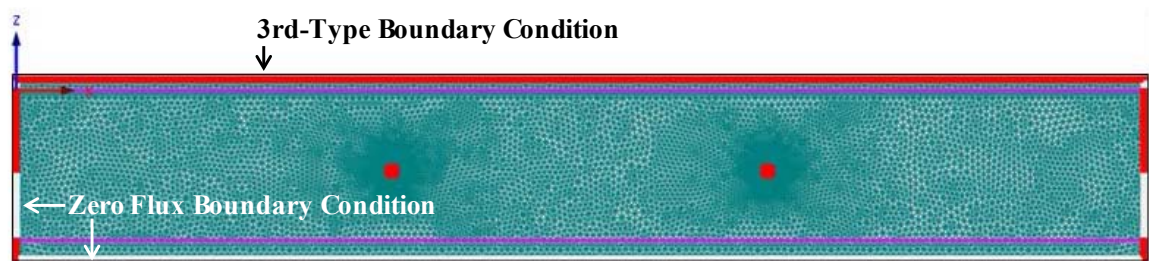


Figure 5.7. Solute transport boundary condition used for all simulations.

CHAPTER 6: RESULTS AND DISCUSSION

6.1 2009 Field Results

6.1.1 Soil Properties

Soil properties of the four main soil materials are shown in Table 6.1. As described by the soil texture classes triangle (Haynes, 2005), the glaciolacustrine is classified as a silt, the glacial till as a loam and B series sand as a sand. The dry bulk density measurements show an increasing density with depth, indicating compaction is occurring with increasing depth. The cation exchange capacity (CEC) values calculated were compared to values found in Appelo and Postma (2005). The CEC of the glaciolacustrine unit fit within the range of a glauconite, illite and chlorite while the CEC of the glacial till fit within the range of a glauconite, kaolinite and chlorite.

6.1.2 Tile Drain Flow Response

Irrigation of plot A began on July 9 (day 190) and continued until October 1 (day 274) (Figure 6.1). Tile flow began in the south tile July 20 (day 201) while the north tile flow began July 27 (day 208) (Figure 6.1). The lag time from when irrigation was initiated to when tile effluent was produced was a result of the antecedent soil moisture conditions. Regionally the study site is centered in an arid region that was suffering from a severe soil moisture deficit (Alberta Agriculture, 2009), so prior to tile drain flow, soil had to become saturated and the water table needed to rise to the tile drain elevation. The lag time between north and south initial flow events was unexpected because theoretically north and south drains should behave in a similar fashion if situated in a homogenous material. This indicates that there are factors (soil heterogeneities) that act

as controls on the tile drain's ability to initiate and terminate flow. Once irrigation ended on October 1, the south tile flowed for 7 additional days while the north continued to flow for 16 days. The 2009 field season cumulative discharge from the south tile was 8.75 m^3 or 43.75 mm (half the area of plot A) while the north discharge was 5.46 m^3 or 27.3 mm. Cumulatively, the north and south drains captured the equivalent of 5.9% of the applied irrigation water volume.

The variability in tile drain flow rates and response to precipitation events illustrates that although both drains were installed at the same depth and only 10 m apart, soil heterogeneity had a large impact on drain flow. Although both the north and south tiles responded quickly to irrigation/precipitation events only after the soils became saturated and the water table was at the tile drain elevation, the peak flow rates of each tile were variable throughout the season. The south tile drain flow rate was consistently greater in the first half of 2009 (average south rate = 14 L/hr, average north rate = 5 L/hr), while the north tile drain reached a higher flow rate in the latter portion of 2009 (south rate = 8 L/hr, north rate = 12 L/hr) (Figure 6.1). The south drain discharged 3.29 m^3 more effluent than the north drain, even though the north drain flowed 2 days longer than the south drain. A analysis of core taken from the northern end of the experimental plot uncovered a 30 cm sand unit at approximately 1.5 m below ground surface that extended laterally north. This sand unit could act as a drain, transporting fresh irrigated water past the north tile drain and beyond the limits of the plot, thereby reducing the volume of water captured by the north tile.

A rough calculation to determine the volume of water needed to overcome the initial soil moisture deficit and raise the water table to the level of the tile drains suggested that theoretically, 18 m^3 of water was needed. In total, 63.6 m^3 of irrigation water was applied before the south drain began to flow. It is postulated then that the additional applied irrigation (45.6 m^3) could have been lost to evapotranspiration, lateral losses beyond the plot or into the deeper B and C sand units.

6.1.3 2009 DFBA Results

6.1.3.1 Tile Drain Effluent

The DFBA tracer was applied on August 18, 2009 (day 230) and initial detection of DFBA in the tile drain effluent was observed 46.75 hours later in both north and south tile drains (Figure 6.1). Tracer concentrations in both north and south tiles followed a similar upward trend with fluctuations that are thought to be a function of irrigation/precipitation events. The infiltration depth of the tracer during the 2009 season was not expected to be greater than 1 m because application of the tracer occurred relatively late in the season and only 298 mm of water was able to be applied post DFBA application. Assuming uniform plug or piston-type flow, a quick calculation suggests the center of DFBA mass would migrate to depths of up to 0.75 meters below surface (298 mm of water applied divided by an average measured porosity of 0.40 equals a depth of 0.745 meters). Peak DFBA concentrations of the north and south tiles were 5.23 mg/L ($C/C_0 = 6.04 \times 10^{-3}$) and 2.36 mg/L ($C/C_0 = 2.72 \times 10^{-3}$), respectively. Overall, 0.45% of the total tracer mass was captured in the tile drains during the 2009 irrigation season.

Due to the quick breakthrough of the tracers (46.75 hours) in the low permeability soils, it is evident that the primary mode of solute transport to the tile drains is through the macroporosity present on site. Furthermore, the low DFBA concentrations measured in the effluent combined with the low mass captured in the tile drains at the end of 2009 (0.45%) suggests the low permeability soils are retaining most of the DFBA. The quick breakthrough times measured in the tile drains support the findings of similar studies conducted by Richard and Steenhuis (1988), Kung et al., (2000) and Zehe and Fluhler (2001). All studies mentioned measured breakthrough times to tile drains between 0.3 – 4.0 hours after tracer application and concluded the quick breakthrough times were likely caused by macropores acting as preferential flow pathways. The lower DFBA breakthrough time measured at the Devon research site could be caused by a lower matrix hydraulic conductivity or a smaller macropore density.

6.1.3.2 Monitoring Wells

Two sampling events occurred during the 2009 field season, one on August 28 (day 240) and the second on October 7 (day 280). All samples were taken from the A series wells completed at a depth of roughly 2 m because no B or C series wells were yet installed. The DFBA detections in the monitoring wells (Figure 6.2) were located primarily along the northern edge of the plot. Monitoring wells MW09-01, MW09-08, MW09-12A and MW09-09 all showed DFBA detections for both the August and October sampling events, while wells located in the southern portion of the plot (MW09-06, MW09-07) showed no DFBA detections. Monitoring well MW09-05 in the south-central region of the plot had a single detection during the August sampling event (0.17 mg/L).

but no DFBA was detected during the October sampling event. Concentrations of DFBA detected in the monitoring well samples averaged 0.74 mg/L while the maximum and minimum concentrations were 4.09 ($C/C_0 = 4.72 \times 10^{-3}$) and 0.11 mg/L ($C/C_0 = 1.27 \times 10^{-4}$) (excluding non-detects). The monitoring well detections support the observed DFBA breakthrough in the tile drains. The quick breakthrough of the DFBA to the monitoring wells indicates that macropores were allowing for rapid transport at depth, but the low concentrations suggest that the low permeability matrix is retaining the bulk of the DFBA mass in the upper portion of the soil profile.

There are a number of possible explanations for the spatial variability in DFBA concentrations measured in the monitoring wells. One possible reason is the non-uniform application of irrigation water as indicated by the consistent water ponding in the northern half of plot A. This could have caused a larger amount of DFBA to be applied in the northern half of the plot relative to the south, increasing the likelihood of monitoring well detections of DFBA in northern monitoring wells. Additionally, the ponding observed in the northern half of the plot could initiate an increased number of preferential flow pathways. Increasing the number of preferential flow pathways by increasing the irrigation intensity was observed by Gjettermann et al., (1997) and could explain the increased DFBA detections in the monitoring wells located in the northern half of Plot A.

Another interesting observation is DFBA detection measured outside of the plot in MW09-12A. The remaining monitoring wells located outside of the plot showed no

detections throughout 2009 so it was thought that little lateral transport was occurring. The MW09-12A DFBA detections could be explained by the presence of a higher hydraulic conductivity 30 cm thick sand lens located approximately 1.5 meters below ground surface below MW09-01. If this sand lens were to extend laterally north, it would allow for preferential flow of DFBA to migrate in the direction of MW09-12A.

6.1.3.3 Tracer Degradation and Sorption Tests

Batch tests were performed to test the potential for sorption of DFBA and PFBA on soils from four depths at the site. Appendix B summarizes the results from the batch tests performed on each tracer. In general, the tracers were found to be conservative at both low (<15mg/L) and high (>15mg/L) concentrations. A linear isotherm was created for both PFBA and DFBA using the results from all four soil depths and the calculated distribution coefficients for each tracer represent the upper limit for sorption. An upper limit for the distribution coefficient of $0.0789 \text{ cm}^3/\text{g}$ and $0.0678 \text{ cm}^3/\text{g}$ was calculated for DFBA and PFBA, respectively. Assuming a bulk density of 1.40 g/cm^3 and a porosity of 0.35, this equates to a retardation factor of 1.3 for both DFBA and PFBA. To determine if any measureable DFBA degradation could be observed, a laboratory experiment was designed to test if DFBA degraded over time. As previously discussed in Section 4.7.5, no measurable DFBA mass loss was observed over the test period. Results are shown in Appendix B

6.1.3.4 Soil Extractions

Soil cores were taken at the end of the 2009 field season and analyzed at various depth intervals for DFBA. Results of the soil extractions for DFBA are shown in Figure 6.3. Cores were taken from a North-South transect through the center of the plot (Figure 4.8) and core depths ranged from 1.7 m (over tile) to 5.6 m. Calculated DFBA pore water extract concentrations in the top 10 cm of the soil profile ranged from 233 to 0 mg/L with higher concentrations of DFBA located in the southern portion of the plot. The site averaged depth profile (Figure 6.3) indicates 55% of the initial input DFBA mass lies in the top 10 cm of the profile and 83% of the initial mass lies in the top 20 cm. In total, 116% of the DFBA mass was accounted for in the soil extractions at the end of the 2009 field season (Table 6.2). The lack of overall movement of the tracer mass within the soil profile indicates a minimal amount of vertical advective transport occurs through the soil matrix. Vertical transport in the low permeability surface soils is mainly controlled by macroporosity (fractures, root holes) and is the primary cause of low DFBA concentrations at depths of up to 5 meters. These results are similar to the findings of a study conducted by Chen et al., (1999) in that 40 days after a surface applied bromide application; the center of bromide mass resided in the top 26 cm of the soil profile, while bromide was detected at low concentrations in the deepest sample at 60 cm. These results suggest that preferential flow (macropores) were able to quickly transport solutes at low concentrations, deep into the soil profile while the majority of the mass remains close to the surface.

The small number of soil samples resulted in a relatively large amount of uncertainty in the extraction results. This may, in part, explain the 116% DFBA mass recovery in the soil (Figure 6.3). Increasing the sample size to account for heterogeneities within the soil could decrease the error of the total mass accounted for in the soil. An additional source of error within this measurement is found in the extraction procedure used to remove DFBA from the soil. As previously discussed in Section 4.7.4 the DFBA extraction technique for the soil samples was tested and showed that 32.5% of the DFBA remained on the soil on average. Although, the reported results have been corrected to account for this unrecovered tracer mass, there is likely to be variability between samples. Fine-tuning the soil extraction process used for the DFBA would also decrease the uncertainty within the measurement.

6.2 2010 Field Results

6.2.1 Tile Drain Flow Response

The 2010 flow results (Figure 6.4) yielded significantly different results than the 2009 season as both north and south tiles were flowing prior to irrigation. Average flow rates and cumulative discharge volumes were higher for both the north and south tiles in 2010. One event that had a major influence on tile drain behaviour was a large precipitation event that occurred on July 13 (day 194), which applied 51.7 mm of water over a 24 hour period. The south tile had a peak discharge rate of 203 L/h, 3.4 times greater than the north tile (62 L/hr) during the July 13 rainfall event. The cumulative discharge in 2010 was 78.5 m³ from the south tile and 60.1 m³ from the north tile. Altogether, the tiles captured the equivalent of 51 % of the applied water volume

(including irrigation and precipitation). The tile drains in 2010 were able to capture a total volume of 9.7 times more water than in 2009.

Both north and south tile drains responded very similar (almost identical) to all irrigation and precipitation events in 2010, with the notable exception of the large July 13 rainfall event. One observation made during the 2010 season was the plateau reached by the north tile's discharge during the July 13 event. The north tile was not able to flow beyond 62 L/hr which differed from the south's response during the same period. One hypothesis for this behaviour is that the sand lens (previously discussed in Sec 6.1.2) located in the northern half of the plot could function as a lateral drain when exposed to saturated conditions. This sand lens could limit the volume of water available to be captured by the north tile drain by transporting any excess water laterally away.

One of the key reasons for the difference between the 2009 and 2010 seasons was the lack of soil moisture present at the start of the 2009 field season that severely hindered tile drain effluent production. The winter leading into 2009 saw a “below average” to “very low” snowpack in the Devon research site region as defined by Alberta Agriculture (Alberta Agriculture, 2009), which amplified the drought conditions experienced in the region. The large amount of winter precipitation prior to the 2010 field season (approximately 90 mm more than the previous year) helped replenish the soil moisture deficit, increasing the water table elevation and resulting in earlier tile drain production. Continuous precipitation and irrigation throughout the summer helped maintain wet conditions on site, allowing for a more consistent tile drain flow.

6.2.2 Hydraulic Response in Monitoring Wells

Only the 2010 hydraulic head data will be discussed due to the limited number of large irrigation events and the limited number of monitoring wells present in 2009. Results presented in Wilkinson (2011) show that the hydraulic response to precipitation and irrigation events in each set of wells (A,B,C series) provide an understanding of how each unit is connected hydraulically and how each response is influenced by the lithology that the well is completed in.

It is assumed that the A series wells have a strong hydraulic connection to the ground surface because of the quick response to irrigation and precipitation events. The degree of hydraulic connection is also supported by the rapid detection of DFB in monitoring well samples (Sec 6.1.3.2). Monitoring wells completed next to tile drains (MW09-04, MW09-03 and MW09-12A) showed little hydraulic response during minor irrigation and precipitation events (less than 25 mm). This is likely because the tile drains regulated the hydraulic head in these monitoring wells dampening the hydraulic response. The hydraulic response of the B and C series monitoring wells was similar to the A series wells when irrigation events occurred, but the magnitude of the responses was lower. This suggests that although both B and C series wells are influenced by irrigation events, their connection to the glaciolacustrine unit is buffered by the glacial till layer.

The seasonal hydraulic gradient between the A-B and B-C series wells indicated that localized flow is mostly in a vertically downward direction. One exception to this was the upward hydraulic gradients observed at the beginning of July that lasted roughly two weeks, likely caused by an increase in evapotranspiration. The large volume of water applied during the July 13 rain event then caused a reversal in vertical flow gradients between the A and B series lithological units. Immediately after the large rainfall event the hydraulic gradients reversed, showing a downward groundwater flow direction. Roughly one week after the large rain event, the vertical gradient reversed again, moving water from the B series sand unit upwards. As discussed in Wilkinson (2011), this is likely due to the over-pressurization of the B series sand unit relative to the glaciolacustrine unit.

Advective transport of tracer will follow this gradient and flow in the direction of the groundwater. For a large portion of the season, this would be towards the C series sand unit. Low concentrations of DFBA have been found in monitoring wells samples taken from the C series sand (Sec 6.2.3.2 and Appendix A) which lends support to the idea that measureable flow exists between the major lithological units on site. The fact that solutes are able to be transported to the deeper sand layers is troublesome in terms of salt remediation due to the higher hydraulic conductivities these sands exhibit. Once DFBA and salts are transported to these lower sand units, increased lateral flow will likely occur, carrying the salts and DFBA beyond the limits of the tile drains.

6.2.3 2010 DFBA Results

6.2.3.1 Tile Drain Effluent Concentrations

The 2010 DFBA tracer results (Figure 6.4) showed a more dynamic response to irrigation and precipitation events than the 2009 DFBA results (Figure 6.1). The tiles were able to capture 6.6% of the initial applied mass, representing 13 times more mass than the 2009 results. The south tile captured 64% more mass than the north tile through 2010 because it typically had higher DFBA concentrations and higher flow volumes than the north tile. One reason for the difference in DFBA mass captured between the north and south tile drain is due to the July 13, 51.7 mm precipitation event in which the south tile captured nearly twice as much DFBA mass as the north tile. Peak DFBA concentrations for the north and south tiles were 3.44 mg/L and 4.97 mg/L, respectively.

One observation of the 2010 tile effluent DFBA concentrations was the concentration response in both north and south tiles to the large July 13 precipitation event. The traditional response of tile DFBA concentrations early in the season was to increase simultaneously with increased tile flows, whereas the large flow increase during the July 13 flow event caused a sharp decrease in DFBA concentrations. This sharp decrease could be caused by the large influx of fresh water. The excess loading of fresh water on the surface allowed the macropores to continually transmit water to the tile drains, flushing the macropores clean of most of the DFBA. Only DFBA stored in the matrix was available for transport to the tile drains once the initial macropore flush occurred. Supplying the macropores with DFBA would then be dependent on the delivery of DFBA from the matrix into the macropore domain, occurring via diffusion

and advection. During the July 13 rainfall event, the solute transfer rate occurring from the matrix into the macropores was not able to replenish the macropores with DFBA quickly enough to maintain a steady concentration. All DFBA that was transferred into the macropore continually got flushed due to the fresh water influx, resulting in a concentration drop measured in both the north and south tile drains. This observation is important in that future irrigation planning should try to avoid such occurrences. A decrease in solute concentration in the tile drains would likely be observed when a volume of water is applied to the surface that exceeds a specific “threshold” volume. This is due to the limiting rate at which solutes can move from the matrix domain into the macropores. A rough estimate from the 2010 data indicates that when a water depth of over 40 mm is applied to the surface the resulting tile drain flux will be greater than 35 L/hr. Analysis of the tile data shows that once the tile drains (north and south) exceed a discharge of 35 L/hr, the DFBA effluent concentrations drop as shown in the 2010 DFBA tile drain data. An irrigation management plan should be developed that would take into consideration this matrix-macropore transfer rate and base the irrigation volume/frequency applied on maximizing the mass of solute flushed per unit volume of irrigation water.

Another interesting observation is the switch of the north and south effluent DFBA concentrations between the 2009 and 2010 seasons. During the 2009 season, north tile DFBA concentrations were consistently higher than the south, but the 2010 data shows the south tile consistently had higher concentrations than the north. Currently no working hypothesis has been formed to explain why the switch occurred.

6.2.3.2 Monitoring Well Detections

Monitoring wells sampling occurred five times during the 2010 season at approximately 30 day intervals from June through to October (Appendix A). Figures 6.5, 6.6 and 6.7 show the monitoring well DFBA concentrations during the five sampling events in the A, B and C series wells, respectively. The spatial distribution of DFBA detections that occurred during the 2009 monitoring wells sampling is repeated in the 2010 samples. MW09-01, MW09-12A, MW09-09 and MW09-08 near the northern edge of the plot all show consistent DFBA detections throughout the 2010 season (Figure 6.5). Additionally, deeper wells in the northern portion of the plot (MW10-12B & C, MW10-15B & C) showed DFBA tracer detections, although at lower concentrations (Figure 6.7 and 6.8). A greater proportion of A series wells showed DFBA detections in the 2010 season (11 of 12) when compared to the 2009 season (4 of 12). Several of the A series wells located in the southern half of the plot (MW09-06, MW09-04, MW09-03) have consistent DFBA detections throughout the 2010 season which differs from 2009. The increase in A series DFBA detections suggest that the DFBA mass is migrating vertically down the soil profile throughout the irrigation plot.

During the 2010 season, no upward or downward concentration trends were observed in any of the A, B or C series monitoring wells. The lack of decrease or increase in DFBA concentrations makes it difficult to speculate on the location of the DFBA center of mass. DFBA detections in both B and C sand units indicate that transport (most likely via macropores) is occurring across the glacial till units overlying

both the B and C series and units. The B and C series monitoring well detections located outside of the plot suggest that increased lateral flow occurs in the deeper B and C series sand units relative to the upper glacial units. No obvious spatial correlation exists between DFBA detections in the monitoring wells and the tile drains.

6.2.3.3 Suction Lysimeter Concentrations

Two nests of suction lysimeters were installed at the beginning of the 2010 field season, one in the center of the plot (South) between tile drains and the other above the north tile drain (North) (Figure 4.4). Similar to the monitoring wells, the lysimeters were sampled five times throughout the season at approximately 30 day intervals from June to October. Both north and south lysimeter nests show concentrations decreasing with time between the June and October sampling events (Figure 6.8), suggesting vertical migration of DFBA tracer is occurring. Peak concentrations in the south lysimeter nest reached 30.4 mg/L while the north nest reached a peak concentration of 18.5 mg/L, both occurring at a depth of 30 cm during the June sampling event. The measured decrease in DFBA concentrations in both north and south lysimeters suggest that matrix flushing is occurring and that DFBA mass is being transported vertically downwards.

One of the noticeable changes that occur during the 2010 season is the increasing DFBA concentration with time in the three lower sampling locations paired with the decreasing DFBA concentration in the upper two sampling locations in the north lysimeter nest. This suggests that flushing is occurring in the top 30 cm of the soil profile, while DFBA is migrating deeper into the soil. This is also observed in the south

lysimeter nest, but not to the same degree. Decreases in DFBA concentrations are measured in the top three lysimeters, paired with slight increases in the bottom two lysimeters. The differences in DFBA flushing between the north and south lysimeter nests could be caused by the proximity to the tile drains. The north lysimeter nest is located directly above the north tile drain, which should cause enhanced fluid drainage and an increase in solute movement. The tile drain could enhance drainage by creating a lower water table which increases the unsaturated zone directly above the drain. This unsaturated zone could enhance the solute transport relative to areas with a higher water table. The south nest, which is situated in the center of the plot and away from the tile drains, should experience less drainage due to the lack of tile drain influence.

Uncertainty arises when interpreting the lysimeter data due to the vertical separation between sampling points. The five sampling points cover 1.5 meters depth, translating into a relatively coarse depth profile. It is difficult to determine whether the center of mass actually moves further down the soil column due to the absence of intermediate sample locations between 30 and 60 cm depth.

6.2.3.4 Soil Extraction

A total of 42 boreholes with depths ranging between 1.5 and 6 m were drilled in a grid pattern across the plot at the end of the 2010 field season to aid in characterizing the DFBA tracer distribution (Figure 6.9). A total of 394 samples were analyzed. The results from the soil extractions showed that 55% of the mass measured in the cores was situated in the top 75 cm of the soil profile (Figure 6.3). In total, 32% of the applied DFBA mass

was accounted for in the soil extractions. Samples taken to a depth of 1.5 m outside the plot (Figure 4.7) all showed non-detectable levels of DFBA indicating that little lateral transport is occurring in the upper 1.5 m. In total, 16 of the 26 profiles show a similar distribution with the center of mass residing between 25 and 75 cm below ground surface (Figure 6.9 and Appendix C). The fact that the DFBA depth profiles show similar distributions between boreholes is somewhat surprising given the high level of lithological heterogeneity observed. Results from the 2010 DFBA soil extraction support previous observations that advection within the low permeability soil matrix is quite slow and accounts for a small amount of DFBA transport.

Four of the five soil cores located on the northern edge of the plot (boreholes 64-67) show non-detections for in samples located above 1 m. This indicates that solutes are being transported quickly enough that nearly all DFBA has been transported beyond 1 m depth. This supports the quick breakthrough of DFBA in the monitoring wells located in the northern edge of the plot. This quick breakthrough and enhanced solute transport can be caused by an increased macropore density relative to other sections in the plot, or increased macropore flow due to surface ponding as previously discussed in Sec 6.1.2.

A similar pattern is observed in the southern edge of the plot with 3 sample locations (62, 68 and 69) showing a comparable depth distribution. It would be expected that increased DFBA monitoring well detections would be measured in samples taken from the wells located in the southern half of the plot, but that did not occur. Boreholes located above the tile drains all produced similar depth distributions with the center of

mass lying between 0.5-0.7 meters below ground surface. In total, it appears that the top 50 cm of soil are being flushed of DFBA in 14 of the 26 borehole locations. Additionally, it appears that boreholes located above the south tile drain are experiencing greater flushing compared to the borehole located above the north tile due to their decrease in DFBA in the top 50 cm. Boreholes located in between the north and south tile drains appear to be experiencing the least amount of DFBA flushing which supports the lysimeter results (Sec 6.2.3.3) in that locations above the tile drains are being more efficiently flushed, relative to locations in between the tile drains. Although results from all soil core samples showed an increase in DFBA infiltration compared to the 2009 soil extraction results, and showed an overall mass reduction of DFBA indicating that matrix flushing is occurring, these spatial concentration differences could be due to the varying initial distribution of DFBA. Unfortunately no initial DFBA concentration distribution was measured directly after application, so no certain conclusions can be made on the spatial differences in DFBA flushing. Literature searches have been unable to find any studies that have tracked solute movement in tile drained, macroporous soils over a two year time period, making it difficult to compare the results found.

Although a large portion of the 1.5 m DFBA depth profiles had non-detectable DFBA for many of the deepest samples (80-90 cm), nine of the boreholes had a continuous detection of DFBA extending to the deepest sample available. This indicates that some of the DFBA mass could have been left unaccounted for below the maximum sampling depths. Because a small portion of the boreholes (4 of the 42) extended beyond

1.5 m depth and DFBA has been recovered in cores as deep as 5 meters, a degree of uncertainty arises on where the DFBA mass is residing below 1.5 meters.

6.2.3.5 DFBA Mass Balance

The total DFBA mass accounted for at the end of the 2010 season was 38% of the initial applied mass (Table 6.3). The tile drains were able to capture 6.5% of the initial applied mass during the 2010 season, giving a total tile drain capture of 7.0% of the initial mass over the two seasons. Extractions of DFBA from the soil cores accounted for 32% of the total mass remaining in the soil. Of the mass that remained in the soil profile at the end of 2009, 73% of that mass was removed by the end of the 2010 field season. One possible mechanism that could account for the loss of DFBA is transport into the lower sand units, presumably along macropores. This is indicated by DFBA detections in the monitoring well samples collected in both B and C sand units. Due to the lateral hydraulic gradients and increased hydraulic conductivity values measured in the B and C unit sands, the mobility of the DFBA would increase in the sand units and potentially be transported down gradient away from the site. The possibility for DFBA degradation has been tested (Sec 4.7.5) and has shown that no measureable degradation occurs.

6.2.4 PFBA Injection Results

Two PFBA injections occurred over a two day period between July 20 and 21, 2010. The first injection occurred above the north tile at a depth of 1.72 m and breakthrough was monitored at the tile drain sump. Initial breakthrough of PFBA took

place 13 hours after injection, with the peak concentration arriving 32.2 hours after application (Figure 6.10). Approximately 75% of the total PFBA mass was captured in the north tile drain over a 58 day period. The breakthrough curve characteristics suggest two different mechanisms could influence the PFBA transport to the tile drain. Macropores are most likely responsible for the quick initial breakthrough and concentration peak, while the sustained PFBA concentration after the recession of the peak is attributed to slower diffusive transport from the matrix into the macropores followed by rapid transport to the drain. This second “matrix diffusion” mechanism was first noted by Foster (1975) and has been shown to effectively reduce the rate of migration of solutes through macropores (Maloszewski and Zuber, 1993; Shapiro 2001).

The second PFBA injection occurred in MW09-13A on July 21. The intent of this injection was to examine how hydraulically connected the upper glaciolacustrine unit is to the lower B series sand unit. Routine samples were collected every 6 hours from MW09-13B and analyzed for PFBA. No detection of PFBA occurred within the 72 day sampling program. Although the absence of PFBA in MW09-13B samples suggests that a limited hydraulic connection exists between each unit, a simple explanation is that PFBA detection in MW09-13B was unlikely from the onset of the experiment due to the low probability that the injected PFBA would be captured by MW09-13B. Therefore, no conclusions can be made from the results of the second PFBA injection.

6.3 Model Calibration and Sensitivity Analysis

6.3.1 Calibration

6.3.1.1 Flow Parameters

Calibration of the flow and transport model was done primarily by comparing observed and simulated water and DFBAT tile drain fluxes. Additionally, matching observed hydraulic heads in monitoring wells (MW09-01, MW09-03, MW09-05, MW09-13A and MW09-13B) helped calibrate the flow and transport model. Water tile drain fluxes and hydraulic head measurements were calibrated by modifying the hydraulic parameters of each soil layer within the model (top soil, glaciolacustrine, glacial till, B series sand). Calibration of the upper infiltration unit was not required because it only served to limit the amount of water lost to runoff.

Initially, van Genuchten matrix parameters were taken from the measured values obtained from the pressure plate extraction and further adjusted when needed. Calibration of each parameter was done systematically by changing a specific variable (ex. K_{sf}) for an individual material and documenting the results. The main variables used to calibrate the model were the macropore hydraulic conductivity variable (K_{sf}), macropore volume (ω) and matrix block half width (a). The results showed that the model was highly sensitive to changes in these variables. Table 6.4 provides a summary of the effect each of the main calibration variables had on the tile drain flow in the numerical simulations. Initial values for the calibrated variables were set using literature values used in similar modeling exercises (Simunek et al., 2003; Gerke and Kohne, 2004; Gardenas et al, 2006). All remaining hydraulic parameters (γ , β , θ_{rf} , θ_{sf} and

l) were set using literature sources. The model's sensitivity to these parameters was minimal and it was determined they would be omitted from the calibration procedure.

6.3.1.2 Transport Parameters

The main solute transport calibration parameter was the mass transfer coefficient (α_s) between the matrix and fracture domain. This parameter characterizes the exchange of solutes between the matrix and macropore domains. Calibration of α_s was done step-wise similar to that of the previous calibration of the hydraulic flow parameters. Calibration was achieved by matching the observed DFBA concentrations in the south tile drain measured in 2010. A base value of 0.05 was used (HYDRUS default) and several simulations were run with decreased or increased values. The calibration procedure was completed by matching the high and low observed DFBA concentration peaks with the simulated peaks.

6.3.2 Sensitivity Analysis

Sensitivity analysis of the model parameters was done simultaneously with the calibration procedure. This was primarily completed by evaluating the goodness of fit of the simulated tile drain flow results and DFBA tile drain concentration results to the measured data. Quantitative evaluation was conducted by calculating the root mean square error (RMSE) (Equation 6.1) between simulated, x_s , and observed results, x_o , as follows:

$$RMSE = \sqrt{\frac{1}{n} \sum (x_m - x_s)^2} \quad (6.1)$$

where n is the number of data points. This allowed all model simulation results to be compared against each other in a consistent manner. A large number of simulations were conducted in a systematic fashion by varying one parameter at a time and evaluating the quality of the simulation results using the RMSE and visual observations of the goodness of each fit. Although the RMSE method provides a quantitative measure for comparing simulations, it can occasionally be misleading. Therefore, the ability of the model to match the timing and magnitude of fluctuations in tile drain flow and tile effluent concentrations was also used to evaluate the simulation results.

As part of the calibration process, a set of parameters that was determined to be the “best fit” to both observed tile drain flow and tile drain effluent DFBA concentrations was arrived at. This set of parameters will be referred to as the base case and are summarized in Table 6.5. Note that the RMSE results for all sensitivity analysis runs have been normalized by dividing the simulated RMSE values for any given run by the base case RMSE values. The sensitivity analysis focused primarily on the hydraulic parameters in the glaciolacustrine unit because they tended to have the largest influence on the flow system response. The parameters tested were n_m , α_m , K_{sf} , K_{as} , a , ω and α_s . The changes in normalized RMSE for selected sensitivity runs are presented in Table 6.6 and the corresponding influence on tile drain flow and concentration response is given in Figures 6.11 and 6.12. The parameters that caused the largest change in the RMSE

results were the a (matrix block half width) and ω (macropore volume) variables for both simulated tile drain flow and solute transport and α_s for solute transport (Table 6.6). Changes in K_{sa} , α_m , n_m and K_{sf} had a relatively small (up to 12%) influence on calculated RMSE values but impacted the timing and shape of the tile flow peaks in comparison to the observed data (Figure 6.11).

6.4 Simulated Flow Results

6.4.1 Tile Drain Discharge

Flow was simulated by modeling a 138 day period spanning from May 29, 2010 (day 149) until October 13, 2010 (day 286). Only flow from the south tile was simulated as it offered the greatest magnitude of change between high and low flows. The model results showed that the dual-permeability method accurately captured the timing of peak flows during the simulation period, but overestimated tile drainage during the simulation period (Figure 6.13). The July 13 (day 194) rainfall peak was the only event in which the model underestimated flows. Additionally, results from the flow simulations showed that macropores accounted for 99% of the cumulative tile drain flow. Overall, the model overestimated flow by 50% with the tiles capturing 80% of the irrigation water volume applied to plot A (irrigation + precipitation without subtracting evapotranspiration) compared to the actual measured amount of 51%. In order to successfully simulate the cumulative flow volumes the macropore contribution must be reduced. Reducing the amount of flow contributed by the macropores by decreasing K_{sf} and ω values (see Figure 6.11, K_{sf} value of 5000 mm/day) allowed the correct cumulative flow volumes to

be simulated, but the timing of the tile drain response to irrigation/precipitation events was adversely affected (Figure 6.11).

One possible reason for the overestimation in tile drain flow is an inaccurate flux boundary condition used for the top of the model. Underestimating the evapotranspiration component of the flux will lead to an overestimation of infiltration, which would increase the amount of water in the domain. The model's overestimation of tile drain flow could also be due in part to the lack of drainage from the base sand unit (B series sand). Flow within this unit is limited by the fact that it can only enter or exit at the lateral edges of the model domain (1D), whereas realistically flow in the lower sand unit could move radially (2D) or vertically down into the underlying till unit. As discussed in a similar modeling exercise completed by Gardenas et al. (2006), the dual permeability approach does an excellent job at matching peak drain response, but overestimates the total drain flow due to a lack of drain bypass into the deeper units.

Another explanation for the overestimation in the simulated drain flow is the absence of vertical anisotropy due to computational limitations. Soil fractures and root holes at the site have been observed to be near vertical, which is expected to give rise to increased permeability in the vertical direction relative to the lateral directions. This anisotropy in the macropore domain currently cannot be simulated with HYDRUS. Furthermore, representing a heterogeneous, 3 dimensional system with a 2 dimensional, homogenous model will create difficulties when attempting to match observed field data with the simulation results. The lack of vertical anisotropy may mean that vertical and

horizontal flow components in the macropores are not being accurately represented. If vertical anisotropy were implemented in the model, it would increase the magnitude of flow occurring vertically, while decreasing the lateral flow component. Reducing the amount of lateral flow in the macropore domain should decrease the effective capture zone of the tile drains, resulting in an increase in the amount of flow bypassing the tile drains and decreasing the total volume captured by the drains. Further work is needed to characterize the measurable vertical anisotropy in soil cores from the site. Additionally, incorporating vertical anisotropy in both matrix and macropore domains in the numerical model should produce more realistic results. Currently, no substantial amount of research has been done in the scientific community on characterizing vertical anisotropy in macroporous soils and this is an area that could benefit from additional research.

6.4.2 Hydraulic Head Response

The simulated hydraulic heads were similar to the observed hydraulic heads in the response to irrigation events throughout the simulation period, but were consistently underestimated relative to the observed heads (Figure 6.14). This underestimation could also be attributed to the lack of vertical anisotropy in the simulations. Decreasing the amount of lateral flow occurring in the domain would reduce the overall amount of drainage occurring, resulting in an increase in hydraulic heads throughout the domain.

Temporally, the simulation did an adequate job at matching changing hydraulic heads with time (Figure 6.15). Simulated hydraulic heads for selected monitoring wells were able to capture some of the time varying fluctuations. All simulated monitoring

wells respond similarly to the large July 13 precipitation event, but differ in how they respond before and after. The simulated response of monitoring wells located on the north and south edge of Plot A (MW09-01 and MW09-05) were able to match the observed response with better accuracy than wells located in the center of the plot (MW09-13A). Results from monitoring well MW09-03, which is located close to the south tile drain, appear to be the least accurate as they are underestimated by approximately 0.5 meters throughout the entire simulation period.

The primary reason why the fixed head boundary conditions were used instead of a no flow symmetry boundary (Figure 5.3) was due to the lateral influx of water observed when the water table surrounding the plot increased in July and August of 2010. Although the total volume of water entering the domain was minimal, the model was able to successfully capture the influx of water along the boundaries on both the north and south sides. The overall impact this influx had on the simulated results is minimal as less than 0.01% of water entered the domain from these hydraulic boundaries. It would be recommended for future simulations to simulate this boundary as a no flow boundary, which would significantly reduce computational time.

6.4.4 Simulated Fluid Mass Balance

Results from the simulated fluid mass balance show that 64% of the applied water volume equivalent exits the domain via the tile drains during the simulation period. The B series sand unit accounts for less than 1% of the flow exiting the system. Flow into and out of the domain through the glaciolacustrine head boundaries accounted for a very

small percentage of water flow (less than 0.01%). Transpiration accounted for 22% and evaporation accounted for 12% of water exiting the system. One possible factor contributing to the overestimation of the tile drain discharge could be the absence of vertical anisotropy in the domain. By implementing vertical anisotropy in future simulations, it is expected that tile drain discharge will decrease, while increasing the bypass to the lower sand unit.

6.5 Simulated DFBA Transport

6.5.1 Tile Drain Effluent Concentrations

The results of DFBA transport simulations are presented in Figure 6.16. The early time response of the simulated DFBA tracer is similar in both magnitude and timing to the observed south tile concentrations. As previously mentioned in Section 6.3.1.2, the simulated results track the observed data closely up until the July 13 rain event, when the simulated results begin to deviate considerably from the observed data. The simulated base case results show that 28% of the initial 2010 DFBA mass is removed during the 2010 field season, with 98% of that mass removed via the north and south tile drains. Macropores accounted for 99% of the DFBA transport to the drains, which is consistent with the simulated flow results. Field measurements show that of the initial DFBA mass in 2010, 31% remained at the end of 2010 (69% removed), indicating the model underestimates the total mass removal that occurred in 2010.

The large discrepancy between the observed versus simulated DFBA mass removal could be due to a number of factors. First, the model does not accurately

simulate the lateral migration of the tracer beyond the plot as observed in the monitoring well DFBA detections in 2009 and 2010. Second, transport of DFBA into the lower sand units and beyond is not able to take place due to the presence of a no flow boundary at the base of the simulated B series sand unit. The current no flow boundary condition is not allowing DFBA to infiltrate deeper, which could account for a portion of the discrepancy in tracer mass.

Although 98% of the tracer transport occurs via the macropores, the model results show that flushing of the matrix domain is occurring. This is important in terms of salt removal as the salt mass resides primarily in the soil matrix. Simulation results show that the main mechanism of advective solute transport is through the macropores, but flushing of the matrix is occurring due to the transfer of solute from the matrix to the macropores. The transfer of solutes from the matrix to the macropores is sustaining transport in the macropore domain, allowing the macropores to continually be supplied with salt or tracer

One challenge that regularly occurred during model calibration was attempting to fit the peak responses of the tile drain DFBA concentrations in both the early time (prior to 50 simulation days) and the late time responses (after 50 days) while simultaneously calibrating for fluid flow. As shown in Figure 6.12, manipulating the solute mass transfer coefficient (α_s) allows for either early or late time simulated DFBA tile drain data to be matched to the observed DFBA tile drain data. Figure 6.12 illustrates that when using a ω value of 0.025 the simulation can successfully match the peak response of the DFBA in early and late time. But as shown in Figure 6.11, using the same ω value of 0.025, tile

drain flows are vastly overestimated throughout the entire simulation period. This required a compromise on both ends to adequately fit the fluid flow and DFBA simulated data to the observed.

The difficulty experienced in successfully fitting the simulated data to the observed DFBA concentration data could be caused by the numerical representation of how the solute mass is initially distributed in the model. When the solute is partitioned into the matrix domain, the concentration is assumed to be distributed equally throughout the node (Figure 6.17a). This approach does not account for the variable concentration distribution within the soil matrix that would occur as a result of the variable time allowed for the solute to migrate or diffuse into the matrix (Figure 6.17b). Multiple studies have shown that the solute concentration is not equally distributed through the matrix-macropore region (van Genuchten et al., 1984; Aliaire-Leung et al., 2000). A major factor controlling the matrix solute distribution is the length of time the solute has had to migrate or diffuse into the matrix block. A longer exposure time will allow the solute to migrate deeper into the matrix, while a shorter exposure time will result in a shallow solute distribution, close to the matrix-macropore interface (van Genuchten et al., 1984). The short residence time of the DFBA tracer in this study translates into a solute distribution that resides close to the matrix-macropore interface (Figure 6.17b). The numerical representation of the solute distribution in the model does not accurately describe the processes occurring on site.

Another issue that must be taken into account is the errors that arise when constructing an initial solute distribution from a limited number of core samples (Figure 4.8). The limited data set that was used to construct the initial solute distribution contained a large uncertainty because only five borehole locations were available to represent the DFBA depth distribution over the entire experimental plot. The alternative to using the 2009 DFBA core data would have been to use the north and south suction lysimeter results. This was not considered because there were even fewer lysimeter locations available (only two locations with five sampling depths at each).

6.5.2 Lysimeter Concentrations

Observation nodes were inserted into the model domain at the same locations and depths as the lysimeters in the south nest. The simulated and observed concentration profiles in the lysimeters are shown in Figure 6.18. Comparisons between the observed and simulated results indicate that the model is capturing the decrease of DFBA mass through the 2010 season, but is unable to simulate the observed change in vertical DFBA distribution for each simulated sampling event. The simulated results show the center of mass moving vertically down the soil profile through the field season. This is not shown in the observed lysimeter results as the center of mass remains situated at 30 cm depth and does not appear to migrate downward. Discrepancies between the simulated and observed results suggest the model is overestimating the degree of tracer movement through the soil profile. The results from the simulated lysimeters suggest that too much vertical transport is occurring in the model. This is shown by the large increase (3.2 mg/L) in DFBA concentrations in the simulated 1.5 m lysimeter that was not measured in

the field. Although the field lysimeter does show a slight increase (0.72 mg/L) in DFBA concentration, the simulations overestimate the DFBA increase at depths of 1.5 m.

The simulated lysimeter results also did not properly capture the low tracer concentrations present below 90 cm, which were observed in the south lysimeter. This problem is likely due to the initial vertical DFBA distribution used in the model. The initial depth distribution for the transport simulation was determined using the 2009 DFBA soil extraction results (Figure 6.3) and not the June 2010 lysimeter results. The 2009 DFBA soil extraction results represent a site wide average concentration depth distribution with a small sample size, and thus a relatively large degree of uncertainty.

6.5.3 Simulated Tracer Migration

The evolutions of DFBA concentrations through the simulation in the matrix and macropore domains are shown in Figures 6.19 and 6.20. The matrix domain DFBA concentration distribution (Figure 6.19) shows a slow vertical migration through the soil profile and a decrease in DFBA concentrations throughout the simulation period. Throughout the simulation time, the matrix appears to be losing DFBA mass and the center of DFBA mass is migrating deeper below the ground surface. The DFBA migration through the matrix domain shows similar results to the DFBA soil core depth distribution (Appendix C) in that the center of mass remains above the tile drains, primarily in the top 1 m of the simulated domain.

The migration of the macropore DFBA (Figure 6.20) initially starts with zero mass at the initial condition, but as the simulation progresses the DFBA mass from matrix transfers into the macropore domain and remains throughout the simulation. The DFBA concentrations in the macropores were consistently lower compared to the matrix DFBA concentrations throughout the simulation, but the macropore DFBA was able to infiltrate to greater depths, particularly early in the simulation period (prior to day 80). The model does a poor job at simulating DFBA migration into the lower sand layer, likely due to the no flow boundary located at the base of the sand. Data from the B series monitoring wells have shown that measurable quantities of DFBA have been transported to this lower sand unit. Much of the DFBA mass loss occurring in the field is believed to be a result of DFBA bypassing the tile drains, and infiltrating deeper into lower units. Currently, this is not being captured in the simulations and is likely a factor that is causing the underestimation in the simulated DFBA flushing to the lower units.

Both matrix and macropore domains showed little lateral migration beyond the extent of Plot A. This supports the idea that little lateral tracer or salt migration is occurring on site, and that solute transport above the tile drains is a vertically dominated process. The capture zone of the tile drains appears to be larger than previously assumed and is likely due to the fact that vertical anisotropy of the macropore domain is not included in the model. A smaller tile drain capture zone is expected to transport larger amounts of tracer and salt past the tile drains, moving the tracer and salt deeper into the lower units. Current field observations detected DFBA in both the B and C series sand units but no measurable amounts of DFBA were present in the simulated B series sand.

Introducing vertical anisotropy in the model is expected to increase tile drain bypass in the simulations, thereby increasing DFBA concentrations in the lower sand unit and better replicating field observations. Furthermore, both tile drains exhibit an “upwelling” effect that forces water from the sand layer directly below each drain vertically upward into the drain, similar to that observed by Van Schaik and Milne (1961). This increases the capture zone of the tile drain which subjects larger areas of soil to drainage, increasing the efficiency of each drain. This allows for salts and tracer that may have originally passed in between a set of drains to be “recaptured” in the future. The implications of the simulated upwelling are an increased flow discharge, as water would be pulled from above and below the drains. The simulated upwelling could be a contributor to the overestimation in tile flow. This would be similar for solutes, as any DFBA residing below the drains would be transported to the drains. Whether this upwelling is real or an artifact of the simulation is currently unknown.

Table 6.1. Properties of soils on site

Material	Particle Size Analysis (% Composition)				Dry Bulk Density (g/cm ³)	Porosity	CEC (meq/kg)
	clay	Silt	Fine Sand	Medium Sand			
Top Soil	N/A	N/A	N/A	N/A	1.05	0.475	N/A
Glaciolacustrine	15	83	2	-	1.545	0.417	219.66
Glacial Till	11	34	40	15	1.735	0.345	112.43
B Series Sand	-	17	75	8	N/A	N/A	N/A

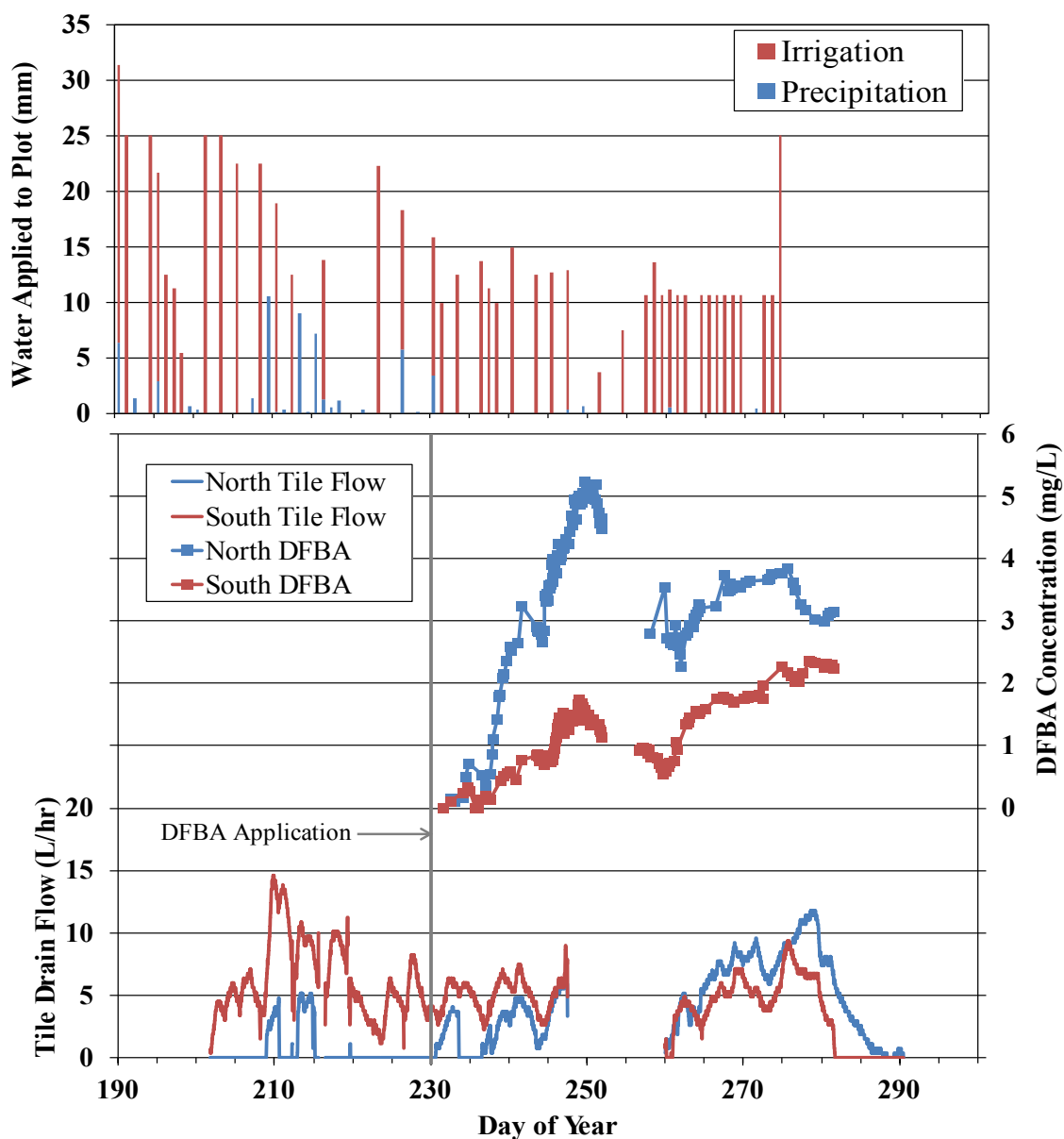


Figure 6.1. Applied irrigation/precipitation (mm), measured tile drain flow (L/hr) and DFBA concentration in water samples recovered from the north and south tile drains in 2009. DFBA surface application occurred August 18 (day 230).

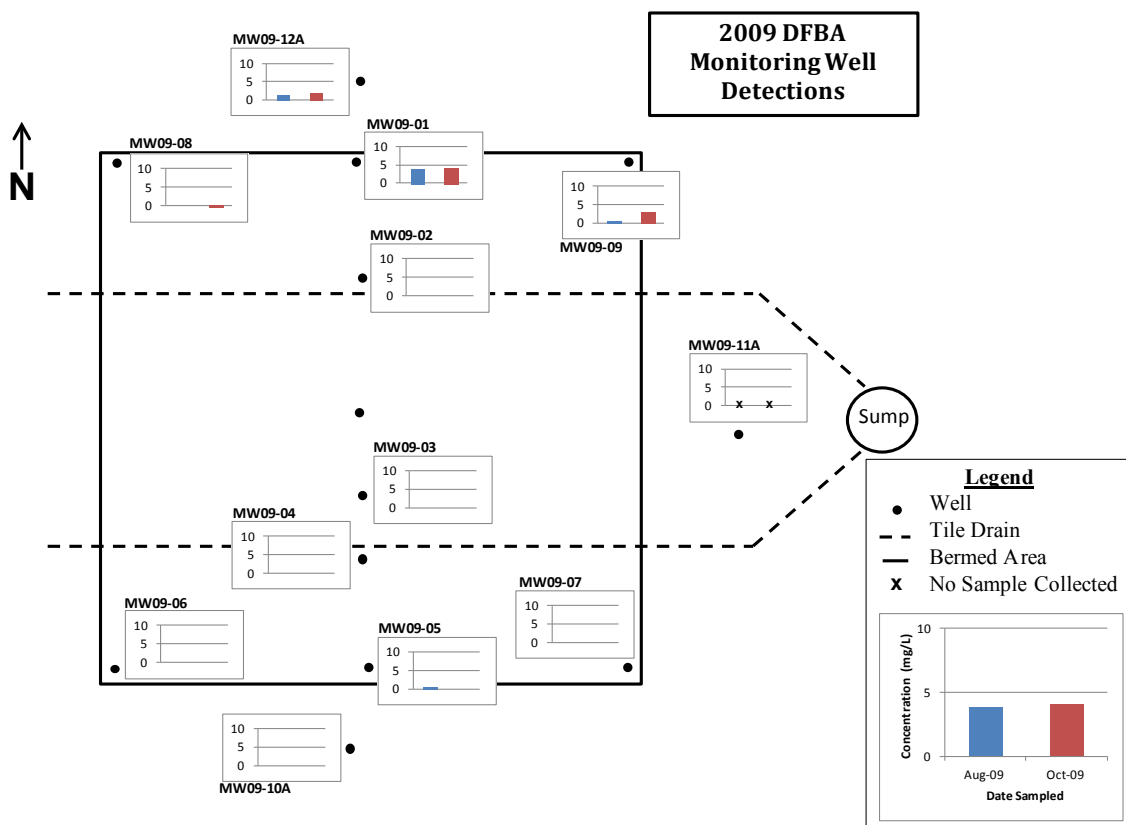


Figure 6.2. Plan view map of monitoring well DFBA concentrations in 2009.

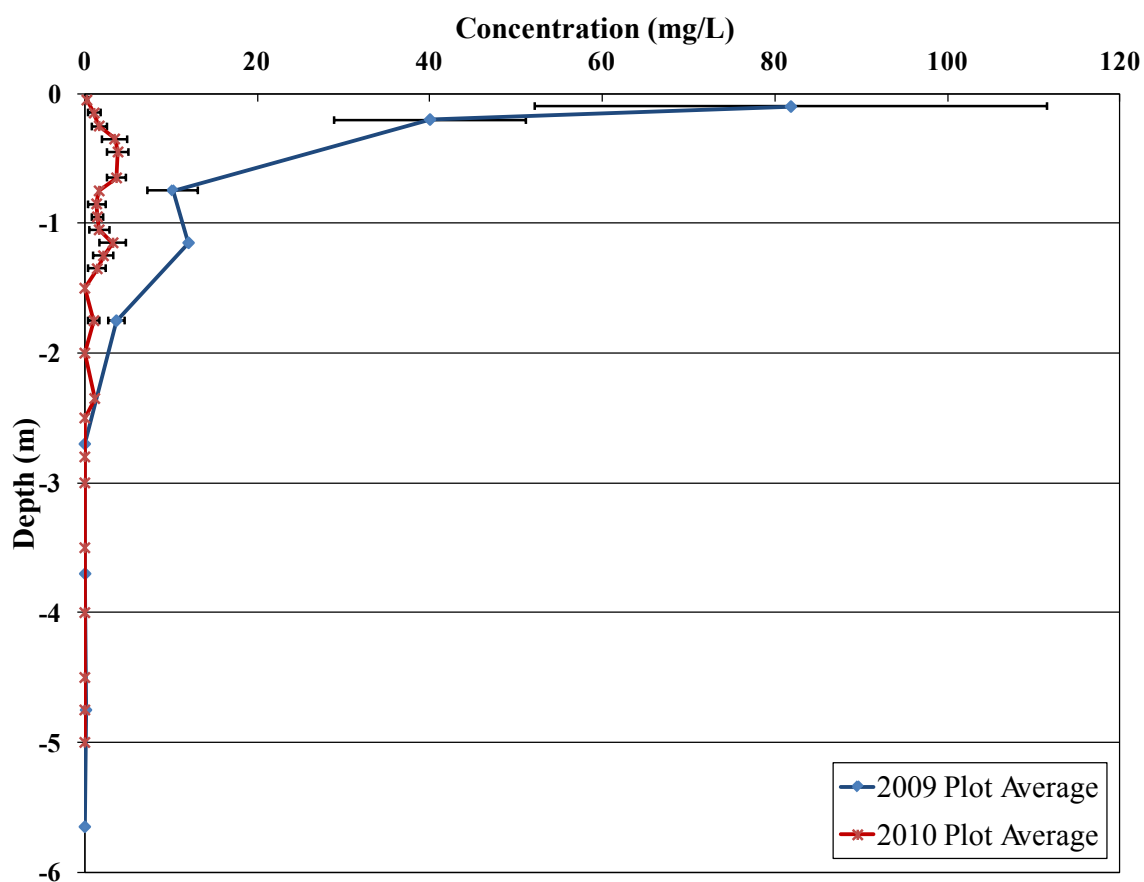


Figure 6.3. Depth profile of average DFBA soil pore water extract concentrations in Plot A. Data are derived from 2:1 soil extracts collected in 2009 (blue) and 2010 (red). Error bars represent the standard error calculated from the sample population.

Table 6.2. Summary of DFBA mass recovery at the end of the 2009 season. Soil corrected values indicate the total DFBA mass accounted for after a correction had been applied based on the DFBA soil extraction method (Section 4.5.2.2).

	2009 Mass Recovered (g)	M/M_o (%)
South Tile	7.01	0.16
North Tile	14.9	0.33
Combined	21.9	0.49
Soil Extraction (Corrected)	5230	116.13
Total	5250	116.62

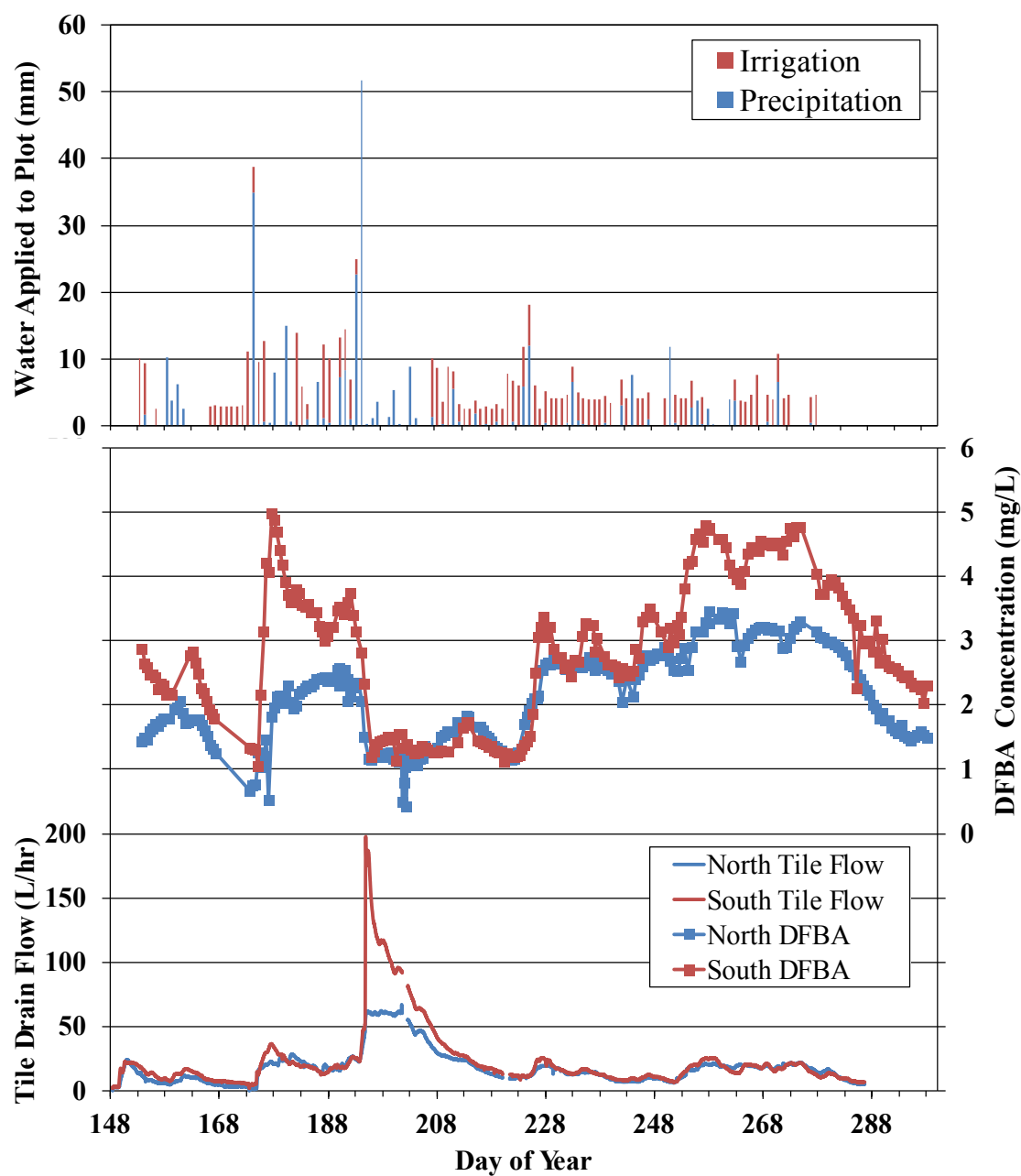


Figure 6.4. Applied irrigation/precipitation (mm), measured tile drain flow (L/hr) and DFBA concentration in water samples recovered from the north and south tile drains in 2010.

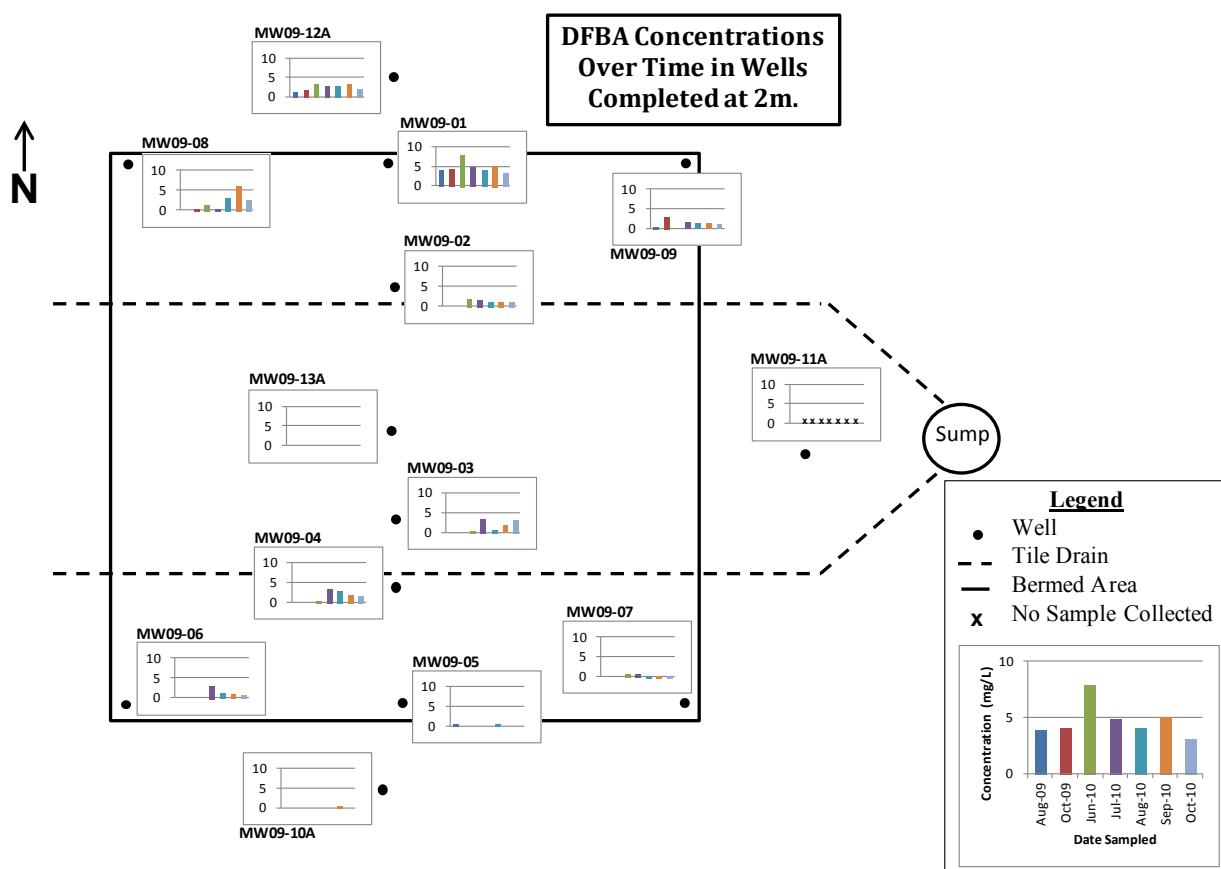


Figure 6.5. Plan view map of DFBA detections in A series monitoring wells during 2009 and 2010.

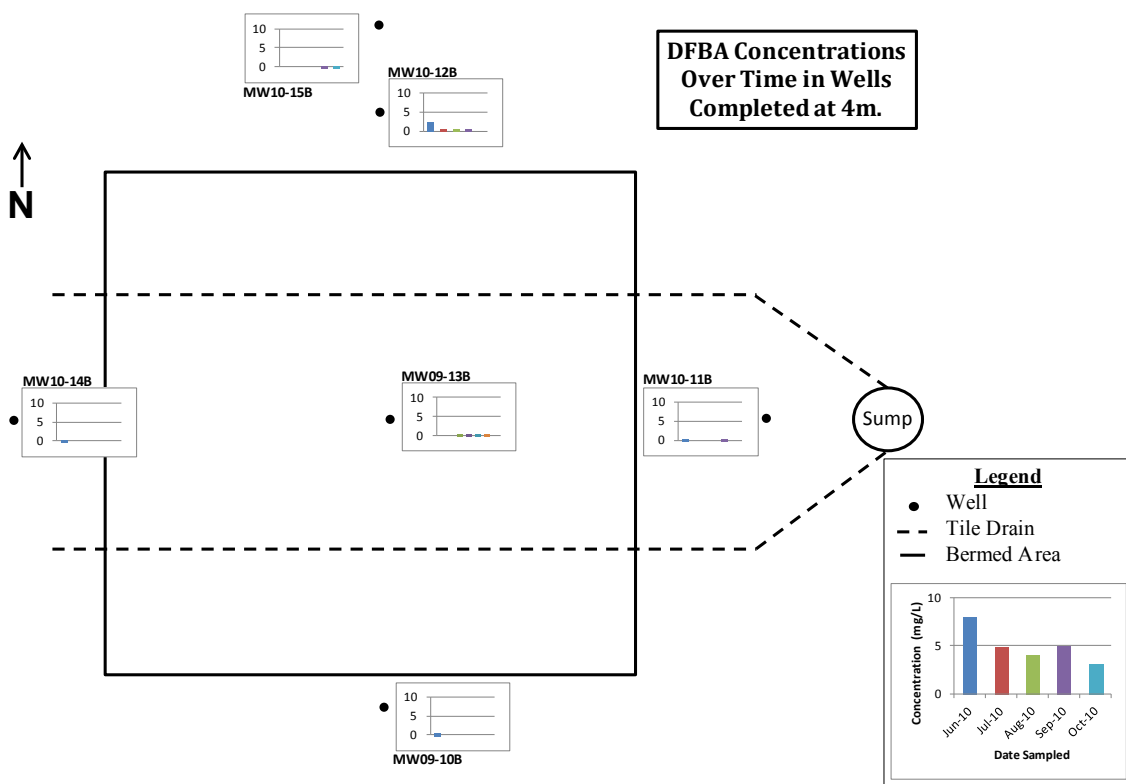


Figure 6.6. Plan view map of DFBA detections in B series monitoring wells in 2010.

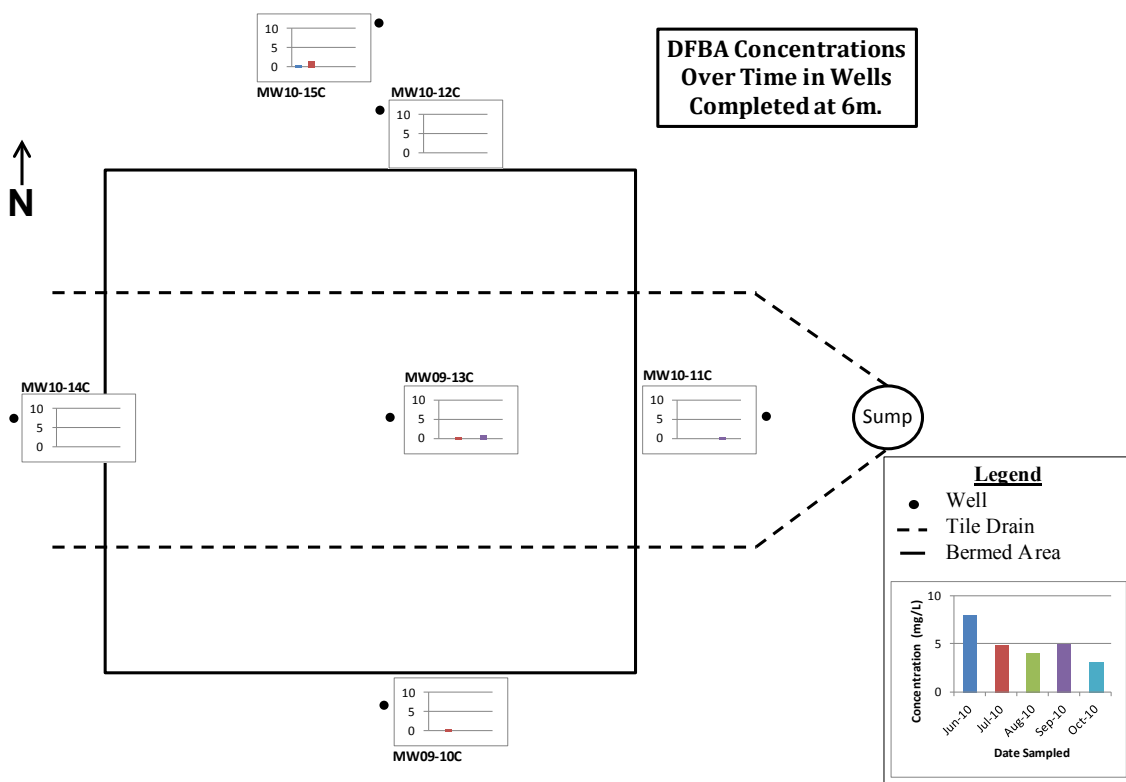


Figure 6.7. Plan view map of DFBA detections in C series monitoring wells in 2010.

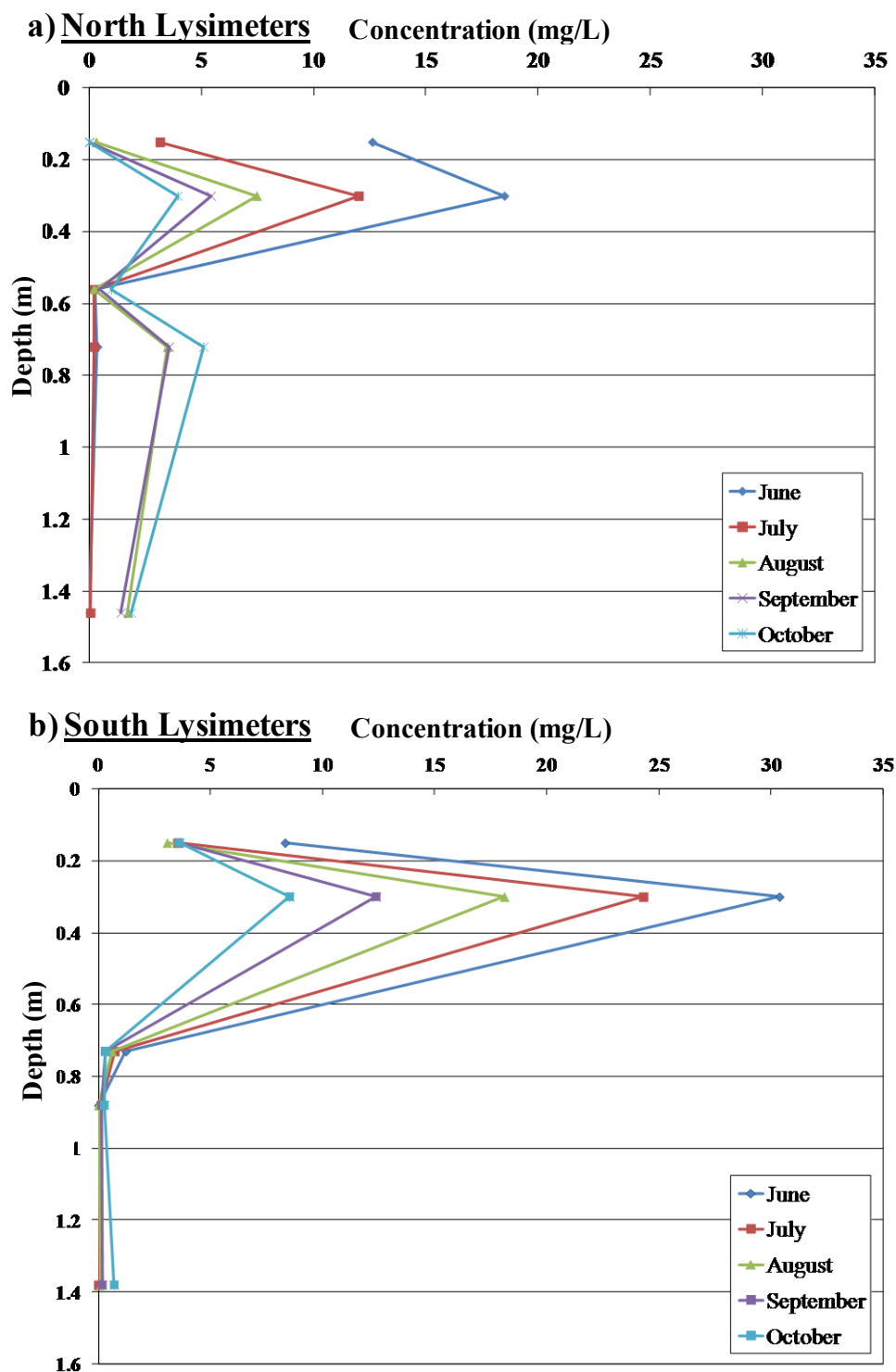


Figure 6.8. North (a) and south (b) lysimeter DFBA depth profiles from June 2010 to October, 2010. The north nest lies above the north tile drain and the south nest lies in the center of the plot, between the tile drains.

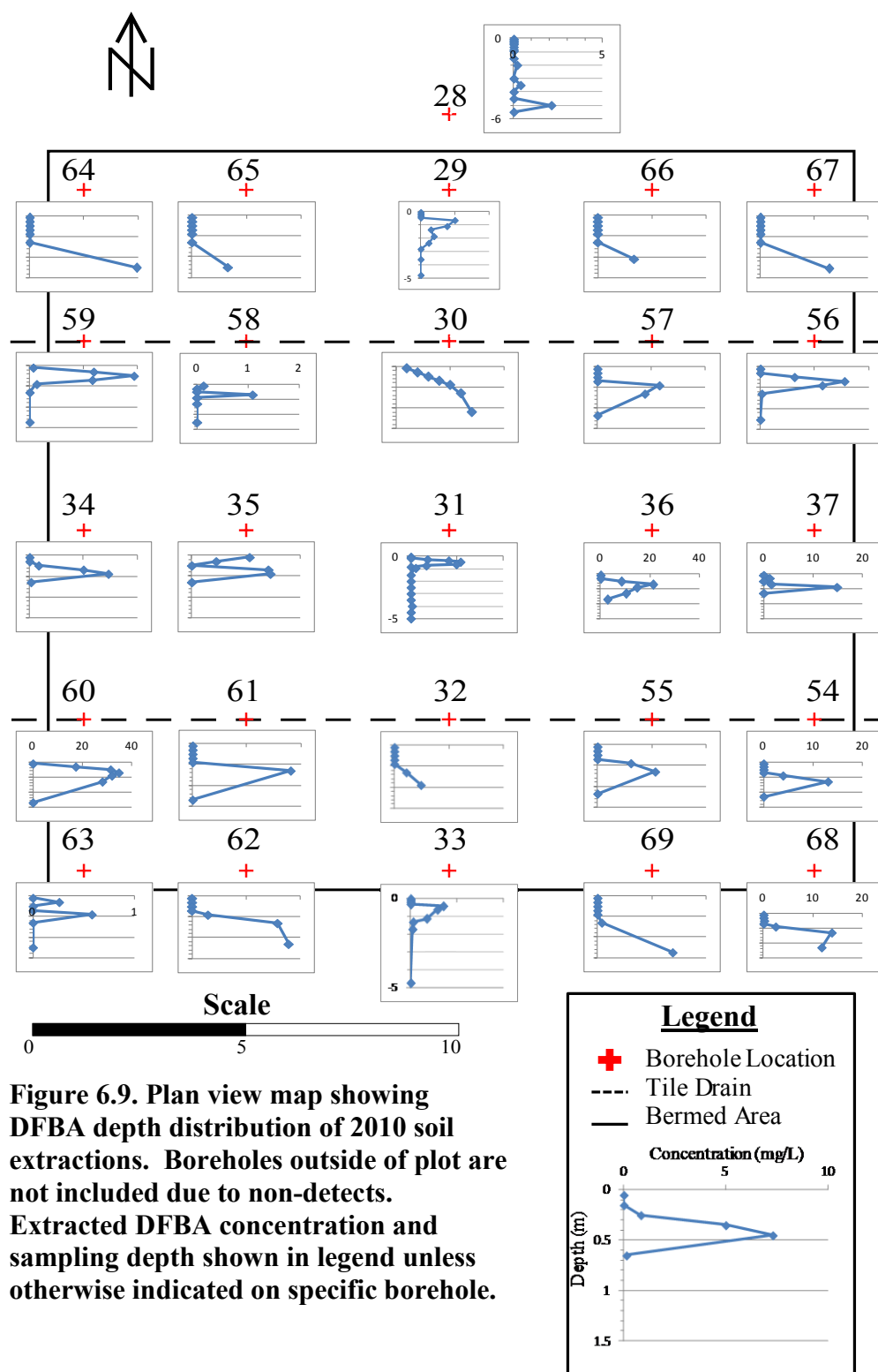


Table 6.3. Summary of DFBA mass recovery at the end of the 2010 season compared against the total mass applied (M_0) at the beginning of the 2009 season. Soil extraction numbers have been corrected based on the DFBA soil extraction method (Section 4.5.2.2)

	2010 Mass recovered (g)	M/M_0
South Tile	180	4.00
North Tile	116	2.58
Combined Tile Flow	296	6.58
Soil Extraction (Corrected)	1430	31.76
Total	1730	38.34

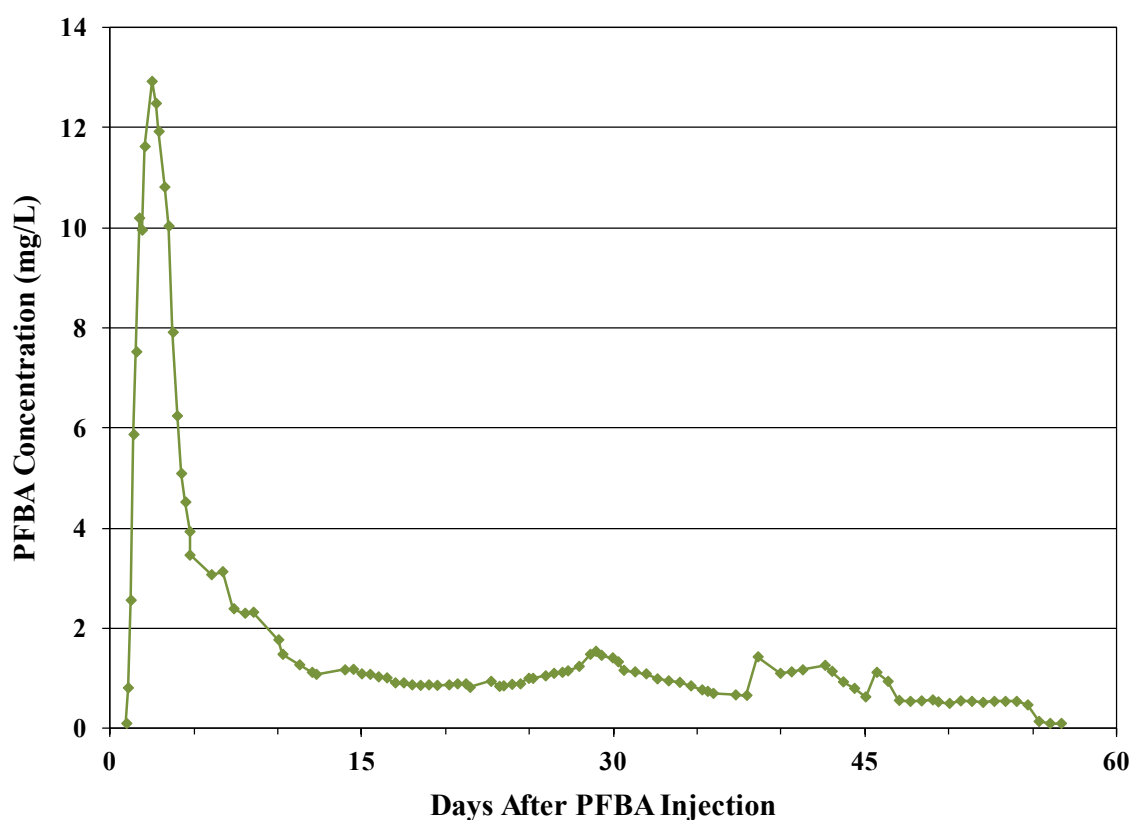


Figure 6.10. Monitored breakthrough of PFBA in North tile during the 2010 season.

Table 6.4. Summary of the reported literature values of the main calibration variables K_{sf} , ω and a as well as their effect on the simulated tile drain flow.

Calibrated Parameter	Literature Value	Simulated Tile Drain Response to Changing Parameter	Literature Sources
$K_{sf} (mm/day)$	3300 - 22288	Magnitude of peak flow and responsiveness to precip/irrigation events largely determined by K_{sf} . Matching magnitude and timing of flow events was done by changing this value for the glaciolacustrine and top soil unit.	Simunek et al., 2003; Gerke and Kohne, 2004; Gardenas et al., 2006
ω	0.03 - 0.05	Literature values increased the tile drain flow higher than observed values. Decreasing the value too low resulted in a tile drain response unable to capture precip/irrigation events.	Simunek et al., 2003; Gerke and Kohne, 2004; Gardenas et al., 2006
$a (mm)$	10	Controlled the rate and sensitivity of the macropore influence in tile drain response. Decreasing the value increased the tile drain sensitivity to precip/irrigation events. Increasing the value slowed the transfer rate of fluid moving from the matrix domain into the macropores.	Simunek et al., 2003; Gerke and Kohne, 2004

Table 6.5. Parameters used in base case simulation for matrix, macropore, fluid mass transfer and solute mass transfer.

Material	Matrix Hydraulic Parameters					
	θ_r	θ_s	α_m (mm ⁻¹)	n_m	K_{sat} (mm/d)	l
Top Soil	0.0001	0.39	0.001	1.48	120	0.5
Glaciolacustrine silt	0.0001	0.38	0.002	1.23	0.5	0.5
Glacial Till	0.07	0.36	0.0005	1.09	0.5	0.5
B Series Fine - Medium Sand	0.045	0.43	0.0145	2.68	125	0.5
Infiltration Unit	0	0.8	0.01	2	7000	0.5

Material	Macropore Hydraulic Parameters					
	θ_{rf}	θ_{sf}	α_f (mm ⁻¹)	n_f	K_{sf} (mm/d)	l
Top Soil	0	0.8	0.01	2	35000	0.5
Glaciolacustrine silt	0	0.8	0.01	2	35000	0.5
Glacial Till	0	0.8	0.01	2	35000	0.5
B Series Fine - Medium Sand	0.045	0.43	0.0145	2.68	125	0.5
Infiltration Unit	0	0.8	0.01	2	7000	0.5

Material	Fluid Mass Transfer Parameters					Solute Mass Transfer Parameter
	ω	β	γ	a (mm)	K_{as} (mm/d)	α_s (d ⁻¹)
Top Soil	0.0025	3	0.4	7	0.01	0.25
Glaciolacustrine silt	0.0025	3	0.4	5	0.01	0.25
Glacial Till	0.0025	3	0.4	25	0.01	0.25
B Series Fine - Medium Sand	0.0025	3	0.4	5	0.01	0.25
Infiltration Unit	0.0025	3	0.4	7	0.01	0.25

Table 6.6. Results of sensitivity analysis normalized against base case simulation. Values less than 1 indicate the simulation results fit closer to observed data than base case results.

Parameter Tested	Normalized RMSE of Simulated Tile Drain Flow	Normalized RMSE of Simulated Tile Drain Effluent DFBA
$\alpha_m = .0005$	1.12	1.05
$\alpha_m = .006$	1.13	0.98
$n = 1.13$	1.03	1.00
$n = 1.35$	1.02	1.05
$K_{sa} = .05$	1.01	0.97
$K_{sa} = .005$	1.13	1.06
$\omega = .00075$	1.26	1.27
$\omega = .025$	4.50	1.21
$K_{sf} = 5000$	1.37	0.96
$K_{sf} = 50000$	1.03	1.01
$a = 2.5$	1.20	1.52
$a = 15$	1.38	2.08
$\alpha_s = 1$	N/A	1.14
$\alpha_s = .01$	N/A	1.69
$\alpha_s = .1$	N/A	1.49
$\alpha_s = 0.05$	N/A	1.02
Retardation ($K_d = 0.0789$)	N/A	1.07
Base case	1	1

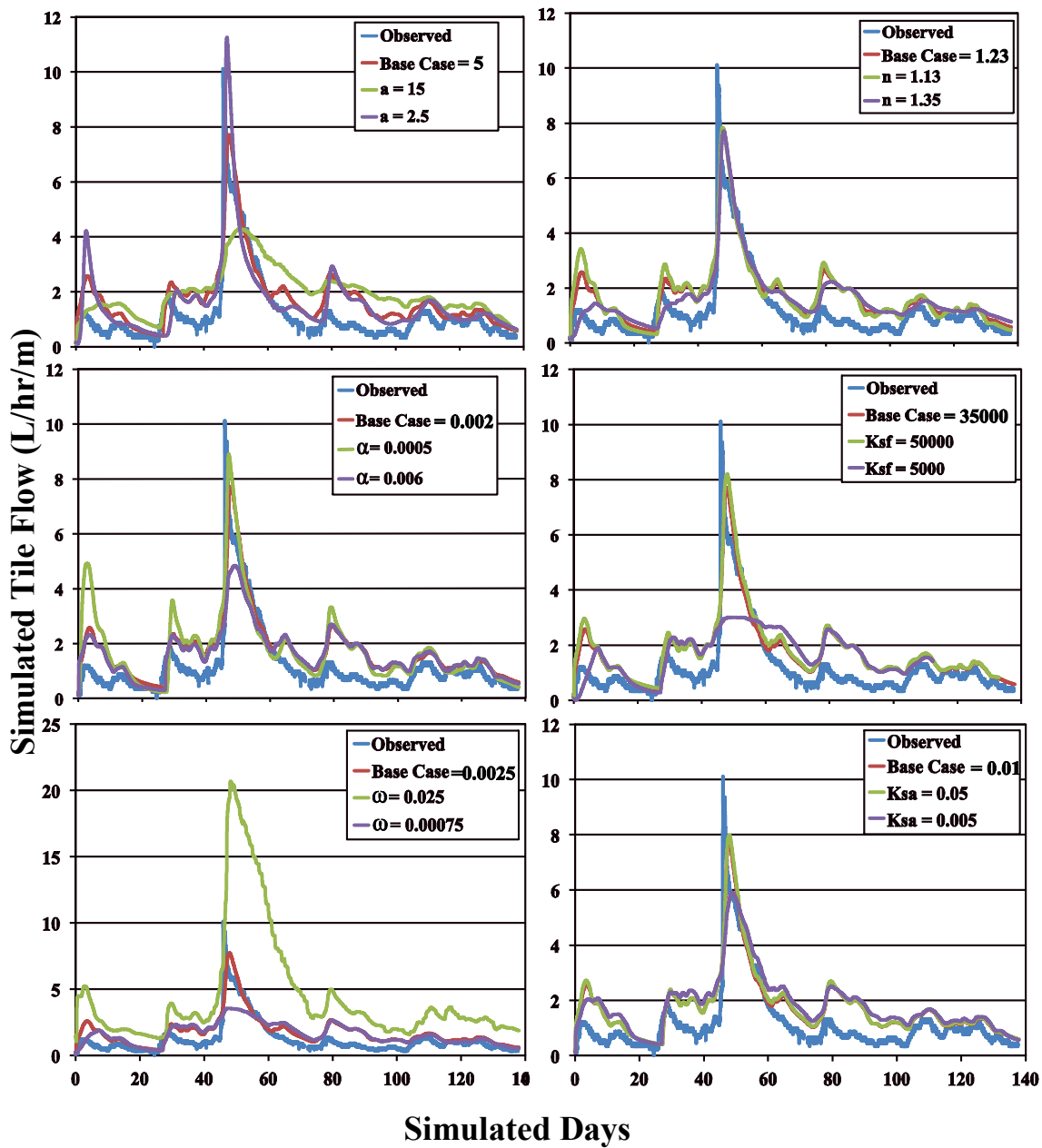
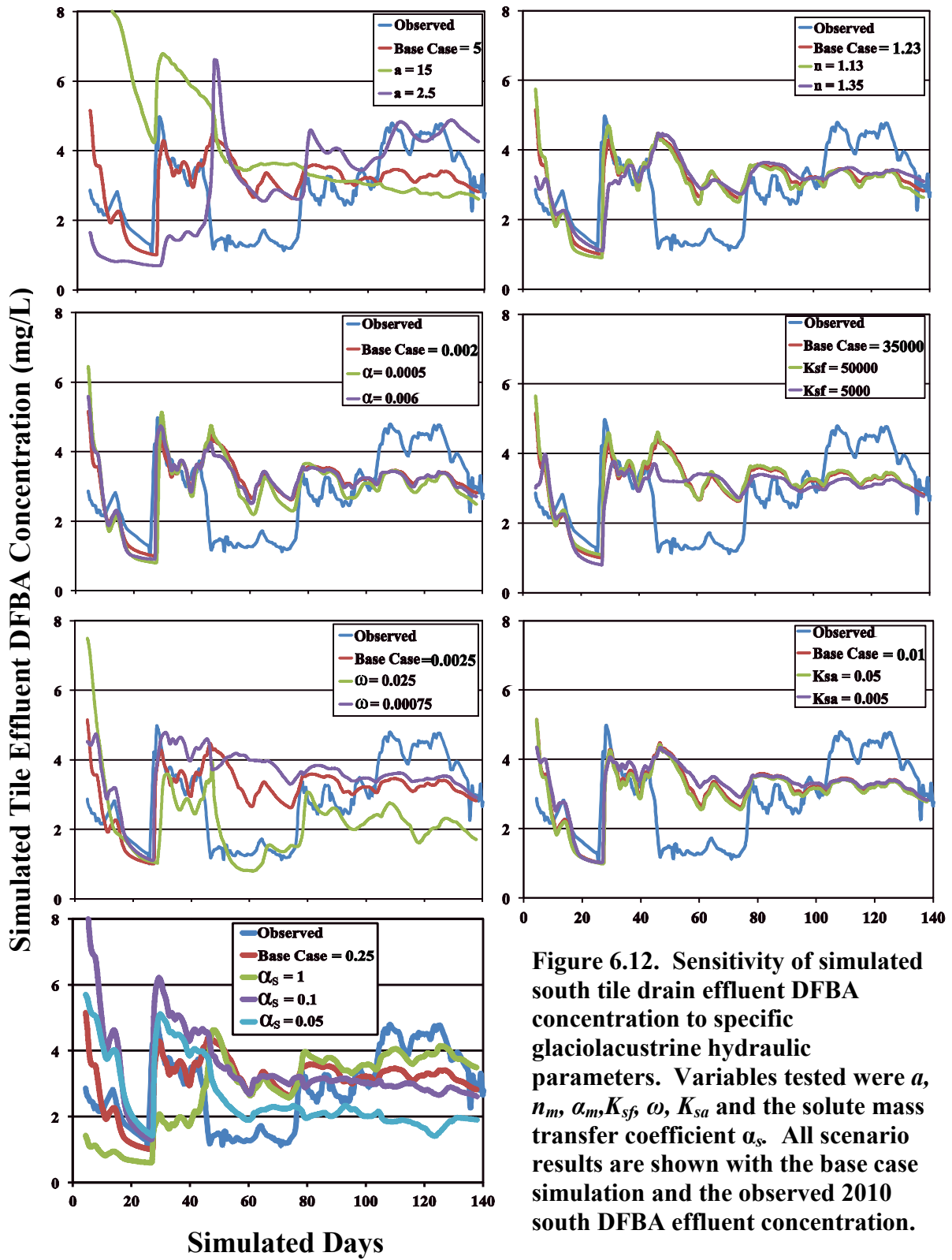


Figure 6.11. Sensitivity of simulated tile drain flow when specific glaciolacustrine hydraulic parameters were changed. Variables tested were a , n_m , α_m , K_{sf} , ω , K_{sa} . Results are shown with the base case simulation results and the observed 2010 south tile drain flow. Note the different scale used for the ω simulations.



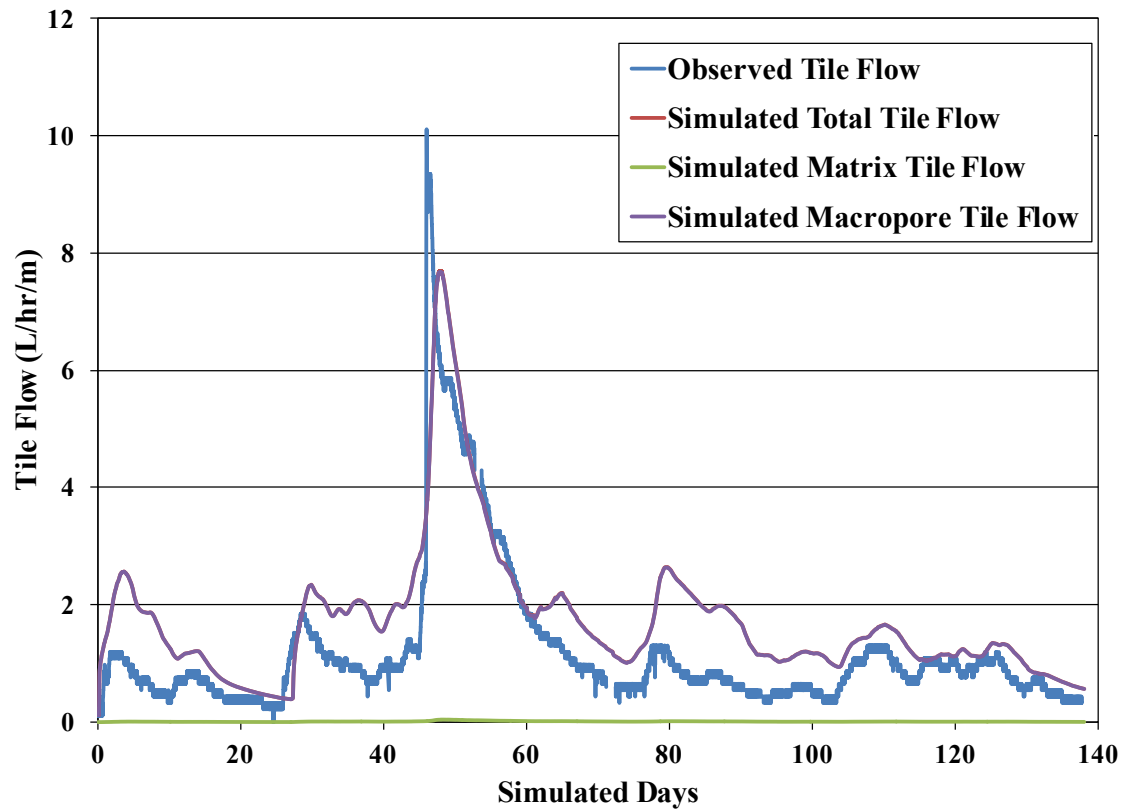


Figure 6.13. Results of base case 2010 simulation of south drain tile flow. Flow measured in tile drain is separated into matrix, macropore and combined flow components all of which are compared to the observed 2010 south tile drain flow.

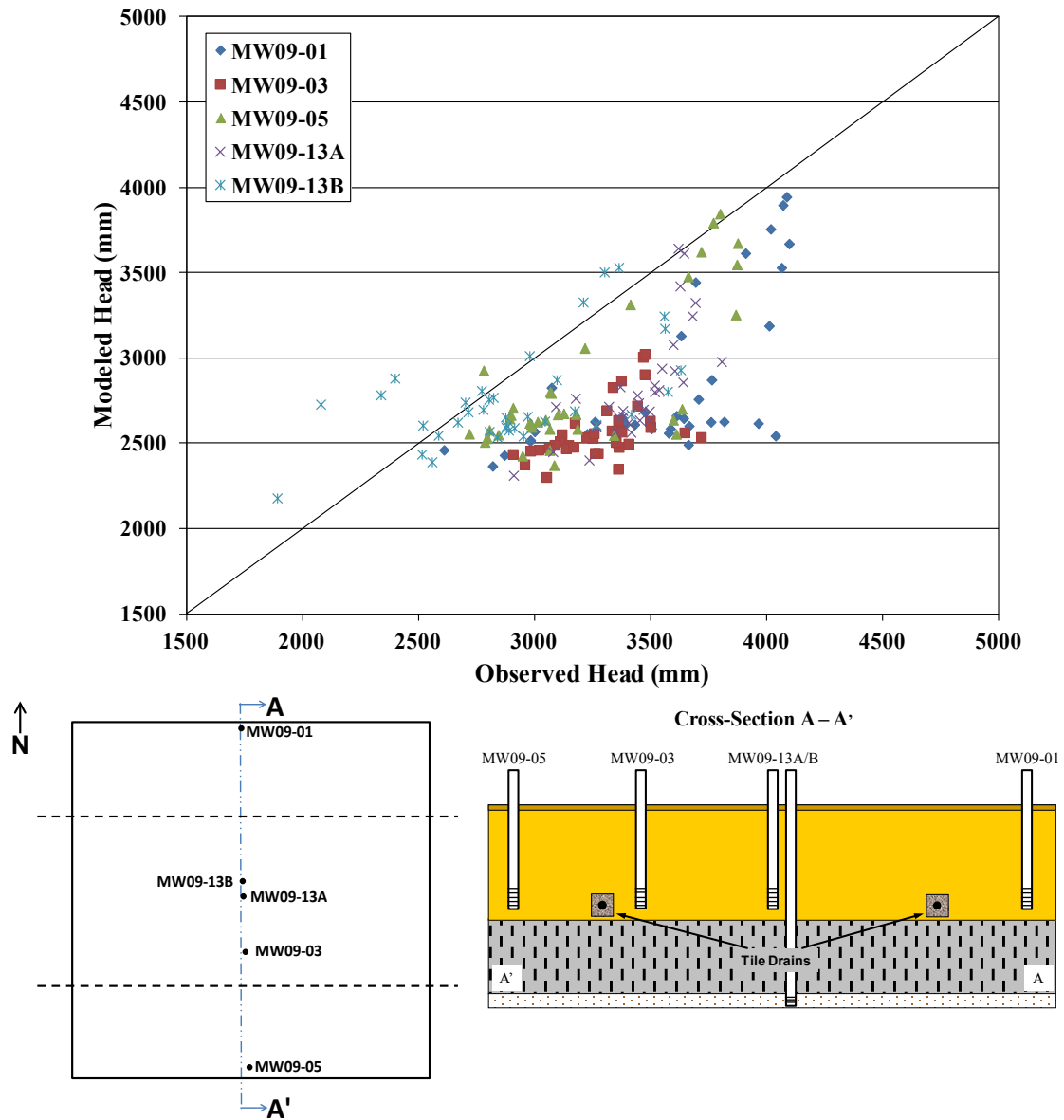


Figure 6.14. Comparison of observed and simulated hydraulic heads selected monitoring wells at 37 different times throughout the simulation period. Locations of wells are indicated in the map and cross-section shown below.

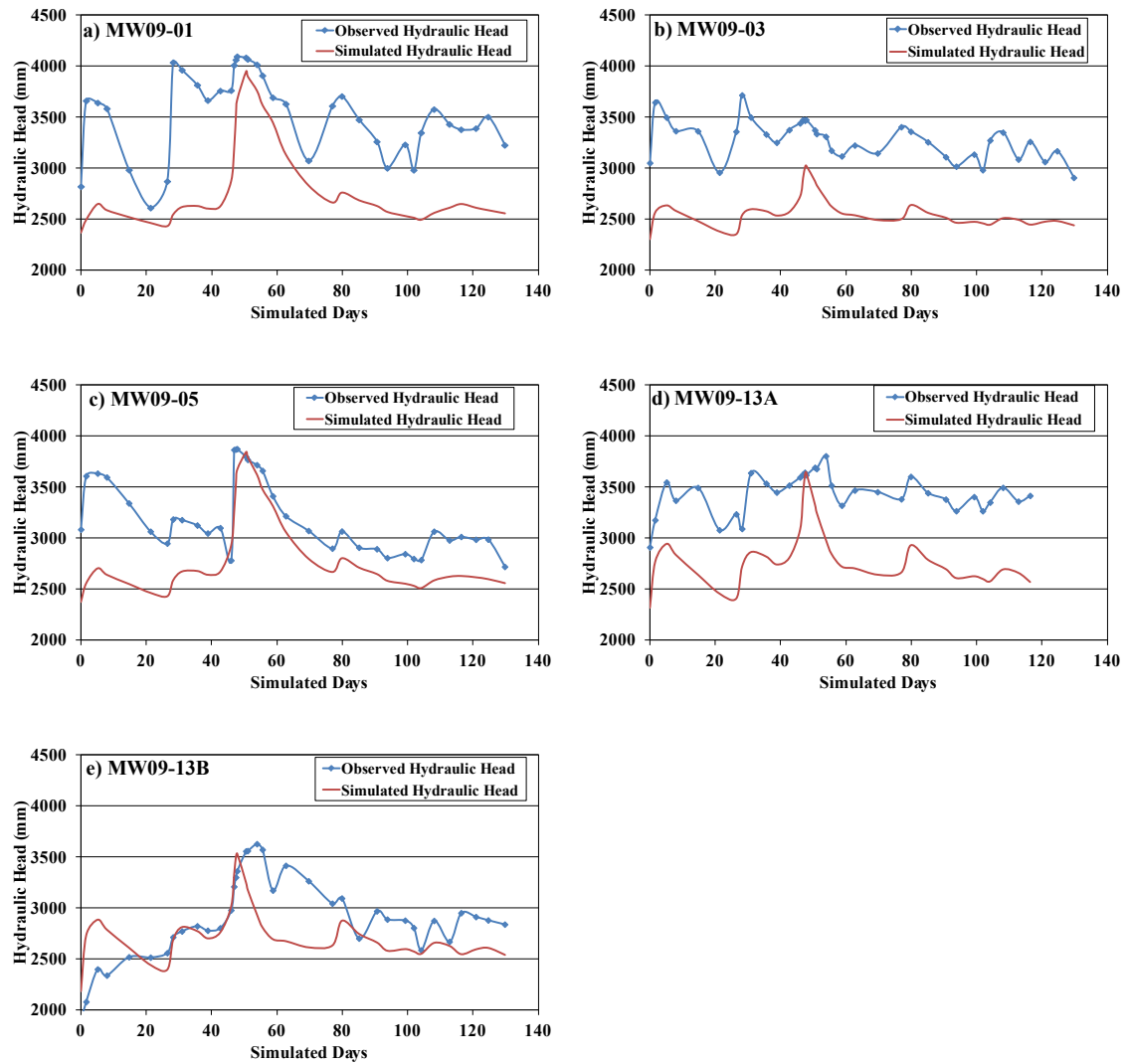


Figure 6.15. Comparison of simulated and observed hydraulic heads measured throughout the simulation period of 2010. Monitoring wells compared are MW09-01 (a), MW09-03 (b), MW09-05 (c), MW09-13A (d) and MW09-13B (e).

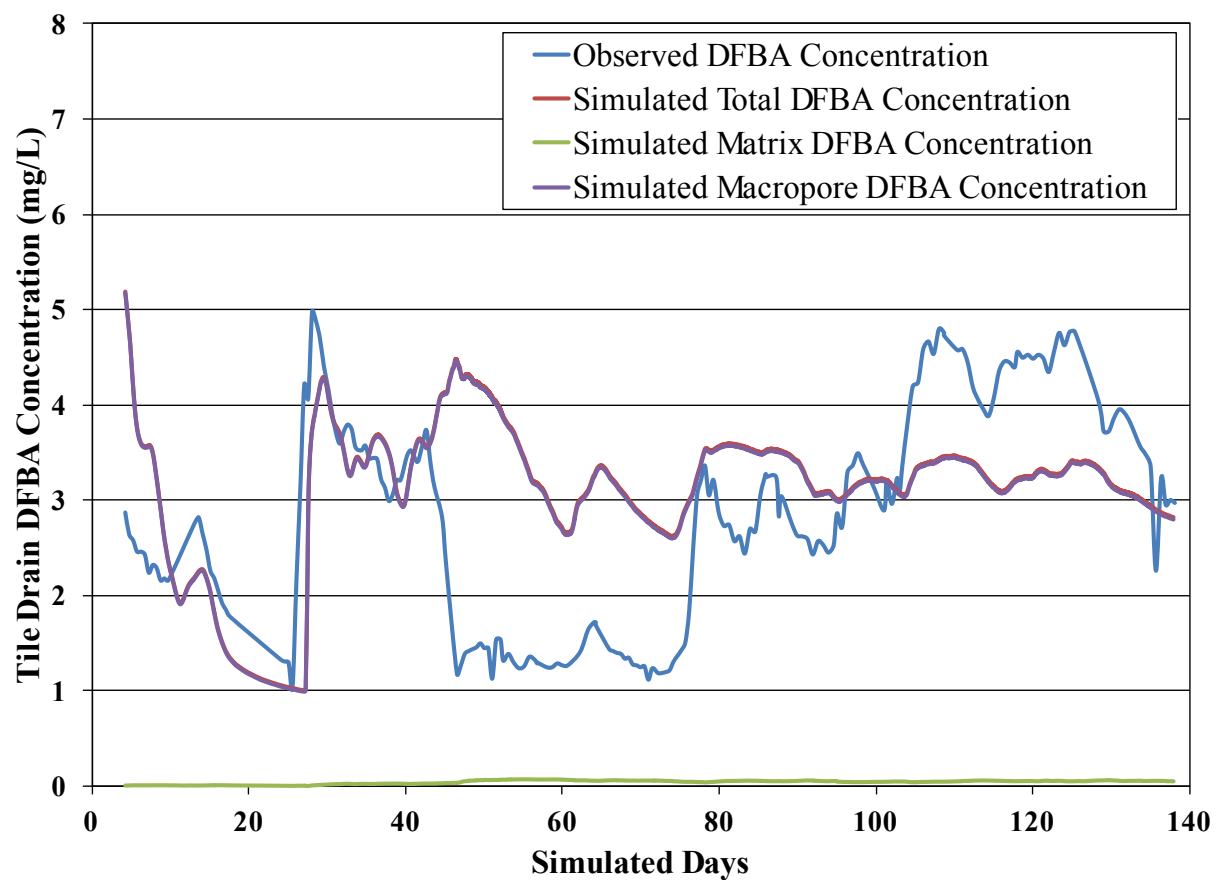
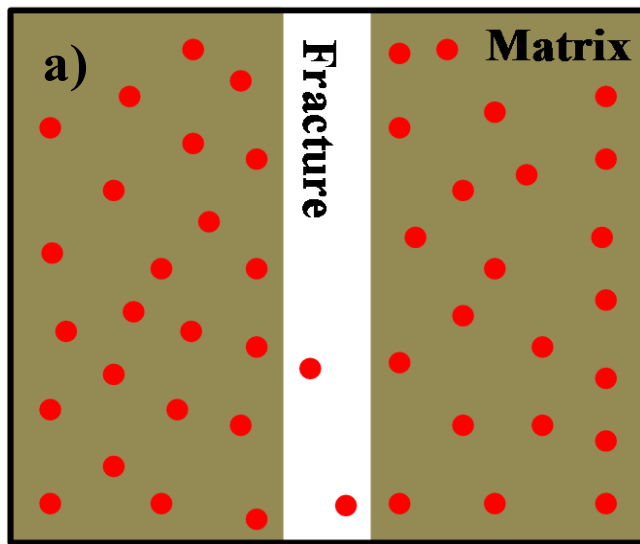
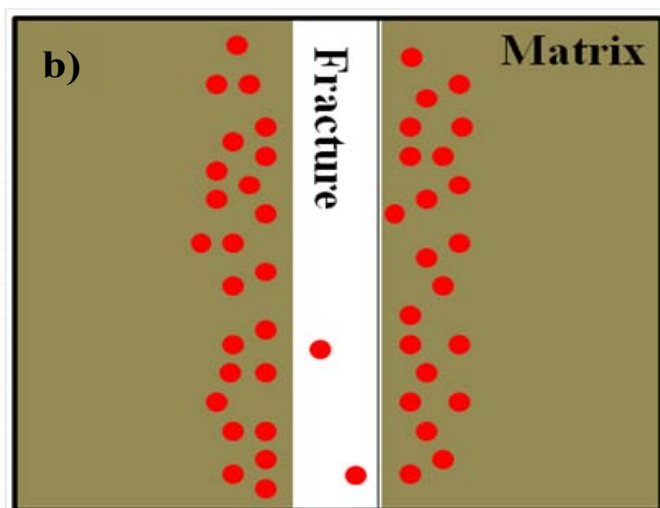


Figure 6.16. Results of base case simulation of the 2010 south drain effluent DFBA concentration. DFBA transport into tile drain is separated into matrix, macropore and combined flow components all of which are compared to the observed 2010 south effluent DFBA measured concentration.

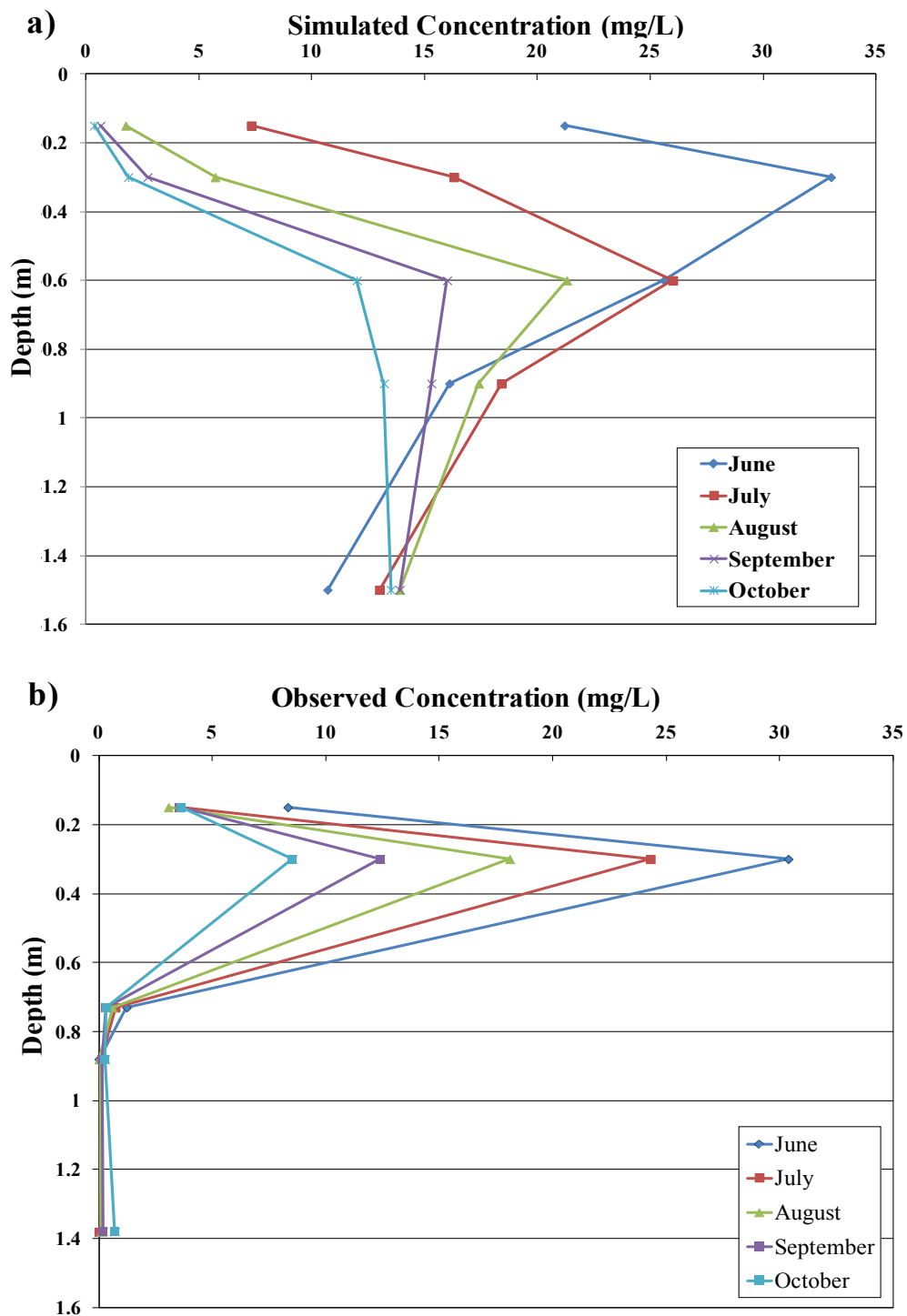


● DFBA



● DFBA

Figure 6.17. Schematic diagram comparing how DFBA tracer mass is spatially distributed in (a) the numerical model versus (b) the field at the start of the 2010 season.



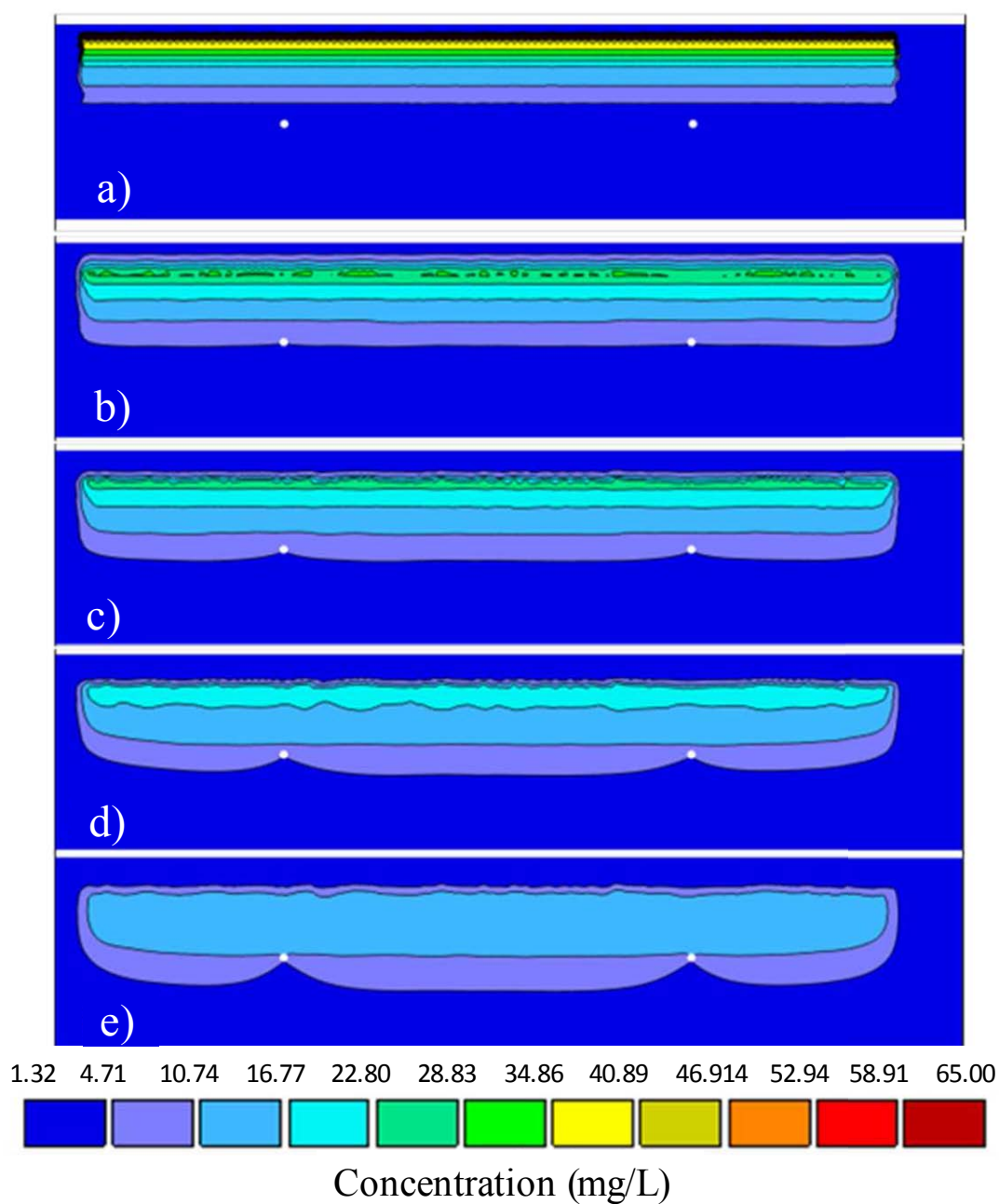


Figure 6.19. Time lapse of simulated DFBA concentrations in the matrix domain at (a) $t=0$ days, (b) $t=36$ days, (c) $t=51$ days, (d) $t=80$ days, (e) $t=138$ days.

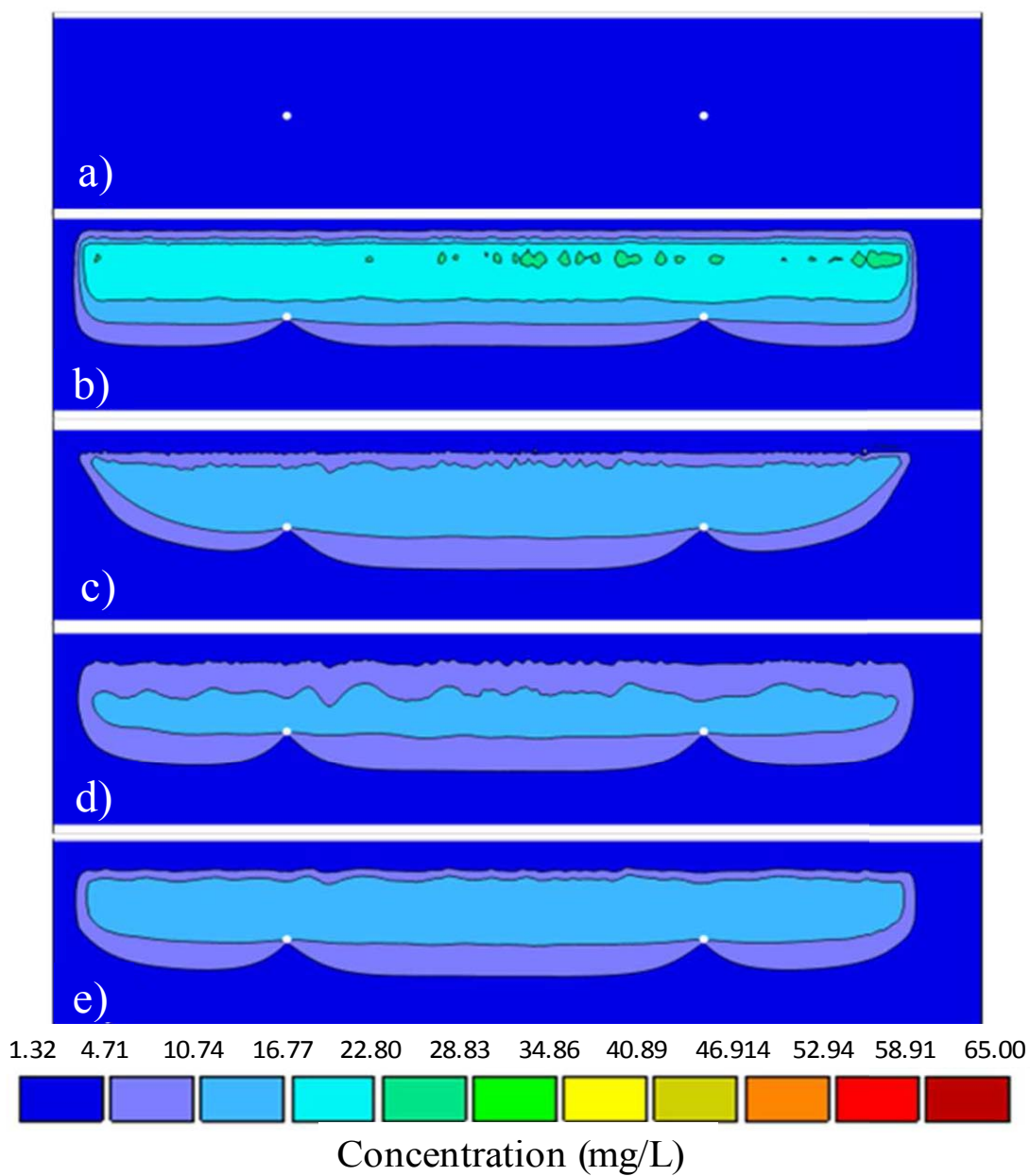


Figure 6.20. Time lapse of simulated DFBA concentration in the macropore domain at (a) $t=0$ days, (b) $t=36$ days, (c) $t=51$ days, (d) $t=80$ days, (e) $t=138$ days.

CHAPTER SEVEN: CONCLUSIONS AND FUTURE WORK

7.1 Conclusions

Results from both the tile drain monitoring and tracer experiments showed macropores were influential in both fluid flow and solute transport in low permeability soils. The quick DFBA (46.75 hrs) and PFBA (13 hrs) tile drain breakthrough and the rapid response of the tile drains to irrigation/precipitation events indicated that macropores were controlling how water and solutes were transported to subsurface tile drains. The large macropore influence was also illustrated by the quick detection of DFBA in monitoring well samples and the results from the numerical simulations showed that 99% of the fluid flow and solute transport occurred in the macropores. The significance of having a large macropore influence in a remediation site is that limited volume water passes through the matrix, hindering the salt flushing capabilities. The macropores are able to transmit large portions of the water to the drains, while only exposing a small percentage of the matrix to fresh water.

Although macropores are responsible for almost all solute transport to the tile drains, matrix flushing appears to be occurring. This is shown by the reduction of DFBA concentrations observed in the suction lysimeters and by the reduction of mass in the soil core extractions at the end of the 2010 season. Results from the soil degradation experiments have shown that no measurable amount of DFBA degradation has occurred, therefore, it can be concluded that removal of DFBA has occurred via mass transfer between the matrix and the macropores and subsequent transport deeper in the soil profile (i.e., to the tile drains or deeper sand units). Results from the numerical model further

support the hypothesis that matrix flushing has occurred with simulated DFBA mass loss observed in the matrix domain and in the simulated lysimeters. Understanding the solute mass transfer process that occurs between the matrix and macropore domains and determining the rate at which solute migrates from the matrix into the macropores will allow for a quicker, more efficient remediation of in situ salt. Determining the optimal irrigation rates for maximizing salt removal will help accelerate the remediation process and limit the amount of water required for irrigation and disposal.

Numerically, the model does a successful job at simulating the breakthrough and the dynamic response of the tile drain flow, but cumulatively overestimates the total drain discharge by 50 %. Additionally, the model consistently underestimates observed hydraulic heads, which could be caused by not incorporating vertical anisotropy in the matrix and macropore domains. The DFBA transport simulations do not accurately capture most of the observed tile drain DFBA concentration response. The model is able to simulate the early time tile drain DFBA response (before 40 days), but struggles to match the observed data for the remainder of the simulation. The solute mass transfer term in the model does not appear to accurately represent the physical processes occurring. Furthermore, the model underestimates the transport of DFBA beyond the tile drains and into the lower sand unit. Additional model refinement is needed in order to accurately capture the transport of DFBA and salt to the lower sand unit.

7.2 Future Work

Continual monitoring (soil geochemistry, near surface geophysics) of the field site is needed until soil conditions meet Alberta Environment remediation guidelines. Furthermore, developing a strategy targeted at reducing the volume of water and time needed to remediate a site would help this remediation technique to be used in similar sites in the future. More advanced modeling of the site will also require the use of vertical anisotropy as well as geochemical modeling to describe how the major ion chemistry influences solute transport and the hydraulic parameters of the soils. As previously mentioned in Sec 3.1, hydraulic conductivities of soil can vary when exposed to changing levels of sodium. Removing salts will alter the geochemistry of the soil, changing the hydraulic parameters. This should be accounted for in future simulations. Additionally, accurately deriving the van Genuchten macropore properties by running small scale laboratory experiments on soil core would help constrain the simulated macropore properties used in the model. This could help reduce the model uncertainty and provide more accurate results.

In conjunction with this project, large amounts of chloride data have been collected during the monitoring program. Although the chloride flushing analysis lies outside this project's scope of work, much of the model construction and calibration has created a foundation for future model runs to be completed. The chloride has a much different initial distribution than the benzoic acid tracers and together with the observed tile concentration data will be used to further improve the flow and transport model, particularly calibration of the solute mass exchange parameters. The revised model will

allow for estimations of salt remediation times under various conditions. Additional forward model runs with differing tile drain spacing and alternative flushing methods (continual irrigation vs infrequent irrigation pulses) will help in designing more efficient remediation strategies for future salt contaminated sites. Construction of a site wide 3-dimensional model would be beneficial to develop a stronger understanding of the salt migration and to determine if any further remediation methods are needed (additional soil removal from site).

Finally, additional long-term studies investigating the influence macropores have on solute transport are needed to better understand how solute transfer processes may vary with time. Most research programs are only aimed at looking at the initial breakthrough and migration of solutes, lasting no more than four months. By increasing the length of time monitoring the migration of the solute, a stronger understanding can be developed on how solute mass transfer processes evolve. Developing a stronger understanding of matrix-macropore mass transfer processes would help create more robust dual domain models.

REFERENCES

- Abrol, I.P., Yadav, J.S.P, and Massoud, F.I., 1988. Salt-Affected Soils and Their Management. FAO Soils Bulletin 39. Food and Agriculture Organization of the United Nations. Rome, 1988.
- Alberta Agriculture. 1991. Dryland Saline Seep Control. Agdex 518-11. Alberta Agriculture and Agriculture Canada. 12 pp.
- Allaire-Leung, S.E., Gupta, S.C. and Moncrief, J.F., 2000. Water and Solute Movement in Soil as Influenced by Macropore Characteristics 1. Macropore Continuity. *Journal of Contaminant Hydrology*, 41: 283-301.
- Allen, R.G., Pereira, L.S., Raes. D. and Smith, M., 1998. Crop Evapotranspiration – Guidelines for Computing Crop Water Requirements – FAO Irrigation and Drainage Paper 56. Natural Resources Management and Environment Department.
- Allison, G.B., Gee, G.W. and Tyler, S.W., 1994. Vadose-Zone Techniques for Estimating Groundwater Recharge in Arid and Semiarid Regions. *Soil Science Society of America Journal*, 58: 6-14.
- Amrhein, C., and Suarez, D.L., 1990. Procedure for Determining Sodium-Calcium Selectivity in Calcareous and Gypsiferous Soils. *Soil Science Society of America Journal*, 54: 999-1007.
- Appelo, C.A.J. and Postma, D., 2005. *Geochemistry, Groundwater and Pollution*. Second Edition. A.A.Balkema, Amsterdam, 649 pp.
- ASTM International., 2007. Standard Test Method for Measurement of Hydraulic Conductivity of Porous Material Using a Rigid-Wall, Compaction-Mold Permeameter. Designation: D 5856 -95 (Reapproved 2007). ASTM International, West Conshohocken, PA.
- Balasubramanian, V., Kanehiro, Y., Rao, P.S.C, and Green, R.E., 1973. Field Study of Solute Movement in a Highly Aggregated Oxisol with Intermittent Flooding: 1. Nitrate. *Journal of Environmental Quality*, 2: 359-362.
- Beven, K. and Germann, P., 1982. Macropores and Water Flow in Soils. *Water Resources Research*, 18: 1311-1325.
- Bouma, J., 1981. Soil Morphology and Preferential Flow Along Macropores. *Agricultural Water Management*, 3: 235-250.
- Bowman, R.S., 1984a. Evaluation of Some New Tracers for Soil Water Studies. *Soil Science Society of America Journal*, 48: 987-993.

- Bowman, R.S., 1984b. Analysis of Soil Extracts for Inorganic and Organic Tracer Anions via High-Performance Liquid Chromatography. *Journal of Chromatography*, 285: 467-477
- Bowman, R.S. and Gibbens, J.F., 1992. Difluorobenzoates as Nonreactive Tracers in Soil and Ground Water. *Ground Water*, 30: 8-14
- Brusseasu, M.L. and Rao, P.S.C., 1990. Modeling Solute Transport in Structured Soils: A Review. *Geoderma*, 46: 169-192.
- Chen, S., Franklin, R.E., Quisenberry, V.L. and Dang, P., 1999. The Effect of Preferential Flow on the Short and Long-Term Spatial Distribution of Surface Applied Solutes in a Structured Soil. *Geoderma*, 90: 229-241.
- Dahan, O. and Ronen, Z., 2001. Analytical Procedure of Simultaneous Use of Seven Fluorobenzoates in Multitracer Tests. *Ground Water*, 39: 366-370.
- Environment Canada, 2011. Canadian Climate Normals 1971 – 2000. Environment Canada Weather Office.
- Fetter, C.W., 1999. Contaminant Hydrogeology. Second Edition. Prentice Hall Inc., Upper Saddle River, New Jersey. 500 pp.
- Fetter, C.W., 2001. Applied Hydrogeology. Prentice Hall Inc., Upper Saddle River, New Jersey, 598 pp.
- Freeze, R.A. and Cherry, J.A., 1979. Groundwater. Prentice Hall Inc., Englewood Cliffs, New Jersey, 604 pp.
- Foster, S.S.D, 1975. The Calk Groundwater Tritium Anomaly – A Possible Explanation. *Journal of Hydrology*, 25: 159-165.
- Gardenas, A.I., Simunek, J., Jarvis, N. and van Genuchten, M.T., 2006. Two-Dimensional Modeling of Preferential Water Flow and Pesticide Transport from Tile-Drained Field. *Journal of Hydrology*, 329: 647-660
- Gelhar, L.W., Welty, C., and Rehfeldt, K.R., 1992. A Critical Review of Data on Field-Scale Dispersion in Aquifers. *Water Resources Research*, 28: 1955-1974.
- Gerke, H.H., and van Genuchten, M.T., 1993a. A Dual-Porosity Model for Simulating the Preferential Movement of Water and Solutes in Structured Porous Media. *Water Resources Research*, 29: 305-319.

- Gerke, H.H and van Genuchten, M.T., 1993b. Evaluation of a First-Order Water Transfer Term for Variably Saturated Dual-Porosity Flow Models. *Water Resources Research*, 29: 1225-1238.
- Gerke, H.H., and van Genuchten, M.T., 1996. Macroscopic Representation of Structural Geometry for Simulating Water and Solute Movement in Dual-Porosity Media. *Advances in Water Resources*, 19: 343-357.
- Gerke, H.H and Kohne, M.J., 2004. Dual-Permeability Modeling of Preferential Bromide Leaching from a Tile-Drained Glacial Till Agricultural Field. *Journal of Hydrology*, 289: 239-257.
- Gish, T.J. and Kung, K-J.S., 2007. Procedure for quantifying a solute flux to a shallow perched water table. *Geoderma*, 138: 57-64.
- Gjettermann, B., Nielsen, K.L., Petersen, C.T., Jensen, H.E. and Hansen, S., 1997. Preferential Flow in Sandy Loam Soils as Affected by Irrigation Intensity. *Soil Technology*, 11: 139-152.
- Government of Alberta, Department of Agriculture. 2010. Management of Sodic Soils in Alberta. *Agri-Facts*. June 2010.
- Government of Alberta, Department of Agriculture and Rural Development. 2009. Drought Report for the Agricultural Region of Alberta, June 23, 2009. *Agriculture Soil Moisture Updates*.
- Government of Alberta, Industry and Economy. 2011. <http://alberta.ca/home/181.cfm>. Page accessed December 6, 2011.
- Haynes, R.H., 2005. The Canadian System of Soil Classification, Third Edition. NRC Research Press., Ottawa, Ontario. 187 pp.
- Hu, Q. and Moran, J.E., 2005. Simultaneous Analyses and Applications of Multiple Fluorobenzoate and Halide Tracers in Hydrologic Studies. *Hydrological Processes*, 19: 2671-2687
- Jamieson, R.C., Gordon, R.J., Sharples, K.E., Stratton, G.W., and Madani, A., 2002. Movement and Persistence of Fecal Bacteria in Agricultural Soils and Subsurface Drainage Water: A Review. *Canadian Biosystems Engineering*. 44: 1.1-1.9.
- Jarvis, N.J., 1995. Simulation of Soil Water Dynamics and Herbicide Persistence in Silt Loam Soil Using the MACRO Model. *Ecological modeling*, 81: 97-109.

- Jarvis, N.J., 2007. A Review of Non-Equilibrium Water Flow and Solute Transport in Soil Macropores; Principles, Controlling Factors and Consequences for Water Quality. *European Journal of Soil Science*, 58: 523-546.
- Jaynes, D.B., 1994. Evaluation of Fluorobenzoate Tracers in Surface Soils. *Ground Water*, 32: 532-53.
- Jaynes, D.B., Colvin, T.S., Karlen, D.L., Cambardella, C.A., and Meek, D.W., 2001. Nitrate Loss in Subsurface Drainage as Affected by Nitrogen Fertilizer Rate. *Journal of Environmental Quality*, 30:1305-1314.
- Johnson, G.R., Gupta, K., Putz, D.K., Hu, K. and Brusseau, M.L., 2003. The Effect of Local-Scale Physical Heterogeneity and Nonlinear, Rate-Limited Sorption/Desorption on Contaminant Transport in Porous Media. *Journal of Contaminant Hydrology*, 64: 35-58.
- Kladivko, E.J., Grochulska, J., and Turco, R.F., 1999. Pesticide and Nitrate Transport into Subsurface Tile Drains of Different Spacings. *Journal of Environmental Quality*, 28: 997-1004.
- Kladivko, E.J., Frankenberger, J.R., Jaynes, D.B., Meek, D.W., Jenkinson, B.K., and Fausey, N.R., 2004. Nitrate Leaching to Subsurface Drains as Affected by Drain Spacing and Changes in Crop Production System. *Journal of Environmental Quality*, 33: 1803-1813.
- Klute, A., 1986. *Methods of Soil Analysis, Part 1. Physical and Mineralogical Methods*. Second Edition. Soil Science Society of America. Madison, Wisconsin, 1188 pp.
- Kodikara, J.K., Rahman, F., and Barbour, S.L., 2002. Towards a More Rational Approach to Chemical Compatibility Testing of Clay. *Canadian Geotechnical Journal*, 39: 597-607.
- Kohne, M.J., and Gerke, H.H., 2005. Spatial and Temporal Dynamics of Preferential Bromide Movement Towards a Tile Drain. *Vadose Zone Journal*, 4: 79-88.
- Komex International, 1997. Assessment Report for the Satellite at XX-XX-50-26 W4M. Komex International LTD.
- Komex International, 1999. Supplementary Site Characterization of the Abandoned Satellite at XX-XX-50-26 W4M. Komex International LTD. Report Number KE-460.9.
- Komex International, 2003. Construction Report Drainage Field Installation XX-XX-50-26 W4M. Komex International LTD. Report Number E04600910.
- Komex International, 2005. 2004 Monitoring Program XX-XX-50-26 W4M Drainage Field. Komex International LTD. Report Number E04600913-17.

Kung, K.-J. S., Klavdivko, E.J., Gish, T.J., Steenhuis, G., Bubenzer and G., Helling, C.S., 2000. Quantifying Preferential Flow by Breakthrough of Sequentially Applied Tracer: Silt Loam Soil. *Soil Science Society of America Journal*, 64: 1296-1304.

Lee, J., Jaynes, D.B. and Horton, R., 2000. Evaluation of a Simple Method for Estimating Solute Transport Parameters: Laboratory Studies. *Soil Science Society of American Journal*, 64: 492-498.

Maloszewski, P., and Zuber, A., 1993. Tracer Experiments in Fractured Rocks: Matrix Diffusion and the Validity of Models. *Water Resources Research*, 29: 2723-2735.

McCarthy, J.F., Howard, K.M., and McKay, L.D., 2000. Effect of pH on Sorption and Transport of Fluorobenzoic Acid Ground Water Tracers. *Journal of Environmental Quality*, 29: 1806-1813.

Mossop, G. and Shetsen, I., 1994. Geological Atlas of the Western Canada Sedimentary Basin. Canadian Society of Petroleum Geologists and the Alberta Research Council.

Natural Regions Committee, 2006. Natural Regions and Subregions of Alberta. Compiled by D.J. Downing and W.W. Pettapiece. Government of Alberta. Pub. No. T/852.

Nielsen, D.R., van Genuchten M.T. and Biggar, J.W., 1986. Water Flow and Solute Transport Processes in the Unsaturated Zone. *Water Resources Research*, 22: 89S-108S.

Paterson, B.A. and Brook Harker, D., 1980. Tile Drainage of Irrigated Till Soils in Alberta, in Eggleston, J., *Irrigation and Drainage Today's Challenges*, American Society of Civil Engineers. New York, New York. 263-273 pp.

Puls, R.W. and Barcelona, M.J., 1996. Low-Flow (Minimal Drawdown) Ground-Water Sampling Procedures. United States Environmental Protection Agency Ground Water Issue, EPA/504/S-95/504

Richard, T.L. and Steenhuis T.S., 1988. Tile Drain Sampling of Preferential Flow on a Field Scale. *Journal of Contaminant Hydrology*, 3: 307-325.

Shapiro, A.M., 2001. Effective Matrix Diffusion in Kilometer-Scale Transport in Fractured Crystalline Rock. *Water Resources Research*, 37: 507-522.

Simunek, J., Jarvis, N.J., van Genuchten, M.T. and Gardenas, A.I., 2003. Review and Comparison of Models for Describing Non-Equilibrium and Preferential Flow and Transport in the Vadose Zone. *Journal of Hydrology*, 272: 14-35.

- Simunek, J., van Genuchten, M.T. and Senja, M., 2006. The HYDRUS Software Package for Simulating the Two- and Three-Dimensional Movement of Water, Heat, and Multiple Solutes in Variable-Saturated Media. Technical Manual.
- Simunek, J. and van Genuchten, M.T., 2008. Modeling Nonequilibrium Flow and Transport Processes Using HYDRUS. *Vadose Zone Journal*, 7: 782-797.
- Smith, A.D., 2008. Evaluating Tile Drainage Systems as a Method of Salt Remediation in Alberta, Master of Science Thesis, University of Calgary, Department of Geoscience, Calgary, Alberta, Canada.
- Stone, W.W., and Wilson, J.T., 2006. Preferential Flow Estimates to an Agricultural Tile Drain with Implications for Glyphosate Transport. *Journal of Environmental Quality* . 35:1825-1835.
- Tanji, K.K., 1990. Agricultural Salinity Assessment and Management. American Society of Civil Engineers. New York, New York, 619 pp.
- Therrien, R., McLaren, R.G., Sudicky, E.A. and Panday, S.M., 2010. HydroGeoSphere: A Three-Dimensional Numerical Model Describing Fully-Integrated Subsurface and Surface Flow and Solute Transport. Technical Manual.
- van Genuchten, M.T., 1980. A Closed-form Equation for Predicting the Hydraulic Conductivity of Unsaturated Soils. *Soil Science Society of America Journal*, 44: 892-898.
- van Genuchten, M.T., Tang, D.H. and Guennelon, R., 1984. Some Exact Solutions for Solute Transport Through Soils Containing Large Cylindrical Macropores. *Water Resources Research*, 20: 335-346.
- van Genuchten, M.T., Leiji, F.J. and Yates, S.R., 1991. The RETC Code for Quantifying the Hydraulic Functions of Unsaturated Soils. Version 1.0. EPA Report 600/2-91/065, U.S. Salinity Laboratory, USDA, ARS, Riverside, California.
- Van Schaik, J.C. and Milne, R.A., 1961. Reclamation of a Saline-Sodic Soil with Shallow Tile Drainage. *Canadian Journal of Soil Science*, 42: 43-48.
- Weatherill, D., Graf, T., Simmons, C.T., Cook, P.G., Therrien, R., and Reynolds, D.A., 2008. Discretizing the Fracture-Matrix Interface to Simulate Solute Transport. *Ground Water*, 46: 606-615.
- Weiler, M., and Naef, F., 2003. An Experimental Tracer Study of the Role of Macropores in Infiltration in Grassland Soils. *Hydrological Processes*, 17: 477-493.

Wilkinson, A., 2011. Subsurface flow in an interbedded silt-sand unit containing tile drains, Bachelor of Science Thesis, University of Calgary, Department of Geoscience, Calgary, Alberta, Canada.

Wise, W.R., Clement, T.P. and Molz, F.J., 1994. Variably Saturated Modeling of Transient Drainage: Sensitivity of Soil Properties. *Journal of Hydrology*, 161: 91-108.

Zehe, E. and Fluhler, H., 2001. Preferential Transport of Isoproturon at a Plot Scale and a Field Scale Tile-Drained Site. *Journal of Hydrology*, 247: 100-115.

APPENDIX A: TRACER DATA

2009 North and south tile drain DFBA concentrations

North Tile		South Tile	
Date	Concentration (mg/L)	Date	Concentration (mg/L)
8/19/09 14:00	0.00	8/19/09 14:00	0.00
8/20/09 14:00	0.15	8/20/09 14:00	0.11
8/21/09 2:00	0.15	8/22/09 2:00	0.24
8/21/09 2:00	0.11	8/22/09 17:00	0.33
8/22/09 2:00	0.16	8/22/09 23:00	0.27
8/22/09 11:00	0.49	8/23/09 17:00	0.00
8/22/09 20:00	0.71	8/24/09 2:00	0.00
8/24/09 14:00	0.53	8/24/09 5:00	0.14
8/25/09 2:00	0.36	8/25/09 2:00	0.20
8/25/09 14:00	0.54	8/25/09 14:00	0.13
8/25/09 20:00	0.86	8/27/09 0:00	0.443
8/25/09 23:00	1.10	8/27/09 9:00	0.51
8/26/09 12:00	1.42	8/27/09 21:00	0.56
8/26/09 18:00	1.79	8/28/09 3:00	0.58
8/26/09 21:00	1.81	8/28/09 21:00	0.45
8/27/09 6:00	2.09	8/29/09 16:00	0.77
8/27/09 9:00	2.14	8/31/09 14:30	0.84
8/27/09 18:00	2.36	8/31/09 17:30	0.85
8/28/09 3:00	2.58	8/31/09 20:30	0.82
8/28/09 6:00	2.53	8/31/09 23:30	0.75
8/29/09 4:00	2.65	9/1/09 2:30	0.76
8/29/09 16:00	3.23	9/1/09 5:30	0.76
8/31/09 14:30	2.90	9/1/09 8:30	0.84
8/31/09 17:30	2.85	9/1/09 11:30	0.69
8/31/09 20:30	2.82	9/1/09 17:30	0.81
8/31/09 23:30	2.89	9/1/09 20:30	0.79
9/1/09 2:30	2.78	9/1/09 23:30	0.78
9/1/09 5:30	2.66	9/2/09 2:30	0.76
9/1/09 8:30	2.84	9/2/09 5:30	0.77
9/1/09 11:30	2.85	9/2/09 8:30	0.75
9/1/09 14:30	3.40	9/2/09 11:30	0.80
9/1/09 17:30	3.32	9/2/09 14:00	0.83
9/1/09 20:30	3.44	9/2/09 14:00	0.78
9/1/09 23:30	3.32	9/2/09 14:30	0.78

9/2/09 2:30	3.57
9/2/09 5:30	3.52
9/2/09 8:30	3.59
9/2/09 11:30	3.91
9/2/09 14:00	3.63
9/2/09 14:00	3.69
9/2/09 14:30	3.99
9/2/09 17:00	3.76
9/2/09 20:00	3.90
9/2/09 23:00	3.99
9/3/09 2:00	3.77
9/3/09 5:00	4.05
9/3/09 8:00	4.24
9/3/09 14:00	3.98
9/3/09 17:00	4.04
9/3/09 20:00	4.24
9/3/09 23:00	4.16
9/4/09 2:00	4.17
9/4/09 2:00	4.19
9/4/09 5:00	4.23
9/4/09 8:00	4.31
9/4/09 16:00	4.23
9/4/09 20:00	4.43
9/5/09 0:00	4.69
9/5/09 4:00	4.54
9/5/09 8:00	4.95
9/5/09 12:00	4.88
9/5/09 16:00	4.62
9/5/09 20:00	4.96
9/6/09 0:00	5.01
9/6/09 4:00	4.87
9/6/09 8:00	4.90
9/6/09 12:00	5.05
9/6/09 16:00	5.23
9/6/09 20:00	5.03
9/7/09 0:00	5.09
9/7/09 4:00	4.99
9/7/09 12:00	5.01
9/7/09 16:00	5.05
9/7/09 20:00	4.96

9/2/09 17:00	0.87
9/2/09 20:00	0.96
9/2/09 23:00	1.07
9/3/09 2:00	1.13
9/3/09 5:00	1.28
9/3/09 8:00	1.34
9/3/09 11:00	1.45
9/3/09 14:00	1.35
9/3/09 17:00	1.38
9/3/09 20:00	1.36
9/3/09 23:00	1.52
9/4/09 2:00	1.20
9/4/09 2:00	1.30
9/4/09 5:00	1.25
9/4/09 8:00	1.31
9/4/09 16:00	1.26
9/4/09 20:00	1.41
9/5/09 0:00	1.39
9/5/09 4:00	1.39
9/5/09 8:00	1.5
9/5/09 12:00	1.47
9/5/09 16:00	1.41
9/5/09 20:00	1.66
9/6/09 0:00	1.74
9/6/09 4:00	1.58
9/6/09 8:00	1.67
9/6/09 12:00	1.62
9/6/09 16:00	1.57
9/6/09 20:00	1.41
9/7/09 0:00	1.46
9/7/09 4:00	1.49
9/7/09 8:00	1.4
9/7/09 12:00	1.33
9/7/09 16:00	1.36
9/7/09 20:00	1.42
9/8/09 0:00	1.35
9/8/09 4:00	1.35
9/8/09 8:00	1.33
9/8/09 12:00	1.35
9/8/09 15:00	1.25

9/8/09 0:00	4.94
9/8/09 4:00	5.18
9/8/09 8:00	4.89
9/8/09 12:00	4.74
9/8/09 15:00	4.62
9/8/09 15:00	4.56
9/8/09 18:00	4.64
9/8/09 21:00	4.64
9/8/09 21:00	4.47
9/15/09 2:00	2.79
9/17/09 0:15	3.54
9/17/09 6:15	2.72
9/17/09 18:15	2.65
9/17/09 21:15	2.69
9/18/09 0:15	2.62
9/18/09 3:15	2.73
9/18/09 6:15	2.93
9/18/09 12:15	2.73
9/18/09 15:00	2.60
9/18/09 21:00	2.46
9/19/09 0:00	2.26
9/19/09 15:00	2.77
9/19/09 21:00	2.81
9/20/09 3:00	2.94
9/20/09 15:00	2.91
9/20/09 18:00	3.04
9/21/09 0:00	3.10
9/21/09 6:00	3.15
9/21/09 9:00	3.26
9/21/09 12:00	3.21
9/23/09 11:00	3.24
9/24/09 15:00	3.74
9/25/09 3:00	3.48
9/25/09 7:00	3.60
9/25/09 7:00	3.50
9/25/09 14:00	3.53
9/25/09 14:00	3.55
9/26/09 8:00	3.57
9/26/09 8:00	3.57
9/26/09 14:00	3.54

9/8/09 18:00	1.22
9/8/09 21:00	1.13
9/9/09 0:00	1.16
9/9/09 6:00	1.16
9/9/09 9:00	1.09
9/9/09 15:00	1.18
9/9/09 18:00	1.12
9/9/09 21:00	1.08
9/10/09 0:00	1.11
9/12/09 16:00	0.88
9/12/09 19:00	1.00
9/12/09 22:00	0.94
9/13/09 1:00	0.95
9/13/09 16:00	0.95
9/13/09 16:00	0.92
9/13/09 19:00	0.93
9/14/09 1:00	0.97
9/14/09 4:00	0.96
9/14/09 13:00	0.95
9/14/09 20:00	0.88
9/14/09 23:00	0.93
9/15/09 5:00	0.81
9/15/09 11:00	0.81
9/16/09 0:15	0.80
9/16/09 6:15	0.71
9/16/09 12:15	0.65
9/16/09 18:15	0.54
9/17/09 3:15	0.59
9/17/09 12:15	0.67
9/17/09 15:15	0.73
9/18/09 3:15	0.75
9/18/09 9:15	1.05
9/18/09 12:15	0.93
9/19/09 15:00	1.34
9/19/09 18:00	1.34
9/20/09 0:00	1.37
9/20/09 3:00	1.45
9/21/09 0:00	1.56
9/21/09 9:00	1.51
9/21/09 12:00	1.54

9/27/09 8:00	3.61
9/27/09 20:00	3.64
9/30/09 2:00	3.66
9/30/09 8:00	3.68
9/30/09 14:00	3.75
10/1/09 16:00	3.77
10/1/09 22:00	3.76
10/2/09 16:00	3.84
10/3/09 10:00	3.62
10/3/09 16:00	3.50
10/4/09 10:00	3.27
10/4/09 22:00	3.18
10/6/09 4:00	3.03
10/7/09 10:00	3.00
10/7/09 21:00	3.09
10/8/09 3:00	3.13
10/8/09 15:00	3.15

9/22/09 3:00	1.58
9/23/09 15:00	1.75
9/24/09 11:00	1.79
9/24/09 23:00	1.76
9/25/09 3:00	1.74
9/25/09 20:00	1.69
9/25/09 20:00	1.71
9/27/09 2:00	1.75
9/27/09 14:00	1.77
9/27/09 14:00	1.80
9/28/09 2:00	1.79
9/29/09 2:00	1.81
9/29/09 14:00	1.76
9/29/09 14:00	1.97
10/1/09 22:00	2.26
10/2/09 16:00	2.18
10/3/09 4:00	2.11
10/3/09 16:00	2.02
10/4/09 4:00	2.03
10/4/09 16:00	2.16
10/5/09 10:00	2.36
10/5/09 16:00	2.34
10/6/09 4:00	2.33
10/7/09 10:00	2.25
10/7/09 15:00	2.31
10/8/09 9:00	2.29
10/8/09 15:00	2.24

2010 North and south tile drain DFBA concentrations

North Tile	
Date	Concentration (mg/L)
6/2/10 19:30	1.43
6/3/10 7:30	1.48
6/3/10 19:30	1.45
6/4/10 7:30	1.59
6/4/10 19:30	1.63
6/5/10 7:30	1.70
6/5/10 19:30	1.67
6/6/10 7:30	1.74
6/6/10 19:30	1.79
6/7/10 7:30	1.78
6/7/10 19:30	1.78
6/8/10 19:30	1.93
6/9/10 7:30	1.95
6/9/10 19:30	2.05
6/10/10 7:30	1.87
6/10/10 19:30	1.71
6/11/10 7:30	1.73
6/11/10 22:00	1.77
6/12/10 10:00	1.76
6/12/10 22:00	1.77
6/13/10 10:00	1.77
6/13/10 22:00	1.69
6/14/10 10:00	1.60
6/14/10 22:00	1.51
6/15/10 10:00	1.37
6/15/10 22:00	1.31
6/16/10 10:00	1.24
6/22/10 15:20	0.66
6/23/10 3:20	0.75
6/23/10 15:20	0.76
6/24/10 3:20	1.25
6/24/10 15:20	1.03
6/25/10 3:20	1.20
6/25/10 15:20	1.45
6/26/10 3:20	0.51

South Tile	
Date	Concentration (mg/L)
6/2/10 19:30	2.87
6/3/10 7:30	2.64
6/3/10 19:30	2.58
6/4/10 7:30	2.46
6/4/10 19:30	2.46
6/5/10 7:30	2.43
6/5/10 19:30	2.24
6/6/10 7:30	2.32
6/6/10 19:30	2.29
6/7/10 7:30	2.16
6/7/10 19:30	2.18
6/8/10 7:30	2.16
6/11/10 16:00	2.76
6/12/10 4:00	2.82
6/12/10 16:00	2.65
6/13/10 4:00	2.48
6/13/10 16:00	2.26
6/14/10 4:00	2.18
6/14/10 16:00	2.05
6/15/10 4:00	1.92
6/15/10 16:00	1.85
6/16/10 4:00	1.78
6/22/10 15:20	1.33
6/23/10 3:20	1.31
6/23/10 15:20	1.30
6/24/10 3:20	1.04
6/24/10 15:20	2.16
6/25/10 3:20	3.13
6/25/10 15:20	4.21
6/26/10 3:20	4.06
6/26/10 15:20	4.97
6/27/10 3:20	4.87
6/27/10 15:20	4.69
6/28/10 3:20	4.40
6/28/10 16:30	4.17

6/26/10 15:20	1.81
6/27/10 3:20	1.96
6/27/10 15:20	2.13
6/28/10 3:20	2.14
6/28/10 16:30	2.02
6/29/10 4:30	2.13
6/29/10 16:30	2.29
6/30/10 4:30	2.04
6/30/10 16:30	1.94
7/1/10 4:30	1.98
7/1/10 16:30	2.17
7/2/10 4:30	2.21
7/2/10 22:10	2.26
7/3/10 4:10	2.29
7/3/10 22:10	2.28
7/4/10 10:10	2.33
7/4/10 22:10	2.40
7/5/10 10:10	2.39
7/5/10 22:10	2.41
7/6/10 10:10	2.42
7/6/10 22:10	2.37
7/7/10 10:10	2.43
7/7/10 22:10	2.41
7/8/10 17:30	2.36
7/8/10 17:30	2.54
7/9/10 5:30	2.30
7/9/10 5:30	2.57
7/9/10 23:30	2.53
7/10/10 5:30	2.54
7/10/10 17:30	2.06
7/10/10 17:30	2.39
7/11/10 5:30	2.12
7/11/10 5:30	2.25
7/11/10 17:30	2.27
7/12/10 5:30	2.29
7/12/10 17:30	2.34
7/13/10 5:30	2.05
7/13/10 17:30	1.50
7/14/10 14:30	1.15
7/15/10 2:30	1.14

6/29/10 4:30	3.91
6/29/10 16:30	3.70
6/30/10 4:30	3.59
6/30/10 16:30	3.72
7/1/10 4:30	3.79
7/1/10 16:30	3.74
7/2/10 4:30	3.55
7/2/10 22:10	3.52
7/3/10 10:10	3.57
7/3/10 22:10	3.44
7/4/10 10:10	3.44
7/4/10 22:10	3.43
7/5/10 10:10	3.22
7/5/10 22:10	3.13
7/6/10 10:10	2.99
7/6/10 22:10	3.06
7/7/10 10:10	3.21
7/7/10 22:10	3.21
7/8/10 17:30	3.46
7/9/10 5:30	3.52
7/9/10 23:30	3.40
7/10/10 5:30	3.42
7/10/10 17:30	3.59
7/11/10 5:30	3.73
7/11/10 17:30	3.39
7/12/10 5:30	3.14
7/13/10 5:30	2.81
7/13/10 17:30	2.32
7/15/10 2:30	1.18
7/15/10 14:30	1.27
7/16/10 2:30	1.39
7/16/10 14:30	1.42
7/17/10 2:30	1.44
7/17/10 14:30	1.46
7/18/10 2:30	1.50
7/18/10 14:30	1.45
7/19/10 2:30	1.45
7/19/10 14:30	1.13
7/20/10 2:30	1.54
7/20/10 16:00	1.54

7/15/10 14:30	1.19
7/16/10 2:30	1.20
7/16/10 14:30	1.24
7/17/10 2:30	1.19
7/17/10 14:30	1.23
7/18/10 2:30	1.20
7/18/10 14:30	1.25
7/19/10 2:30	1.15
7/19/10 14:30	1.18
7/20/10 2:30	1.12
7/20/10 13:00	1.22
7/20/10 17:00	0.49
7/20/10 21:00	1.22
7/21/10 2:00	1.19
7/21/10 4:00	0.78
7/21/10 6:00	1.03
7/21/10 8:00	1.21
7/21/10 10:00	0.42
7/21/10 12:00	1.20
7/21/10 14:18	1.06
7/21/10 18:18	1.13
7/21/10 22:18	1.20
7/22/10 2:18	1.22
7/22/10 6:18	1.20
7/22/10 10:18	1.23
7/22/10 14:18	1.24
7/23/10 0:18	1.24
7/23/10 6:18	1.16
7/23/10 10:18	1.06
7/23/10 18:30	1.16
7/24/10 0:30	1.16
7/24/10 6:30	1.17
7/24/10 12:30	1.17
7/24/10 18:30	1.35
7/25/10 0:30	1.26
7/25/10 6:30	1.30
7/25/10 6:30	1.29
7/26/10 13:30	1.29
7/27/10 5:30	1.33
7/27/10 21:30	1.50

7/21/10 0:00	1.32
7/21/10 16:00	1.39
7/22/10 8:00	1.30
7/23/10 0:00	1.24
7/23/10 16:00	1.26
7/24/10 8:00	1.36
7/25/10 0:00	1.33
7/25/10 8:00	1.29
7/25/10 8:00	1.30
7/26/10 13:30	1.25
7/27/10 5:30	1.25
7/27/10 21:30	1.29
7/28/10 13:30	1.27
7/29/10 5:30	1.27
7/30/10 19:30	1.41
7/31/10 19:30	1.64
8/1/10 13:30	1.72
8/1/10 19:30	1.72
8/1/10 19:30	1.69
8/3/10 12:30	1.44
8/4/10 0:30	1.42
8/4/10 12:30	1.40
8/5/10 0:30	1.39
8/5/10 12:30	1.34
8/6/10 0:30	1.35
8/6/10 12:30	1.28
8/7/10 0:30	1.27
8/7/10 12:30	1.25
8/8/10 0:30	1.26
8/8/10 12:30	1.12
8/9/10 0:30	1.24
8/9/10 17:30	1.19
8/10/10 5:30	1.19
8/10/10 17:30	1.20
8/11/10 5:30	1.22
8/11/10 17:30	1.31
8/12/10 5:30	1.37
8/12/10 17:30	1.43
8/13/10 5:30	1.51
8/13/10 17:30	1.85

7/28/10 13:30	1.53
7/29/10 1:30	1.59
7/30/10 13:30	1.57
7/30/10 19:30	1.73
7/31/10 19:30	1.72
8/1/10 13:30	1.82
8/1/10 19:30	1.81
8/3/10 12:30	1.66
8/4/10 0:30	1.65
8/4/10 12:30	1.60
8/5/10 0:30	1.51
8/5/10 12:30	1.48
8/6/10 0:30	1.43
8/6/10 12:30	1.36
8/7/10 0:30	1.33
8/7/10 12:30	1.28
8/8/10 0:30	1.28
8/8/10 12:30	1.21
8/9/10 0:30	1.22
8/9/10 17:30	1.14
8/10/10 5:30	1.16
8/10/10 17:30	1.22
8/10/10 23:30	1.26
8/12/10 5:30	1.70
8/12/10 17:30	1.81
8/12/10 23:30	1.91
8/13/10 11:30	2.02
8/13/10 23:30	2.10
8/14/10 11:30	2.10
8/14/10 17:30	2.14
8/15/10 11:30	2.54
8/15/10 23:30	2.63
8/16/10 11:30	2.65
8/16/10 19:30	2.62
8/17/10 11:30	2.69
8/18/10 3:30	2.69
8/18/10 11:30	2.65
8/18/10 19:30	2.64
8/19/10 11:30	2.57
8/19/10 19:30	2.55

8/14/10 5:30	2.50
8/14/10 17:30	3.05
8/15/10 5:30	3.21
8/15/10 17:30	3.36
8/16/10 5:30	3.05
8/16/10 19:30	3.21
8/17/10 11:30	2.87
8/18/10 3:30	2.73
8/18/10 19:30	2.74
8/19/10 11:30	2.57
8/20/10 3:30	2.62
8/20/10 19:30	2.44
8/21/10 11:30	2.70
8/22/10 3:30	2.67
8/22/10 19:30	3.06
8/23/10 11:30	3.27
8/23/10 11:30	3.24
8/24/10 19:30	3.24
8/25/10 3:30	2.83
8/25/10 11:30	3.04
8/26/10 19:30	2.75
8/27/10 11:30	2.63
8/28/10 3:30	2.62
8/28/10 19:30	2.59
8/29/10 11:30	2.43
8/30/10 3:30	2.57
8/30/10 19:30	2.53
8/31/10 11:30	2.45
9/1/10 3:30	2.53
9/1/10 13:30	2.86
9/2/10 5:30	2.72
9/2/10 21:30	3.29
9/3/10 13:30	3.36
9/4/10 5:30	3.49
9/4/10 21:30	3.37
9/6/10 5:30	3.14
9/7/10 13:30	2.89
9/7/10 21:30	3.19
9/8/10 13:30	2.96
9/9/10 5:30	3.23

8/20/10 3:30	2.57
8/20/10 19:30	2.60
8/21/10 11:30	2.59
8/22/10 3:30	2.58
8/22/10 19:30	2.58
8/23/10 11:30	2.61
8/24/10 3:30	2.74
8/24/10 19:30	2.69
8/25/10 3:30	2.54
8/25/10 11:30	2.67
8/26/10 19:30	2.56
8/27/10 11:30	2.54
8/28/10 3:30	2.48
8/29/10 11:30	2.36
8/30/10 3:30	2.04
8/30/10 19:30	2.41
9/1/10 3:30	2.12
9/1/10 13:30	2.40
9/2/10 5:30	2.46
9/2/10 21:30	2.59
9/3/10 13:30	2.76
9/4/10 5:30	2.69
9/4/10 21:30	2.72
9/5/10 13:30	2.79
9/6/10 5:30	2.77
9/6/10 21:30	2.90
9/7/10 13:30	2.79
9/7/10 21:30	2.68
9/8/10 13:30	2.54
9/9/10 5:30	2.52
9/9/10 21:30	2.72
9/10/10 13:30	2.88
9/11/10 5:30	2.54
9/11/10 21:30	2.90
9/12/10 13:30	3.13
9/13/10 5:30	3.14
9/13/10 21:30	3.13
9/14/10 13:30	3.28
9/15/10 5:30	3.45
9/15/10 5:30	3.26

9/9/10 13:30	3.09
9/9/10 21:30	3.36
9/10/10 13:30	3.81
9/11/10 5:30	4.19
9/11/10 21:30	4.23
9/12/10 13:30	4.58
9/13/10 5:30	4.66
9/13/10 21:30	4.53
9/14/10 13:30	4.79
9/15/10 5:30	4.75
9/15/10 5:30	4.72
9/16/10 21:30	4.57
9/17/10 13:30	4.58
9/18/10 5:30	4.44
9/18/10 21:30	4.18
9/19/10 13:30	4.05
9/20/10 5:30	3.95
9/20/10 21:30	3.88
9/21/10 13:30	4.07
9/22/10 5:30	4.35
9/22/10 21:30	4.45
9/23/10 13:30	4.44
9/24/10 5:30	4.39
9/24/10 13:30	4.55
9/25/10 5:30	4.49
9/25/10 21:30	4.52
9/26/10 13:30	4.48
9/27/10 5:30	4.52
9/27/10 21:30	4.48
9/28/10 13:30	4.34
9/29/10 5:30	4.55
9/29/10 21:30	4.75
9/30/10 13:30	4.62
10/1/10 5:30	4.76
10/1/10 21:30	4.76
10/4/10 21:30	4.04
10/5/10 13:30	3.72
10/6/10 5:30	3.72
10/6/10 21:30	3.86
10/7/10 13:30	3.95

9/16/10 21:30	3.34
9/17/10 13:30	3.44
9/18/10 5:30	3.38
9/18/10 21:30	3.27
9/19/10 13:30	3.42
9/20/10 5:30	2.91
9/20/10 21:30	2.67
9/21/10 13:30	2.92
9/22/10 5:30	3.03
9/22/10 21:30	3.11
9/23/10 13:30	3.17
9/24/10 5:30	3.20
9/24/10 13:30	3.21
9/25/10 5:30	3.21
9/25/10 21:30	3.16
9/26/10 13:30	3.19
9/27/10 5:30	3.15
9/27/10 21:30	3.15
9/28/10 13:30	2.88
9/29/10 5:30	2.90
9/29/10 21:30	3.04
9/30/10 13:30	3.18
10/1/10 5:30	3.22
10/1/10 21:30	3.28
10/1/10 21:30	3.30
10/4/10 21:30	3.14
10/5/10 13:30	3.05
10/6/10 5:30	3.04
10/6/10 21:30	2.96
10/7/10 13:30	2.98
10/8/10 5:30	2.93
10/8/10 21:30	2.90
10/9/10 13:30	2.82
10/10/10 5:30	2.77
10/10/10 21:30	2.63
10/11/10 13:30	2.59
10/12/10 5:30	2.47
10/12/10 21:30	2.40
10/13/10 11:30	2.30
10/14/10 1:30	2.23

10/8/10 5:30	3.91
10/8/10 21:30	3.82
10/9/10 13:30	3.69
10/10/10 5:30	3.56
10/10/10 21:30	3.48
10/11/10 13:30	3.35
10/12/10 5:30	2.26
10/12/10 21:30	3.23
10/13/10 11:30	2.95
10/14/10 1:30	3.0
10/14/10 15:30	2.97
10/15/10 5:30	2.82
10/15/10 19:30	3.31
10/16/10 9:30	2.65
10/16/10 23:30	3.02
10/17/10 13:30	2.70
10/18/10 3:30	2.60
10/18/10 17:30	2.57
10/19/10 7:30	2.57
10/19/10 21:30	2.53
10/20/10 11:30	2.45
10/21/10 1:30	2.42
10/21/10 15:30	2.45
10/22/10 5:30	2.34
10/22/10 19:30	2.28
10/23/10 9:30	2.29
10/23/10 23:30	2.24
10/24/10 13:30	2.03
10/25/10 3:30	2.29

10/14/10 15:30	2.15
10/15/10 5:30	1.99
10/15/10 19:30	1.94
10/16/10 9:30	1.79
10/16/10 23:30	1.87
10/17/10 13:30	1.75
10/18/10 3:30	1.75
10/18/10 17:30	1.64
10/19/10 7:30	1.60
10/19/10 21:30	1.56
10/20/10 11:30	1.69
10/21/10 1:30	1.51
10/21/10 15:30	1.48
10/22/10 5:30	1.44
10/22/10 19:30	1.50
10/23/10 9:30	1.53
10/23/10 23:30	1.58
10/24/10 13:30	1.53
10/25/10 3:30	1.49

2010 North tile drain PFBA concentrations

Date	Concentration (mg/L)
7/21/10 6:00	0.10
7/21/10 8:00	0.81
7/21/10 10:00	2.56
7/21/10 12:00	5.87
7/21/10 14:18	7.52
7/21/10 18:18	10.19
7/21/10 22:18	9.95
7/22/10 2:18	11.62
7/22/10 6:18	12.92
7/22/10 10:18	12.48
7/22/10 14:18	11.92
7/23/10 0:18	10.81
7/23/10 6:18	10.03
7/23/10 10:18	7.91
7/23/10 18:30	6.24
7/24/10 0:30	5.09
7/24/10 6:30	4.52
7/24/10 12:30	3.93
7/24/10 18:30	3.46
7/25/10 0:30	3.07
7/25/10 6:30	3.13
7/25/10 6:30	2.39
7/26/10 13:30	2.30
7/27/10 5:30	2.32
7/27/10 21:30	1.77
7/28/10 13:30	1.48
7/29/10 1:30	1.27
7/30/10 13:30	1.12
7/30/10 19:30	1.08
7/31/10 19:30	1.17
8/1/10 13:30	1.18
8/1/10 19:30	1.09
8/3/10 12:30	1.08
8/4/10 0:30	1.03
8/4/10 12:30	1.01
8/5/10 0:30	0.91

8/5/10 12:30	0.91
8/6/10 0:30	0.87
8/6/10 12:30	0.86
8/7/10 0:30	0.87
8/7/10 12:30	0.86
8/8/10 0:30	0.87
8/8/10 12:30	0.89
8/9/10 0:30	0.89
8/9/10 17:30	0.82
8/10/10 5:30	0.94
8/10/10 17:30	0.84
8/10/10 23:30	0.85
8/12/10 5:30	0.88
8/12/10 17:30	0.89
8/12/10 23:30	1.00
8/13/10 11:30	1.00
8/13/10 23:30	1.05
8/14/10 11:30	1.10
8/14/10 17:30	1.12
8/15/10 11:30	1.15
8/15/10 23:30	1.24
8/16/10 11:30	1.48
8/16/10 19:30	1.54
8/17/10 11:30	1.46
8/18/10 3:30	1.41
8/18/10 11:30	1.33
8/18/10 19:30	1.16
8/19/10 11:30	1.13
8/19/10 19:30	1.09
8/20/10 3:30	0.99
8/20/10 19:30	0.95
8/21/10 11:30	0.92
8/22/10 3:30	0.85
8/22/10 19:30	0.77
8/23/10 11:30	0.74
8/24/10 3:30	0.70
8/24/10 19:30	0.67
8/25/10 3:30	0.66
8/25/10 11:30	1.43
8/26/10 19:30	1.10

8/27/10 11:30	1.13
8/28/10 3:30	1.17
8/29/10 11:30	1.26
8/30/10 3:30	1.14
8/30/10 19:30	0.93
9/1/10 3:30	0.80
9/1/10 13:30	0.63
9/2/10 5:30	1.12
9/2/10 21:30	0.94
9/3/10 13:30	0.56
9/4/10 5:30	0.54
9/4/10 21:30	0.55
9/5/10 13:30	0.57
9/6/10 5:30	0.53
9/6/10 21:30	0.50
9/7/10 13:30	0.55
9/7/10 21:30	0.54
9/8/10 13:30	0.52
9/9/10 5:30	0.54
9/9/10 21:30	0.54
9/10/10 13:30	0.54
9/11/10 5:30	0.47
9/11/10 21:30	0.14
9/12/10 13:30	0.10
9/13/10 5:30	0.10
9/13/10 21:30	0.06
9/14/10 13:30	0.10
9/15/10 5:30	0.10

2009 irrigation and precipitation rates

2009 Irrigation and Precipitation Events		
Date	Irrigation (mm)	Precipitation (mm)
7/9/2009	25	6.4
7/10/2009	25	0
7/11/2009	0	1.4
7/12/2009	0	0
7/13/2009	25	0
7/14/2009	18.75	2.9
7/15/2009	12.5	0
7/16/2009	11.25	0
7/17/2009	5.5	0
7/18/2009	0	0.7
7/19/2009	0	0.4
7/20/2009	25	0
7/21/2009	0	0
7/22/2009	25	0
7/23/2009	0	0
7/24/2009	22.5	0
7/25/2009	0	0
7/26/2009	0	1.4
7/27/2009	22.5	0
7/28/2009	0	10.6
7/29/2009	18.75	0.2
7/30/2009	0	0.4
7/31/2009	12.5	0
8/1/2009	0	9
8/2/2009	0	0.2
8/3/2009	0	7.2
8/4/2009	12.5	1.3
8/5/2009	0	0.6
8/6/2009	0	1.2
8/7/2009	0	0
8/8/2009	0	0
8/9/2009	0	0.4
8/10/2009	0	0
8/11/2009	22.25	0
8/12/2009	0	0

8/13/2009	0	0
8/14/2009	12.5	5.8
8/15/2009	0	0
8/16/2009	0	0.2
8/17/2009	0	0
8/18/2009	12.5	3.4
8/19/2009	10	0
8/20/2009	0	0
8/21/2009	12.5	0
8/22/2009	0	0
8/23/2009	0	0
8/24/2009	13.75	0
8/25/2009	11.25	0
8/26/2009	10	0
8/27/2009	0	0
8/28/2009	15	0
8/29/2009	0	0
8/30/2009	0	0
8/31/2009	12.5	0
9/1/2009	0	0
9/2/2009	12.75	0
9/3/2009	0	0
9/4/2009	12.5	0.4
9/5/2009	0	0
9/6/2009	0	0.7
9/7/2009	0	0
9/8/2009	3.75	0
9/9/2009	0	0
9/10/2009	0	0
9/11/2009	7.5	0
9/12/2009	0	0
9/13/2009	0	0
9/14/2009	10.625	0
9/15/2009	13.625	0
9/16/2009	10.625	0
9/17/2009	10.625	0.6
9/18/2009	10.625	0
9/19/2009	10.625	0
9/20/2009	0	0
9/21/2009	10.625	0

9/22/2009	10.625	0
9/23/2009	10.625	0
9/24/2009	10.625	0
9/25/2009	10.625	0
9/26/2009	10.625	0
9/27/2009	0	0
9/28/2009	0	0.5
9/29/2009	10.625	0
9/30/2009	10.625	0
10/1/2009	25	0
10/2/2009	0	0

2010 irrigation and precipitation rates

2010 Irrigation and Precipitation Events		
Date	Irrigation (mm)	Precipitation (mm)
6/2/2010 13:40	10.08	0.00
6/3/2010 11:20	7.62	1.70
6/4/2010 11:20	0.00	0.00
6/5/2010 18:00	2.49	0.00
6/6/2010 18:00	0.00	0.00
6/7/2010 18:00	0.00	10.20
6/8/2010 18:00	0.00	3.80
6/9/2010 18:00	0.00	6.20
6/10/2010 18:00	0.00	2.60
6/11/2010 18:00	0.00	0.00
6/12/2010 18:00	0.00	0.00
6/13/2010 18:00	0.00	0.00
6/14/2010 18:00	0.00	0.00
6/15/2010 18:00	2.99	0.00
6/16/2010 18:00	3.02	0.00
6/17/2010 18:00	2.99	0.00
6/18/2010 18:00	2.98	0.00
6/19/2010 18:00	2.95	0.00
6/20/2010 18:00	2.98	0.00
6/21/2010 18:00	3.03	0.00
6/22/2010 18:00	11.18	0.00
6/23/2010 18:00	3.80	34.90
6/24/2010 18:00	9.30	0.20
6/25/2010 18:00	11.99	0.70
6/26/2010 18:00	0.00	0.40
6/27/2010 18:00	0.00	8.00
6/28/2010 18:00	0.00	0.00
6/29/2010 18:00	0.00	14.90
6/30/2010 18:00	0.00	0.60
7/1/2010 17:19	13.87	0.00
7/2/2010 18:00	5.87	0.00
7/3/2010 18:00	2.34	1.00
7/4/2010 18:00	0.00	0.00
7/5/2010 18:00	0.00	6.50
7/6/2010 18:00	11.05	1.20

7/7/2010 18:00	9.71	0.40
7/8/2010 18:00	0.00	0.00
7/9/2010 18:00	6.03	7.20
7/10/2010 18:00	5.99	8.40
7/11/2010 18:00	6.00	1.00
7/12/2010 18:00	2.35	22.60
7/13/2010 18:00	0.00	51.70
7/14/2010 18:00	0.00	0.20
7/15/2010 18:00	0.00	1.20
7/16/2010 18:00	0.00	3.60
7/17/2010 18:00	0.00	0.00
7/18/2010 18:00	0.00	1.40
7/19/2010 18:00	0.00	5.30
7/20/2010 18:00	0.00	0.20
7/21/2010 18:00	0.00	0.00
7/22/2010 18:00	0.00	8.90
7/23/2010 18:00	0.00	1.10
7/24/2010 18:00	0.00	0.00
7/25/2010 18:00	0.00	0.00
7/26/2010 18:00	8.75	1.40
7/27/2010 18:00	8.68	0.00
7/28/2010 18:00	3.40	0.20
7/29/2010 18:00	8.80	0.00
7/30/2010 18:00	2.61	5.60
7/31/2010 18:00	2.62	0.60
8/1/2010 18:00	2.56	0.00
8/2/2010 18:00	2.58	0.00
8/3/2010 18:00	1.99	1.80
8/4/2010 18:00	2.62	0.00
8/5/2010 18:00	2.66	0.20
8/6/2010 18:00	2.59	0.00
8/7/2010 18:00	2.59	0.60
8/8/2010 18:00	2.59	0.00
8/9/2010 18:00	7.88	0.00
8/10/2010 18:00	6.11	0.70
8/11/2010 18:00	6.07	0.00
8/12/2010 18:00	5.93	5.90
8/13/2010 18:00	6.06	12.00
8/14/2010 18:00	6.08	0.00
8/15/2010 18:00	2.57	0.00

8/16/2010 18:00	4.79	0.40
8/17/2010 18:00	4.09	0.00
8/18/2010 18:00	4.08	0.00
8/19/2010 18:00	4.06	0.00
8/20/2010 18:00	4.08	0.50
8/21/2010 18:00	2.33	6.60
8/22/2010 18:00	4.12	0.80
8/23/2010 18:00	3.93	0.20
8/24/2010 18:00	4.00	0.00
8/25/2010 18:00	3.99	0.00
8/26/2010 18:00	3.98	0.00
8/27/2010 18:00	4.10	0.40
8/28/2010 18:00	3.46	0.00
8/29/2010 18:00	0.00	0.00
8/30/2010 18:00	3.93	3.00
8/31/2010 18:00	4.10	0.00
9/1/2010 18:00	0.00	7.60
9/2/2010 18:00	4.13	0.00
9/3/2010 18:00	4.08	0.00
9/4/2010 18:00	4.12	0.90
9/5/2010 18:00	0.00	0.00
9/6/2010 18:00	0.00	0.00
9/7/2010 18:00	4.17	0.00
9/8/2010 18:00	0.00	11.80
9/9/2010 18:00	4.13	0.50
9/10/2010 18:00	4.15	0.00
9/11/2010 18:00	4.17	0.00
9/12/2010 18:00	3.99	2.70
9/13/2010 18:00	0.00	3.70
9/14/2010 18:00	4.18	0.20
9/15/2010 18:00	0.00	2.60
9/16/2010 18:00	0.00	0.20
9/17/2010 18:00	0.00	0.00
9/18/2010 18:00	0.00	0.00
9/19/2010 18:00	0.00	4.00
9/20/2010 18:00	3.15	3.70
9/21/2010 18:00	3.70	0.00
9/22/2010 18:00	3.65	0.00
9/23/2010 18:00	4.66	0.00
9/24/2010 18:00	7.64	0.00

9/25/2010 18:00	0.00	0.00
9/26/2010 18:00	4.02	0.60
9/27/2010 18:00	4.03	0.00
9/28/2010 18:00	4.10	6.60
9/29/2010 18:00	4.08	0.00
9/30/2010 18:00	4.68	0.00
10/1/2010 18:00	0.00	0.00
10/2/2010 18:00	0.00	0.00
10/3/2010 18:00	0.00	0.00
10/4/2010 18:00	3.93	0.40
10/5/2010 18:00	4.61	0.00

Completed list of monitoring well benzoic acid concentrations during the 2009 and 2010 sampling seasons

Well	Sampling Date and Concentration (mg/L)									
	Aug 2009 DFBA	Oct 2009 DFBA	Jun 2010 DFBA	Jul 2010 DFBA	Aug 2010 DFBA	Aug 2010 PFBA	Sep 2010 DFBA	Sep 2010 PFBA	Oct 2010 DFBA	Oct 2010 PFBA
MW09-01	3.86	4.09	7.94	4.89	4.02	1.12	5.01	0	3.1	0
MW09-02	0	0	1.75	1.68	0.96	2.24	1.18	0	1.18	0
MW09-03	0	0	0.14	3.37	0.58	0	1.72	0	3.19	0
MW09-04	0	0	0.3	3.38	2.73	0	1.74	0	1.71	0
MW09-05	0.14	0	0	0	0.03	0	0	0	0	0
MW09-06	N/A	N/A	0	3.13	1.03	0	0.81	0	0.63	0
MW09-07	0	0	0.47	0.37	0.19	0	0.11	0	0.14	0
MW09-08	0	0.14	1.41	0.23	3.04	0	6.21	0	2.45	0
MW09-09	0.11	2.75	0	1.51	1.28	0	1.13	0	0.96	0
MW09-10A	N/A	N/A	0	0	0	0	0.01	0	0	0
MW09-10B	N/A	N/A	0.39	0	0	0	0	0	0	0
MW09-10C	N/A	N/A	0	0.04	0	0	0	0	0	0
MW09-11A	N/A	N/A	N/A	N/A	N/A	N/A	N/A	N/A	N/A	N/A
MW10-11B	N/A	N/A	0.12	0	0	0	0.01	0	0	0
MW10-11C	N/A	N/A	0	0	0	0	0.08	0	0	0
MW09-12A	1.24	1.75	3.19	2.56	2.58	0	3.3	0	2.02	0
MW10-12B	N/A	N/A	2.26	0.21	0.07	0	0.17	0	0	0
MW10-12C	N/A	N/A	0	0	0	0.02	0	0	0	0
MW09-13A	N/A	N/A	0	0	0	0	0	0	0	0

MW09-13B	N/A	N/A	0.09	0.02	0.11	0	0.1	0	0	0
MW09-13C	N/A	N/A	0	0	0	0.1	0	0	0	0.04
MW10-14B	N/A	N/A	0.06	0	0	0	0	0	0	0
MW10-14C	N/A	N/A	0	0	0	0	0	0	0	0
MW10-15B	N/A	N/A	0	0	0	0	0.01	0	0.05	0
MW10-15C	N/A	N/A	0.21	1.41	0	0	0	0	0	0

2010 Lysimeter Results - Results from the north and south lysimeter sampling nests

		Concentrations (mg/L)									
		June	July		August		September			October	
North	Sampling Depth (m)	Original	Original	Split	Original	Split	Overnight	1 hour Original	1 hour Duplicate	Overnight	1 hour Original
	0.15	12.61	3.15	N/A	0.3	N/A	0	0.02	0.05	0	0.01
	0.3	18.5	12.16	11.85	7.46	N/A	5.42	4.08	2.25	3.94	3.55
	0.56	0.24	0.21	N/A	0.2	0.56	0.45	0.28	0.14	0.97	0.55
	0.72	0.36	0.21	N/A	3.48	N/A	3.55	2.51	N/A	5.08	3.33
	1.46	0.02	0.04	0.06	1.72	1.72	1.41	N/A	N/A	1.86	0

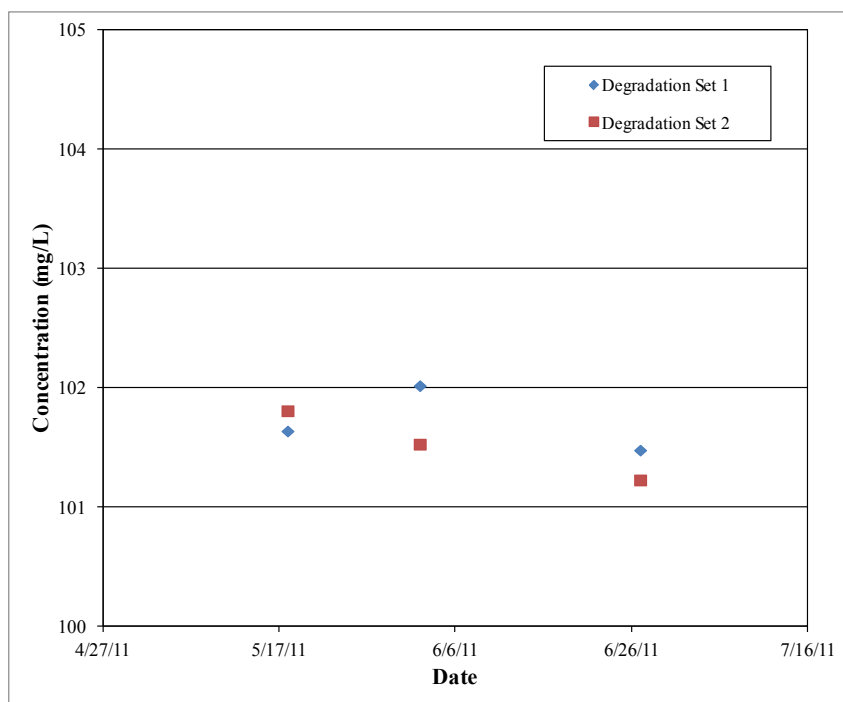
		Concentrations (mg/L)									
		June	July		August		September			October	
South	Sampling Depth (m)	Original	Original	Split	Original	Split	Overnight	1 hour Original	1 hour Duplicate	Overnight	1 hour Original
	0.15	8.32	3.53	N/A	3.06	N/A	3.59	2.28	1.81	3.61	0
	0.3	30.37	24.3	N/A	18.18	18.01	12.39	13.19	8.48	8.53	9.52
	0.73	1.22	0.72	N/A	0.59	N/A	0.31	0.31	N/A	0.33	0
	0.88	0	0.12	N/A	0	0	0.15	0.1	N/A	0.27	0.33
	1.38	0	0	0	0.1	N/A	0.18	N/A	N/A	0.71	0.72

APPENDIX B: SOIL BATCH TESTS

DFBA Soil Degradation Test

Soil Degradation Set 1	
Date	Concentration (mg/L)
5/18/2011	101.64
6/2/2011	102.02
6/27/2011	101.48

Soil Degradation Set 2	
Date	Concentration (mg/L)
5/18/2011	101.81
6/2/2011	101.53
6/27/2011	101.23



Summary of DFBA Soil Extraction Results

Extraction Method	Percent Recovered
H ₂ O	69.5
H ₂ O	40.3
H ₂ O	66.1
H ₂ O	85.1
H ₂ O	81.0
H ₂ O	59.2
H ₂ O	61.5
H ₂ O	75.9
H ₂ O	55.3
H ₂ O	55.3
H ₂ O	84.3
H ₂ O	76.7
Average	67.5

Extraction Method	Percent Recovered
Methanol	41.1
Methanol	32.1
Methanol	58.6
Methanol	46.2
Methanol	46.5
Average	44.9

Extraction Method	Percent Recovered
CaCl	43.3
CaCl	41.5
CaCl	65.0
CaCl	59.3
CaCl	53.3
CaCl	39.3
CaCl	49.3
CaCl	45.5
CaCl	46.5
Average	49.2

Extraction Method	Percent Recovered
Sonication	42.4
Sonication	50.5
Sonication	0.0
Sonication	56.9
Average	37.5

Raw data of batch test trials. In total 4 soil depths were tested over 7 different concentrations.

Depth	Applied Concentration (mg/L)		Measured Concentration (mg/L) (Ceq)				Average Measured Concentration (mg/L)		q (g/g)			
	DFBA	PFBA	DFBA Sample 1	DFBA Sample 2	PFBA Sample 1	PFBA Sample 2	DFBA	PFBA	DFBA Sample 1	DFBA Sample 2	PFBA Sample 1	PFBA Sample 2
2.1-2.4m	0.97	0.68	1.00	1.01	0.79	0.75	1.01	0.77	-6.00E-08	-8.00E-08	-2.20E-07	-1.40E-07
	4.86	3.68	4.79	4.85	3.51	4.23	4.82	3.87	1.40E-07	2.00E-08	3.40E-07	-1.10E-06
	9.54	7.50	9.79	10.46	8.22	7.88	10.13	8.05	-5.00E-07	-1.84E-06	-1.44E-06	-7.60E-07
	14.30	10.25	15.49	19.05	10.97	11.85	17.27	11.41	-2.38E-06	-9.50E-06	-1.44E-06	-3.20E-06
	48.75	45.95	50.53	50.42	46.75	N/A	50.48	46.75	-3.56E-06	-3.34E-06	-1.60E-06	N/A
	105.21	91.87	101.72	102.55	90.94	99.37	102.14	95.16	6.98E-06	5.32E-06	1.86E-06	-1.50E-05
	191.25	195.79	191.91	185.34	192.38	195.29	188.63	193.84	-1.32E-06	1.18E-05	6.82E-06	1.00E-06
1.7-1.9m	0.97	0.68	0.98	0.96	0.69	0.65	0.97	0.67	-2.00E-08	2.00E-08	-2.00E-08	6.00E-08
	4.86	3.68	4.98	4.82	4.17	5.48	4.90	4.83	-2.40E-07	8.00E-08	-9.80E-07	-3.60E-06
	9.54	7.50	10.11	10.39	6.72	6.56	10.25	6.64	-1.14E-06	-1.70E-06	1.56E-06	1.88E-06
	14.30	10.25	16.95	17.49	9.37	9.04	17.22	9.21	-5.30E-06	-6.38E-06	1.76E-06	2.42E-06
	48.75	45.95	49.15	51.03	43.86	43.70	50.09	43.78	-8.00E-07	-4.56E-06	4.18E-06	4.50E-06
	105.21	91.87	99.09	119.13	89.19	92.48	109.11	90.84	1.22E-05	-2.78E-05	5.36E-06	-1.22E-06
	191.25	195.79	215.59	205.42	191.50	198.39	210.51	194.95	-4.87E-05	-2.83E-05	8.58E-06	-5.20E-06

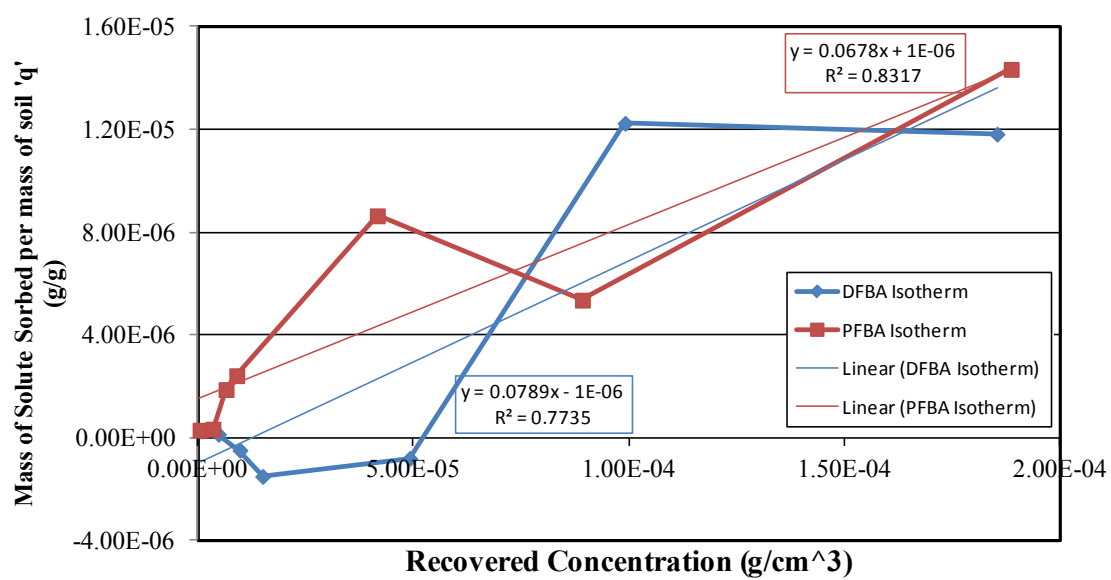
	Applied Concentration (mg/L)		Measured Concentration (mg/L) (Ceq)				Average Measured Concentration (mg/L)		q (g/g)			
Depth	DFBA	PFBA	DFBA Sample 1	DFBA Sample 2	PFBA Sample 1	PFBA Sample 2	DFBA	PFBA	DFBA Sample 1	DFBA Sample 2	PFBA Sample 1	PFBA Sample 2
0.3-0.4m	0.97	0.68	0.98	0.99	0.53	N/A	0.99	0.53	-2.00E-08	-4.00E-08	3.00E-07	N/A
	4.86	3.68	4.99	5.19	3.64	N/A	5.09	3.64	-2.60E-07	-6.60E-07	8.00E-08	N/A
	9.54	7.50	10.09	10.25	7.09	6.96	10.17	7.03	-1.10E-06	-1.42E-06	8.20E-07	1.08E-06
	14.30	10.25	16.90	16.49	9.37	9.67	16.70	9.52	-5.20E-06	-4.38E-06	1.76E-06	1.16E-06
	48.75	45.95	50.14	N/A	41.63	N/A	50.14	41.63	-2.78E-06	N/A	8.64E-06	N/A
	105.21	91.87	111.30	N/A	94.17	N/A	111.30	94.17	-1.22E-05	N/A	-4.60E-06	N/A
	191.25	195.79	200.89	N/A	188.62	N/A	200.89	188.62	-1.93E-05	N/A	1.43E-05	N/A
0.6-0.9m	0.97	0.68	0.84	0.84	0.94	0.87	0.84	0.91	2.60E-07	2.60E-07	-5.20E-07	-3.80E-07
	4.86	3.68	5.00	4.91	4.75	4.58	4.96	4.67	-2.80E-07	-1.00E-07	-2.14E-06	-1.80E-06
	9.54	7.50	9.78	11.17	8.96	8.98	10.48	8.97	-4.80E-07	-3.26E-06	-2.92E-06	-2.96E-06
	14.30	10.25	15.05	15.35	11.01	14.94	15.20	12.98	-1.50E-06	-2.10E-06	-1.52E-06	-9.38E-06
	48.75	45.95	52.10	51.25	48.51	45.46	51.68	46.99	-6.70E-06	-5.00E-06	-5.12E-06	9.80E-07
	105.21	91.87	112.57	106.92	98.06	94.42	109.75	96.24	-1.47E-05	-3.42E-06	-1.24E-05	-5.10E-06
	191.25	195.79	191.75	203.11	197.93	N/A	197.43	197.93	-1.00E-06	-2.37E-05	-4.28E-06	N/A

Summary statistics of applied vs recovered concentrations over all soil depths.

Applied Concentrations (mg/L)		Average Recovered Concentrations (mg/L)		Total Number of Samples		Standard Deviation of Recovered Concentration (mg/L)		Standard Error of Concentration (mg/L)		Average 'q' Value (g/g)		Standard Deviation of 'q' (g/g)		Standard Error of 'q' (g/g)	
DFBA	PFBA	DFBA	PFBA	DFBA	PFBA	DFBA	PFBA	DFBA	PFBA	DFBA	PFBA	DFBA	PFBA	DFBA	PFBA
0.97	0.68	0.95	0.74	8	7	0.065	0.12	0.022	0.048	4E-08	-1E-07	1.3E-07	2.55E-07	4.6E-08	9.65E-08
4.86	3.68	4.94	4.33	8	7	0.120	0.62	0.042	0.23	-1.6E-07	-1E-06	2.41E-07	1.25E-06	8.52E-08	4.73E-07
9.54	7.5	10.25	7.67	8	8	0.416	0.91	0.14	0.32	-1.4E-06	-3E-07	8.33E-07	1.83E-06	2.94E-07	6.47E-07
14.3	10.25	16.59	10.77	8	8	1.23	1.82	0.43	0.64	-4.6E-06	-1E-06	2.47E-06	3.66E-06	8.74E-07	1.29E-06
48.75	45.95	50.66	44.98	7	6	0.86	2.23	0.32	0.91	-3.8E-06	1.9E-06	1.72E-06	4.47E-06	6.51E-07	1.82E-06
105.21	91.87	107.61	94.09	7	7	6.59	3.38	2.49	1.29	-4.8E-06	-4E-06	1.32E-05	6.77E-06	4.98E-06	2.56E-06
191.25	195.79	199.14	194.02	7	6	9.45	3.51	3.57	1.43	-1.6E-05	3.5E-06	1.89E-05	7.03E-06	7.15E-06	2.87E-06

Calculated "Worst Case" Linear Isotherm for both DFBA and PFBA

DFBA "Worst Case" Linear Isotherm			PFBA "Worst Case" Linear Isotherm			Calculated "Worst Case" distribution coefficient (Kd) Value (cm ³ /g)	
Recovered Concentration (mg/L)	Converted Concentration (g/cm ³)	Calculated 'q' (g/g)	Recovered Concentration (mg/L)	Converted Concentration (g/cm ³)	Calculated 'q' (g/g)		
0.84	8.40E-07	2.60E-07	0.53	5.30E-07	3.00E-07	DFBA	PFBA
4.79	4.79E-06	1.40E-07	3.51	3.51E-06	3.40E-07	0.0789	0.0678
9.78	9.78E-06	-4.80E-07	6.56	6.56E-06	1.88E-06		
15.05	1.51E-05	-1.50E-06	9.04	9.04E-06	2.42E-06		
49.15	4.92E-05	-8.00E-07	41.63	4.16E-05	8.64E-06		
99.09	9.91E-05	1.22E-05	89.19	8.92E-05	5.36E-06		
185.34	1.85E-04	1.18E-05	188.62	1.89E-04	1.43E-05		

Calculated isotherms for both DFBA and PFBA

APPENDIX C: FIELD SOIL EXTRACTIONS

Summary statistics and concentrations of 2009 DFBA soil extractions

Core Sample Depth (m)	Borehole Location and Porewater Concentration					
	1 - North Edge Plot A (mg/L)	1- Duplicate (mg/L)	2 - Above North Tile (mg/L)	2- Duplicate (mg/L)	3 - Center of Plot (mg/L)	3- Duplicate (mg/L)
-0.1	0	0	9.84	N/A	110.21	107.72
-0.2	0.36	0	45.13	46.29	12.57	13.33
-0.75	11.64	N/A	20.70	20.19	0	0
-1.15	N/A	N/A	N/A	N/A	N/A	N/A
-1.75	4.45	6.91	N/A	N/A	N/A	N/A
-2.7	0	0	N/A	N/A	N/A	N/A
-3.7	0	N/A	N/A	N/A	0	0.13
-4.75	0	N/A	N/A	N/A	0.40	N/A
-5.65	0	0	N/A	N/A	0	N/A

Borehole Location and Porewater Concentration				
Core Sample Depth (m)	4 - Above South Tile (mg/L)	4- Duplicate (mg/L)	5 - Southern Edge Plot A (mg/L)	5- Duplicate (mg/L)
-0.1	15.88	N/A	233.07	178.03
-0.2	44.0774	34.86	102.01	101.52
-0.75	13.9085	14.02	1.0859	N/A
-1.15	12.029	N/A	N/A	N/A
-1.75	3.04	3.90	0.01	N/A
-2.7	N/A	N/A	0	N/A
-3.7	N/A	N/A	N/A	N/A
-4.75	N/A	N/A	0.01	N/A
-5.65	N/A	N/A	0.01	N/A

Core Sample Depth (m)	Average (mg/L)	Max (mg/L)	Min (mg/L)	Standard Deviation (mg/L)	Standard Error (mg/L)
-0.1	81.84	233.07	0.00	84.06	29.72
-0.2	40.01	102.01	0.00	35.18	11.12
-0.75	10.19	20.70	0.00	8.15	2.88
-1.15	12.03	12.03	12.03	0.00	0.00
-1.75	3.66	6.91	0.01	2.23	1.00
-2.7	0.00	0.00	0.00	0.00	0.00
-3.7	0.04	0.13	0.00	0.06	0.03
-4.75	0.14	0.40	0.00	0.19	0.11
-5.65	0.00	0.01	0.00	0.00	0.00

Summary statistics of 2010 DFBA soil extraction results and porewater concentrations at each borehole

Depth of Core Sample (m)	N	Average (mg/L)	Maximum (mg/L)	Minimum (mg/L)	Standard Deviation (mg/L)	Standard Error (mg/L)
-0.05	30	0.22	5.32	0.00	0.96	0.17
-0.15	28	1.01	17.29	0.00	3.34	0.63
-0.25	37	1.58	31.38	0.00	5.39	0.89
-0.35	29	3.22	34.71	0.00	7.35	1.37
-0.45	31	3.61	31.89	0.00	6.47	1.16
-0.65	31	3.45	28.05	0.00	6.04	1.09
-0.75	2	0.83	1.67	0.00	0.83	0.59
-0.85	3	0.92	2.75	0.00	1.30	0.75
-0.95	3	0.98	2.43	0.00	1.05	0.60
-1.05	2	1.67	3.33	0.00	1.67	1.18
-1.15	8	3.27	11.72	0.00	4.31	1.52
-1.25	9	2.16	9.86	0.00	3.43	1.14
-1.35	6	1.44	6.92	0.00	2.50	1.02
-1.5	3	0.00	0.00	0.00	0.00	0.00
-1.75	2	1.06	1.92	0.19	0.86	0.61
-2	3	0.06	0.19	0.00	0.09	0.05
-2.35	1	1.15	1.15	1.15	N/A	N/A
-2.5	2	0.00	0.00	0.00	0.00	0.00
-2.8	1	0.00	0.00	0.00	N/A	N/A
-3	2	0.00	0.00	0.00	0.00	0.00
-3.5	3	0.13	0.38	0.00	0.18	0.10
-4	2	0.00	0.00	0.00	0.00	0.00
-4.5	2	0.00	0.00	0.00	0.00	0.00
-4.75	2	0.00	0.00	0.00	0.00	0.00
-5	2	1.06	2.11	0.00	1.06	0.75

Core Sample Depth (m)	Borehole Location and Porewater Concentration										
	27	28	29	30	31	32	33	34	35	36	37
-0.05	0	0	0.00	0.00	0.00	0.00	0.00	0.00	5.32	0.00	0.00
-0.15	0	0	0.00	0.45	0.00	0.00	0.00	0.00	2.24	0.00	1.15
-0.25	0	0	0.00	2.37	1.79	0.00	0.00	0.83	0.00	8.39	0.00
-0.35	0	0	0.00	5.19	4.10	0.00	0.00	5.00	7.04	21.20	1.54
-0.45	0	0	0.00	0.96	5.38	0.00	3.52	7.30	7.24	14.67	14.79
-0.65	0	0	5.00	0.00	4.93	1.09	2.88	0.13	0.00	10.25	0.00
-0.75	0				1.67						
-0.85		0			0.00					2.75	
-0.95		0			0.51	2.43					
-1.05				0.00							
-1.15			3.84				1.73				
-1.25											
-1.35			1.47				0.26				
-1.5	0	0			0.00						
-1.75			1.92				0.19				
-2	0	0.19			0.00						
-2.35			1.15								
-2.5	0				0.00						
-2.8			0.00								
-3		0			0.00						
-3.5		0.38	0.00		0.00						
-4		0			0.00						
-4.5		0			0.00						
-4.75			0.00				0.00				
-5		2.11			0.00						

[illegible]

Core Sample Depth (m)	Borehole Location and Porewater Concentration				
	65	66	67	68	69
-0.05	0.00	0.00	0.00	0.00	0.00
-0.15	0.00	0.00	0.00	0.00	0.00
-0.25	0.00	0.00	0.00	0.13	0.00
-0.35	0.00	0.00	0.00	0.00	0.00
-0.45	0.00	0.00	0.00	2.43	0.00
-0.65	0.00	0.00	0.00	13.77	0.38
-0.75					
-0.85					
-0.95					
-1.05		3.33			
-1.15				11.72	
-1.25	3.27		6.34		
-1.35					6.92
-1.5					
-1.75					
-2					
-2.35					
-2.5					
-2.8					
-3					
-3.5					
-4					
-4.5					
-4.75					
-5					

APPENDIX D: QA/QC

Complete List of 2009 and 2010 QA/QC samples analyzed

2010 Soil Extraction Duplicates	
Primary Sample Concentration (mg/L)	Duplicate Sample Concentration (mg/L)
0.21	0.00
0.41	0.15
8.59	6.53
0.00	0.00
0.64	0.45
1.27	1.41
0.80	0.00
0.00	0.00
0.00	0.00
0.00	0.00
0.76	0.00
0.00	0.00
0.00	0.00
0.00	0.00
0.00	0.00
0.00	0.00
0.00	0.00
0.00	0.00
0.00	0.00
0.00	0.00
0.00	0.00
0.00	0.00
0.00	0.00
0.82	0.61
0.00	0.00
0.00	0.00
0.17	0.00
0.00	0.00
1.06	0.92
0.00	0.00
0.00	0.00

2010 Monitoring Well Equipment Blanks	
Date	Concentration (mg/L)
7/8/10 0:00	0
7/8/10 0:00	0
10/4/10 0:00	0
10/4/10 0:00	0
10/4/10 0:00	0

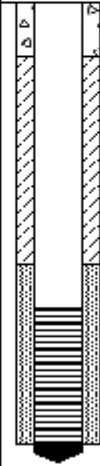
2009-2010 Tile and Monitoring Well Duplicate/Split		
Date	Primary Sample Concentration (mg/L)	Duplicate or Split Sample Concentration (mg/L)
9/3/09 20:00	4.32	4.24
9/3/09 23:00	4.08	4.16
9/4/09 2:00	1.40	1.30
9/5/09 12:00	4.50	4.88
9/8/09 15:00	1.08	1.25
9/21/09 0:00	3.10	3.06
9/21/09 9:00	3.26	3.44
9/27/09 2:00	1.75	1.77
10/3/09 16:00	3.50	3.41
10/6/09 4:00	2.33	2.30
10/6/09 4:00	3.03	3.17
6/27/10 3:20	2.03	1.96
6/28/10 16:30	4.17	4.17
6/29/10 16:30	2.19	2.29
7/2/10 4:30	3.55	3.55
7/9/10 0:00	5.01	5.04
7/9/10 0:00	1.13	1.09
7/9/10 0:00	2.42	2.48
7/9/10 0:00	0.06	0.00
7/10/10 17:30	3.59	3.10
7/13/10 17:30	1.50	1.32
7/25/10 6:30	1.30	1.29
7/25/10 6:30	2.30	2.32
7/25/10 8:00	1.29	1.30
7/26/10 6:00	0.08	0.06
8/1/10 19:30	1.72	1.69
8/3/10 0:00	473.62	475.20
8/3/10 8:30	0.12	0.12
8/7/10 0:00	12.16	11.85
8/7/10 0:00	0.04	0.06
8/7/10 0:00	0.00	0.00
8/7/10 0:00	3.38	1.97
8/7/10 0:00	0.02	0.00
8/7/10 0:00	0.00	0.00

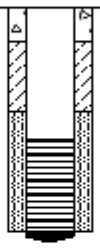
8/7/10 0:00	1.54	1.47
8/10/10 0:00	1.28	1.23
8/10/10 0:00	1.72	1.72
8/10/10 0:00	0.58	0.59
8/10/10 0:00	18.18	18.01
8/13/10 23:30	2.08	2.10
8/14/10 17:30	3.06	3.05
8/17/10 10:30	0.15	0.13
8/19/10 19:30	2.57	2.55
8/23/10 11:30	3.27	3.24
8/24/10 2:30	0.11	0.01
9/1/10 2:30	0.11	0.13
9/8/10 13:30	2.54	2.09
9/8/10 13:30	0.47	0.37
9/8/10 13:30	2.96	2.59
9/15/10 5:30	4.75	4.72
9/15/10 5:30	3.45	3.26
9/21/10 13:30	4.07	4.01
10/1/10 21:30	3.28	3.30
10/2/10 2:30	0.00	0.00

APPENDIX E: BOREHOLE LOGS

PROJECT:				Devon Salt Research		MW09-01/C0X-01	
BORING LOCATION:				Devon site, North edge of plot A		GROUND SURFACE ELEVATION AND DATUM: 725.051 m.a.s.l.	
DRILLING CONTRACTOR:				Envirocore		DATE STARTED: 22-Aug-08	DATE FINISHED: 22-Aug-08
DRILLING METHOD:				Direct Push Macropore 38mm (1.5 in)		BH DEPTH (m): 6.65	Well Stick Up (m): 0.387
DRILLING EQUIPMENT:				Geoprobe 6610 Track Unit		Well hole Diameter (inch): 2	Well Diameter (inch): 1
SAMPLING METHOD:				Coring with PVC liner		LOGGED BY: M. Callaghan	
Easting: 314648.96				Northing: 5907209.362		Well Installation: U of C	REG. NO.
DEPTH (meters)	SAMPLES			OVM Reading	DESCRIPTION NAME (USCS): Density, Color, Classification, Moisture, Sed. Structure, Weathering, Secondary Grain, Local Obs. Surface Elevation: 725.051 m.a.s.l.	WELL CONSTRUCTION DETAILS AND/OR DRILLING REMARKS	
	Sample No.	Sample	Blows/ Foot				
0					Topsoil- Loose, black to brown, dry to wet Glaciolacustrine Silty Loam (Disturbed)- Dense, black to brown, moist to wet, massive, roots	Backfill, 0-0.3m	
1					Glaciolacustrine Silty Loam (Undisturbed)- Dense, yellow to brown, moist to wet, locally thinly bedded, roots to till contact	Bentonite, 0.3-1.63m	
2					Glacial Till- Dense to very dense, grey to brown, moist, locally thinly bedded sand, local oxidization, trace fine gravel	Sandpack, 1.613-2 m Screen, 1.75-2 m	
3							
4					Sand- Loose to dense, yellow to brown, fine to medium grained sand, moist to wet Glacial Till- Dense to very dense, grey to brown, moist, locally thinly bedded sand, local oxidization, trace fine gravel, fractures visible through entirety section, interlayered sands from 4.9-5.1 m		
5							
6					Sand- Loose to dense, yellow to brown, fine to medium grained sand, moist to wet		
7							
University of Calgary - Imperial Oil Limited						04-05-50-26W4M	

PROJECT:		Devon Salt Research			MW09-02/C0X-02		
BORING LOCATION:		Devon site, North of the center of plot A			GROUND SURFACE ELEVATION AND DATUM: 725.086		
DRILLING CONTRACTOR:		Envirocore			DATE STARTED:	22-Aug-08	
DRILLING METHOD:		Direct Push Macropore 38mm (1.5 in)			BH Depth (m):	2.4	
DRILLING EQUIPMENT:		Geoprobe 6610 Track Unit			Well hole diameter (inch):	2	
SAMPLING METHOD:		Coring with PVC liner			Well Diameter (inch):	1	
Easting:		314648.32			Northing:		
					5907202.387		
LOGGED BY:		M. Callaghan			Well Installation:		
					U of C		
REG. NO.							
DEPTH (meters)	SAMPLES				OVM Reading	DESCRIPTION NAME (USCS): Density, Color, Classification, Moisture, Sed. Structure, Weathering, Secondary Grain, Local Obs. Surface Elevation: 725.086 m.a.s.l.	WELL CONSTRUCTION DETAILS AND/OR DRILLING REMARKS
	Sample No.	Sample	Blows/ Foot				
0						Topsoil- Loose, black to brown, dry to wet	<p>Backfill, 0-0.3 m</p> <p>Bentonite, 0.3-1.23 m</p> <p>Sandpack, 1.23-2.4 m</p> <p>Screen, 1.48-2.4 m</p>
						Glaciolacustrine Silty Loam (Disturbed)- Dense, black to brown, moist to wet, massive, roots observed to 0.7 m	
1							
2							
University of Calgary - Imperial Oil Limited					04-05-50-26W4M		

PROJECT: Devon Salt Research					MW09-04/C0X-04				
BORING LOCATION: Devon site, South of central plot A					GROUND SURFACE ELEVATION AND DATUM: 725.161 m.a.s.l.				
DRILLING CONTRACTOR: Envirocore					DATE STARTED: 8-Aug-08		DATE FINISHED: 8-Aug-08		
DRILLING METHOD: Direct Push Macropore 38mm (1.5 in)					BH DEPTH (m): 2.46		Well Stick Up (m): 0.5		
DRILLING EQUIPMENT: Geoprobe 6610 Track Unit					Well hole Diameter (inch): 2		Well Diameter (inch): 1		
SAMPLING METHOD: Coring with PVC liner					LOGGED BY: M. Callaghan				
Easting: 314648.26			Northing: 5907193.786		Well Installation: U of C			REG. NO.	
DEPTH (meters)	SAMPLES				OVM Reading	DESCRIPTION NAME (USCS): Density, Color, Classification, Moisture, Sed. Structure, Weathering, Secondary Grain, Local Obs. Surface Elevation: 725.161 m.a.s.l.	WELL CONSTRUCTION DETAILS AND/OR DRILLING REMARKS		
	Sample No.	Sample	Blows/ Foot						
0						Topsoil - Loam, black to brown, dry to wet	 <p>Bentonite, 0.3-1.46 m</p> <p>Sandpack, 1.46-2.46 m</p> <p>Screen, 1.71-2.46 m</p>		
1						Glaciolacustrine Silty Loam (Disturbed)- Dense, black to brown, moist to wet, massive, roots			
2									
3									
University of Calgary - Imperial Oil Limited							04-05-50-26W4M		

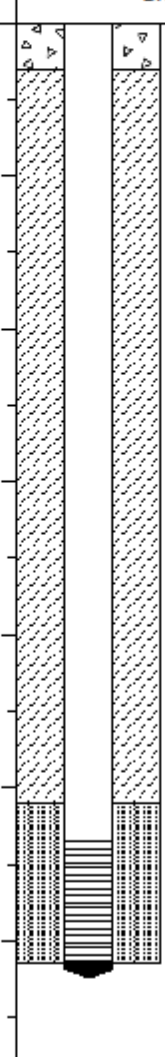
PROJECT:		Devon Salt Research			MW09-05/C0X-05	
BORING LOCATION:		Devon site, South edge of plot A			GROUND SURFACE ELEVATION AND DATUM: 725.259 m.a.s.l.	
DRILLING CONTRACTOR:		Envirocore			DATE STARTED: 22-Aug-08 DATE FINISHED: 22-Aug-08	
DRILLING METHOD:		Direct Push Macropore 38mm (1.5 in)			BH DEPTH (m): 1.98 Well Stick Up (m): 0.5	
DRILLING EQUIPMENT:		Geoprobe 6610 Track Unit			Well hole diameter (inch): 2 Well Diameter (inch): 1	
SAMPLING METHOD:		Coring with PVC liner			LOGGED BY: M. Callaghan	
Easting:		314648.269		Northing:		5907189.181
				Well Installation:		U of C REG. NO.
DEPTH (meters)	SAMPLES				DESCRIPTION NAME (USCS): Density, Color, Classification, Moisture, Sed. Structure, Weathering, Secondary Grain, Local Obs. Surface Elevation: 725.259 m.a.s.l.	WELL CONSTRUCTION DETAILS AND/OR DRILLING REMARKS
	Sample No.	Sample	Blows/ Foot	QVM Reading		
0					Topsoil- Loose, black to brown, dry to wet Glaciolacustrine Silty Loam (Disturbed)- Dense, black to brown, moist to wet, massive, roots	 <p>Bentonite, 0.3-0.93</p> <p>Sandpack, 0.93-1.98 m</p> <p>Screen, 1.18-1.98 m</p>
1					Glaciolacustrine Silty Loam (Undisturbed)- Dense, yellow to brown, moist to wet, locally thinly bedded, roots to till contact, dark grey laminations and brittle fracture at 1.5-2.1 m	
2					Glacial Till- Dense to very dense, grey to brown, moist, locally thinly bedded sand, local oxidization, trace fine gravel, trace sand laminations at 2.45 m, oxidized fracture between 3.04-4.5 m	
3						
4						
5					Sand- Loose to dense, yellow to brown, fine to medium grained sand, moist to wet	
6					Glacial Till- Dense to very dense, grey to brown, moist, locally thinly bedded sand, local oxidization, trace fine gravel	
7					Missing Sand- Loose to dense, yellow to brown, fine to medium grained sand, moist to wet Glacial Till- Dense to very dense, grey to brown, moist, locally thinly bedded sand, local oxidization, trace fine gravel, sand mixed in at 6.34 to 6.45 m	
University of Calgary - Imperial Oil Limited					04-05-50-28W4M	

PROJECT: Devon Salt Research					MW09-11B				
BORING LOCATION: Devon site, East of plot A					GROUND SURFACE ELEVATION AND DATUM: 725.094 m.a.s.l.				
DRILLING CONTRACTOR: Envirocore					DATE STARTED: Nov-09		DATE FINISHED: Nov-09		
DRILLING METHOD: Solid Stem Auger 6 in					BH DEPTH (m): 4.44		Well Stick Up (m): 0.78		
DRILLING EQUIPMENT: Diedrich D-50 Track Unit					Well hole Diameter (inch): 6		Well Diameter (m): 2		
SAMPLING METHOD: None					LOGGED BY: N/A				
Easting: 314665.403			Northing: 5907195.819		Well Installation: Envirocore			REG. NO.	
DEPTH (meters)	SAMPLES				OVM Reading	DESCRIPTION NAME (USCS): Density, Color, Classification, Moisture, Sed. Structure, Weathering, Secondary Grain, Local Obs. Surface Elevation: 725.094 m.a.s.l.	WELL CONSTRUCTION DETAILS AND/OR DRILLING REMARKS		
	Sample No.	Sample	Blows/ Foot						
0						No corresponding borehole log for this well location	Backfill, 0-0.3m		
1									
2							Bentonite, 0.3-3.835 m		
3									
4							Sandpack, 3.835-4.4 m		
							Screen, 4.1-4.4 m		
University of Calgary - Imperial Oil Limited						04-05-50-26W4M			

PROJECT:		Devon Salt Research		MW09-11C		
BORING LOCATION:		Devon site, East of plot A		GROUND SURFACE ELEVATION AND DATUM: 725.096 m.a.s.l.		
DRILLING CONTRACTOR:		Envirocore		DATE STARTED: 14-Aug-09	DATE FINISHED: 14-Aug-09	
DRILLING METHOD:		Solid Stem Auger 6 in		BH DEPTH (m): 6.41	Well Stick Up (m): 0.767	
DRILLING EQUIPMENT:		Diedrich D-50 Track Unit		Well hole Diameter (inch): 6	Well Diameter (m): 2	
SAMPLING METHOD:		None		LOGGED BY: N/A		
Easting: 314664.381		Northing: 5907195.669		Well Installation: Envirocore	REG. NO.	
DEPTH (meters)	SAMPLES				DESCRIPTION NAME (USCS): Density, Color, Classification, Moisture, Sed. Structure, Weathering, Secondary Grain, Local Obs. Surface Elevation: 725.096 m.a.s.l.	WELL CONSTRUCTION DETAILS AND/OR DRILLING REMARKS
	Sample No.	Sample	Blows/ Foot	QVM Reading		
0						Back fill, 0-0.3 m
1					No corresponding borehole log for this location	
2						
3						
4						
5						
6						Bentonite, 0.3-5.8 m
						Sandpack, 5.8-6.4 m
						Screen, 6.1-6.4 m
University of Calgary - Imperial Oil Limited					04-05-50-26W4M	

PROJECT:				Devon Salt Research				MW09-13A/C0X-03					
BORING LOCATION:				Devon site, Center of plot A				GROUND SURFACE ELEVATION AND DATUM: 725.104 m.a.s.l.					
DRILLING CONTRACTOR:				Envirocore				DATE STARTED: 22-Aug-08		DATE FINISHED: 22-Aug-08			
DRILLING METHOD:				Direct Push Macropore 38mm (1.5 in)				BH DEPTH (m): 2.05		Well Stick Up (m): 0.5			
DRILLING EQUIPMENT:				Geoprobe 6610 Track Unit				Well hole Diameter (inch): 2		Well Diameter (inch): 1			
SAMPLING METHOD:				Coring with PVC liner				LOGGED BY: M. Callaghan					
Easting: 314647.894				Northing: 5907198.559				Well Installation: U of C		REG. NO.			
DEPTH (meters)		SAMPLES		DESCRIPTION		WELL CONSTRUCTION DETAILS AND/OR DRILLING REMARKS							
Sample No.		Sample		NAME (USCS): Density, Color, Classification, Moisture, Sed. Structure, Weathering, Secondary Grain, Local Obs.									
		Blows/ Foot		OVM Reading		Surface Elevation: 725.104 m.a.s.l.							
0						Topsoil- Loose, black to brown, dry to wet							
						Glaciolacustrine Silty Loam (Disturbed)- Dense, black to brown, moist to wet, massive, roots							
						Glaciolacustrine Silty Loam (Undisturbed)- Dense, yellow to brown, moist to wet, locally thinly bedded, roots to till contact, grey clay laminations at 2 m							
1													
2								Bentonite, 0.3-1.5 m Sandpack, 1.5-2.03 m Screen, 1.75-2.03 m					
University of Calgary - Imperial Oil Limited				04-05-50-26W4M									

PROJECT:				Devon Salt Research		MW09-13B/C0X-03	
BORING LOCATION:				Devon site, Center of plot A		GROUND SURFACE ELEVATION AND DATUM: 725.59 m.a.s.l.	
DRILLING CONTRACTOR:				Envirocore		DATE STARTED:	Nov-09
DRILLING METHOD:				Solid Stem Auger 6 in		DATE FINISHED:	Nov-09
DRILLING EQUIPMENT:				Diedrich D-50 Track Unit		BH DEPTH (m):	4.52
SAMPLING METHOD:				None		Well Stick Up (m):	0.5
Easting:				314648.663		Well hole Diameter (inch):	6
Northing:				5907198.583		Well Diameter (inch):	1
LOGGED BY:				M. Callaghan		Well Installation:	Envirocore
REG. NO.							
DEPTH (meters)	SAMPLES			OVM Reading	DESCRIPTION NAME (USCS): Density, Color, Classification, Moisture, Sed. Structure, Weathering, Secondary Grain, Local Obs. Surface Elevation: 725.59 m.a.s.l.	WELL CONSTRUCTION DETAILS AND/OR DRILLING REMARKS	
	Sample No.	Sample	Blows/ Foot				
0					Topsoil- Loose, black to brown, dry to wet		
					Glaciolacustrine Silty Loam (Disturbed)- Dense, black to brown, moist to wet, massive, roots		
1					Glaciolacustrine Silty Loam (Undisturbed)- Dense, yellow to brown, moist to wet, locally thinly bedded, roots to till contact, grey clay laminations at 2 m		
2							
					Glacial Till- Dense to very dense, grey to brown, moist, locally thinly bedded sand, local oxidization, trace fine gravel, trace coarse sand		Bentonite, 0.3-3.9 m
3							
4					Sand- Loose to dense, yellow to brown, fine to medium grained sand, moist to wet		Sandpack, 3.9-4.52 m
					Glacial Till- Dense to very dense, grey to brown, moist, locally thinly bedded sand, local oxidization, trace fine gravel, sand lens at 5.13-5.16 m		Screen, 4.15-4.52 m
5							
6							
University of Calgary - Imperial Oil Limited						04-05-50-26W4M	

PROJECT: Devon Salt Research				MW09-13C/C0X-03			
BORING LOCATION: Devon Site, Center of plot A				GROUND SURFACE ELEVATION AND DATUM: 724.864 m.a.s.l.			
DRILLING CONTRACTOR: Envirocore				DATE STARTED: Nov-09		DATE FINISHED: Nov-09	
DRILLING METHOD: Solid Stem Auger 6 in				BH DEPTH (m): 6.14		Well Stick Up (m): 0.5	
DRILLING EQUIPMENT: Diedrich D-50 Track Unit				Well hole Diameter (inch): 6		Well Diameter (m): 1	
SAMPLING METHOD: None				LOGGED BY: M. Callaghan			
Easting: 314649.415		Northing: 5907198.57		Well Installation: Envirocore		REG. NO.	
DEPTH (meters)	SAMPLES			OVM Reading	DESCRIPTION NAME (USCS): Density, Color, Classification, Moisture, Sed. Structure, Weathering, Secondary Grain, Local Obs. Surface Elevation: 724.864 m.a.s.l.	WELL CONSTRUCTION DETAILS AND/OR DRILLING REMARKS	
	Sample No.	Sample	Blows/ Foot				
0					Topsoil- Loose, black to brown, dry to wet		
					Glaciolacustrine Silty Loam (Disturbed)- Dense, black to brown, moist to wet, massive, roots		
1					Glaciolacustrine Silty Loam (Undisturbed)- Dense, yellow to brown, moist to wet, locally thinly bedded, roots to till contact, grey clay laminations at 2 m		
2							
3					Glacial Till- Dense to very dense, grey to brown, moist, locally thinly bedded sand, local oxidization, trace fine gravel, trace coarse sand		
4					Sand- Loose to dense, yellow to brown, fine to medium grained sand, moist to wet		
5					Glacial Till- Dense to very dense, grey to brown, moist, locally thinly bedded sand, local oxidization, trace fine gravel, sand lens at 5.13-5.16 m	Bentonite, 0.3-5.1 m	
6						Sandpack, 5.1-6.14 m	
						Screen, 5.35-6.14 m	
University of Calgary - Imperial Oil Limited				04-05-50-26W4M			

PROJECT: Devon Salt Research					MW09-14B				
BORING LOCATION: Devon site, West of plot A					GROUND SURFACE ELEVATION AND DATUM: 725.198 m.a.s.l.				
DRILLING CONTRACTOR: Envirocore					DATE STARTED: Nov-09		DATE FINISHED: Nov-09		
DRILLING METHOD: Solid Stem Auger 6 in					BH DEPTH (m): 4.66		Well Stick Up (m): 0.88		
DRILLING EQUIPMENT: Diedrich D-50 Track Unit					Well hole diameter (inch): 6		Well Diameter (m): 2		
SAMPLING METHOD: None					LOGGED BY: N/A				
Easting: 314634.05			Northing: 5907197.04		Well Installation: Envirocore			REG. NO.	
DEPTH (meters)	SAMPLES				OVM Reading	DESCRIPTION NAME (USCS): Density, Color, Classification, Moisture, Sed. Structure, Weathering, Secondary Grain, Local Obs. Surface Elevation: 725.198 m.a.s.l.	WELL CONSTRUCTION DETAILS AND/OR DRILLING REMARKS		
	Sample No.	Sample	Blows/ Foot						
0						No corresponding borehole log for this location	Back fill, 0-0.3 m		
1									
2									
3									
4									
							Bentonite, 0.3-4.16 m		
							Sandpack, 4.16-4.66 m		
							Screen, 4.3-4.66 m		
University of Calgary - Imperial Oil Limited						04-05-50-26W4M			

PROJECT: Devon Salt Research					MW09-14C				
BORING LOCATION: Devon site, West of plot A					GROUND SURFACE ELEVATION AND DATUM: 725.169 m.a.s.l.				
DRILLING CONTRACTOR: Envirocore					DATE STARTED: Nov-09		DATE FINISHED: Nov-09		
Drilling Method: Solid Stem Auger 6 in					TOTAL DEPTH (m): 6.63		Well Stick Up (m): 0.883		
DRILLING EQUIPMENT: Diedrich D-50 Track Unit					Well hole Diameter (inch): 6		Well Diameter (m): 2		
SAMPLING METHOD: None					LOGGED BY: N/A				
Easting: 314635.01			Northing: 5907197.016		Well Installation: Envirocore			REG. NO.	
DEPTH (meters)	SAMPLES				OVM Reading	DESCRIPTION NAME (USCS): Density, Color, Classification, Moisture, Sed. Structure, Weathering, Secondary Grain, Local Obs. Surface Elevation: 725.169 m.a.s.l.	WELL CONSTRUCTION DETAILS AND/OR DRILLING REMARKS		
	Sample No.	Sample	Blows/ Foot						
0									
1						No corresponding borehole log for this location			Back fill, 0-0.3 m
2									
3									Bentonite, 0.3-5.9 m
4									
5									
6									
									Sandpack, 5.9-6.63 m
									Screen, 6.3-6.6 m
University of Calgary - Imperial Oil Limited							04-05-50-26W4M		

APPENDIX F: HYDRUS INPUTS

Only available electronically

APPENDIX G: SOIL DATA

C10-01 0-5 cm	
Nominal Pressure (mbar)	Water Content (v/v)
0	0.482
2.49	0.476
10	0.472
30	0.469
63	0.454
125	0.436
250	0.422
500	0.406
1000	0.377
3000	0.338
6000	0.291

C10-02 0-5 cm	
Nominal Pressure (mbar)	Water Content (v/v)
0	0.484
2.49	0.477
10	0.471
30	0.466
63	0.455
125	0.447
250	0.440
500	0.429
1000	0.411
3000	0.408
6000	0.370

C10-03 0-5 cm	
Nominal Pressure (mbar)	Water Content (v/v)
0	0.482
2.49	0.469
10	0.465
30	0.462
63	0.445
125	0.428
250	0.411
500	0.389
1000	0.362
3000	0.346
6000	0.305

C10-04 0-5 cm	
Nominal Pressure (mbar)	Water Content (v/v)
0	0.506
2.49	0.494
10	0.489
30	0.487
63	0.470
125	0.448
250	0.427
500	0.407
1000	0.377
3000	0.355
6000	0.304

C10-05 0-5 cm	
Nominal Pressure (mbar)	Water Content (v/v)
0	0.520
2.49	0.511
10	0.505
30	0.501
63	0.482
125	0.456
250	0.439
500	0.420
1000	0.384
3000	0.364
6000	0.311

C08-03 0.6-0.7 cm	
Nominal Pressure (mbar)	Water Content (v/v)
0	0.541
1.21	0.481
30	0.457
60	0.436
120	0.429
250	0.419
500	0.409
1000	0.387
2040	0.364
4000	0.343
7500	0.323

C08-10 0.6-0.7 cm	
Nominal Pressure (mbar)	Water Content (v/v)
0	0.583
1.21	0.544
10	0.545
30	0.513
60	0.500
120	0.486
250	0.467
500	0.441
1000	0.417
2040	0.391

Van Genuchten parameters calculated using the RETC fitting program

Top Soil Unit	RETC Calculated Values			
Test	θ_r	θ_s	α (mm ⁻¹)	n
C10-01 0-5 cm	0	0.4757	0.00068	1.12
C10-02 0-5 cm	0	0.4791	0.00277	1.04
C10-03 0-5 cm	0	0.4749	0.00177	1.08
C10-04 0-5 cm	0	0.499	0.00144	1.1
C10-05 0-5 cm	0	0.5148	0.00159	1.1

Glaciolacustrine Unit	RETC Calculated Values			
Test	θ_r	θ_s	α (mm ⁻¹)	n
C08-03 0.6-0.7	0	0.429	0.00663	1.06
C08-10 0.6-0.7	0	0.03947	0.01519	1.08